



HAL
open science

Anderson localization in disordered systems with competing channels

Hongyi Dr. Xie

► **To cite this version:**

Hongyi Dr. Xie. Anderson localization in disordered systems with competing channels. Quantum Physics [quant-ph]. Scuola Internazionale Superiore di Studi Avanzati, 2012. English. NNT: . tel-00752118

HAL Id: tel-00752118

<https://theses.hal.science/tel-00752118>

Submitted on 14 Nov 2012

HAL is a multi-disciplinary open access archive for the deposit and dissemination of scientific research documents, whether they are published or not. The documents may come from teaching and research institutions in France or abroad, or from public or private research centers.

L'archive ouverte pluridisciplinaire **HAL**, est destinée au dépôt et à la diffusion de documents scientifiques de niveau recherche, publiés ou non, émanant des établissements d'enseignement et de recherche français ou étrangers, des laboratoires publics ou privés.



SCUOLA INTERNAZIONALE
SUPERIORE di STUDI AVANZATI
International School
for Advanced Studies
via Bonomea 265 • 34136 Trieste • ITALY
T +39 040 3787 111 • F +39 040 3787 249
w w w . s i s s a . i t

INTERNATIONAL SCHOOL FOR ADVANCED STUDIES

CONDENSED MATTER THEORY SECTOR

Anderson Localization in Disordered Systems with Competing Channels

A Dissertation Submitted for the Degree of Doctor of Philosophy

Academic Year 2011/2012

CANDIDATE:

Hong-Yi Xie

SUPERVISORS:

Prof. Michele Fabrizio

Prof. Vladimir E. Kravtsov

Prof. Markus Müller

OCTOBER 2012

SISSA - VIA BONOMEA 265, 34136 TRIESTE - ITALY

Contents

1	Introduction	5
1.1	Basics concepts of Anderson localization	5
1.1.1	Boltzmann theory and Ioffe-Regel criterion	5
1.1.2	Evidence for the breakdown of weak scattering theory	7
1.1.3	Anderson localization and the scaling theory	8
1.2	Few-particle systems–Channel competition	12
1.3	Anderson localization of polaritons	13
1.4	Summary of the results	14
2	Localization of few interacting particles	17
2.1	Thouless block picture	20
2.2	Localization of two interacting particles	21
2.2.1	Two interacting particles in one dimension	21
2.2.2	Two interacting particles in higher dimensions	24
2.3	Localization of N interacting particles in one dimension	26
2.4	Competing channels	38
3	Anderson localization of a hybrid particle–Exciton-polariton	39
3.1	A short introduction to microcavity polaritons	41

3.2	Disorder effects on excitons and polaritons	43
4	Anderson localization on a two-leg ladder	46
4.1	Two-leg Anderson model	49
4.1.1	Disorder free part	51
4.1.2	Disordered part	54
4.2	Two-channel regime	55
4.2.1	Transfer matrix approach	56
4.2.2	Fokker-Planck equation for the distribution function of parameters . . .	59
4.2.3	Parametrization of transfer matrices	59
4.2.4	Physical interpretation of ξ_1 and ξ_2	62
4.2.5	Fokker-Planck equation for the distribution function of $\vec{\lambda}(\mathbf{R})$	64
4.2.6	Coarse graining	66
4.2.7	Calculating the localization lengths	69
4.2.8	Results for the localization lengths	78
4.3	One-channel regime	90
4.3.1	Transfer matrix of an elementary slice	91
4.3.2	Weak disorder analysis of Lyapunov exponents	92
4.3.3	Localization length and evanescent decay rate	96
4.4	Shape and polarization of the wave functions	100
4.4.1	Numerical analysis	100
4.4.2	Perturbative analysis	102
4.5	Limit of vanishing hopping on the “slow” leg	104
4.6	Possible application to polaritons	107
5	Anderson localization on two-layer Bethe lattice	110

5.1	Anderson model and the recursion relation for the local Green's functions . . .	113
5.2	Anderson transition and population dynamics	116
5.3	Phase diagram	119
5.3.1	Numerical results	119
5.3.2	Perturbative analysis	123
6	Discussion	124
A	Transfer matrix of an “elementary slice” in the current-conserving basis Eqs. (4.24) and (4.26)	126
B	Perturbative calculation of $\delta\vec{\lambda}$ up to second order	129
C	Coefficients of Eq. (4.67)	133
D	Transfer matrix of an “elementary slice” in the basis Eqs. (4.24) and (4.106)	136

Chapter 1

Introduction

1.1 Basics concepts of Anderson localization

1.1.1 Boltzmann theory and Ioffe-Regel criterion

Structural, chemical and other imperfections are unavoidable in crystalline solids. Sufficiently reducing their concentration may uncover many intrinsic properties of ideal “pure” materials. Nevertheless, impurities play a substantial role in understanding the transport properties of electronic materials. The conventional theory of electronic conductivity, which is referred to as Boltzmann quasiclassical theory[1], was built on the picture that an electron is multiply elastically scattered by impurities and diffusing through the solid. A cardinal concept in the description of the diffusion of an electron is the mean free path l or the mean free time τ , which are the average distance or time between scatterings by impurities. They are related by $l = \hbar k_F \tau / m_e$, where k_F is the Fermi wavevector of the electrons, and m_e is the effective mass of an electron in a band. The theory results in the Drude formula for the DC conductivity of electrons if the linear size of the system is much larger than the mean free path:

$$\sigma_0 = \frac{ne^2\tau}{m_e}, \quad (1.1)$$

where e is the elementary charge, n is the average density of electrons. The Drude conductivity σ_0 is temperature-independent and proportional to the mean free time τ . The stronger the scattering by impurities, the shorter the mean free time, and the smaller the conductivity.

Yet at finite temperatures T one has to additionally consider the inelastic scattering processes of electrons due to, for example, electron-phonon coupling. Similarly as in the case of impurity (elastic) scattering, the contribution of inelastic scattering to the conductivity is proportional to the corresponding inelastic scattering time, which depends on two temperature regimes:

- (i) At high temperatures, that is, the temperature is much higher than the Debye temperature of phonons, the inelastic scattering time is set by $\hbar/k_B T$, which leads to $1/\sigma(T) - 1/\sigma_0 \propto T$.
- (ii) At low temperatures, however, we have $1/\sigma(T) - 1/\sigma_0 \propto (T/T_0)^p$, where p and T_0 depend on the nature of inelastic scattering. For example, if electrons are scattered by phonons, $p = 5$ and T_0 is the Debye temperature of the phonons. For electron-electron interaction, $p = 2$ and T_0 is the Fermi energy of electrons.

Here we note that the Boltzmann theory gives $d\sigma(T)/dT < 0$, since the inelastic scattering time is shorter if the temperature is higher. The Boltzmann theory has been quite successful in describing the impurity and temperature dependence of the conductivity in ordinary and relatively pure conductors.

Yet the Boltzmann theory is correct only if the elastic mean free path is much larger than the Fermi wave length,

$$k_F l \gg 1. \tag{1.2}$$

In this case quantum interference is not important. Eq. (1.2) is called the Ioffe-Regel criterion[2, 3]. One can naturally expect that $k_F l \sim 1$ will bring us into a totally different regime, where the quantum interference becomes substantial. Combined with Eq. (1.1), in three dimensions $k_F l \sim 1$ leads to a conductivity[4]:

$$\sigma_{0,min} \sim 5 \times 10^{-5} k_F / \Omega. \tag{1.3}$$

The Ioffe-Regel criterion (1.2) implies that in three dimensions only for metals with conductivities much larger than $\sigma_{0,min}$ their transport properties are well captured by the Boltzmann theory.

1.1.2 Evidence for the breakdown of weak scattering theory

The effect of quantum interference on electron conductivity in disordered metals was first taken into account by the diagrammatic perturbation theory[5, 6], which is a systematic series expansion in the small parameter $1/k_F l$. Qualitatively, the effect can be interpreted via the return probability in a semiclassical way. The amplitude of a quantum particle to start at a point 0 and return to it is a sum over Feynman paths[7]:

$$A_{0 \rightarrow 0} = \sum_i A_i e^{iS_i/\hbar}, \quad (1.4)$$

where S_i is the action of the i -th path starting from 0 and returning to it, and A_i are appropriate coefficients. Therefore, the probability of return to the point 0 is

$$P_0 = |A_{0 \rightarrow 0}|^2 = \sum_i |A_i|^2 + \sum_{i \neq j} A_j A_i^* e^{i(S_j - S_i)/\hbar}. \quad (1.5)$$

On the right hand side of Eq. (1.5) the first term is the classical return probability, and the second term represents the effect of quantum interference. Upon averaging over realizations of impurities the second term has strong cancellations. But there exists a large number of paths whose contributions do not vanish when the time-reversal symmetry is present (in the absence of the magnetic field), which are the pairs of time-reversed paths. Since the two paths of each pair have the same phase, they lead to an enhanced return probability compared to the classical one. In this case the probability for transmission is reduced, which leads to a reduced conductivity. The enhancement of the return probability is a precursor to a strongly localized regime where the quantum interference dominates the propagation of particles.

It has long been realized that large enough concentrations of impurities can give rise to a number of phenomena essentially distinct from what are observed in clean or weakly disordered conductors. In particular, for three-dimensional metals with Drude conductivity σ_0

smaller than the value of the order of the one given in Eq. (1.3)[4, 8], the temperature dependence of the conductivity $\sigma(T)$ becomes much weaker or eventually changes direction, that is, $d\sigma(T)/dT \geq 0$. This behavior contradicts the Boltzmann weak scattering theory, which predicts that $d\sigma(T)/dT < 0$, and provides an experimental evidence for the existence of the regime where the Ioffe-Regel condition (1.2) is broken. More interestingly, in some thin wires and films, which are effectively one- and two-dimensional systems in the absence of spin-orbit coupling, respectively, it is found that $\sigma(T) \rightarrow 0$ as $T \rightarrow 0$ and $d\sigma(T)/dT > 0$ at low enough temperatures[9]–[12]. The above properties provide the experimental evidence for the existence of a strongly localized regime, where the strength of disorder is sufficiently strong, or the dimensionality is low.

1.1.3 Anderson localization and the scaling theory

A better starting point for understanding the transport properties in strongly disordered or low-dimensional systems is the concept of Anderson localized states, where a quantum particle is coherently trapped by impurities and does not participate in transport any longer. The existence of such states was predicted and explained in terms of quantum interference by P. W. Anderson in his groundbreaking paper[13]. This phenomenon is referred to as the *Anderson localization*[6, 14, 15]. The theory is based on the fact that for a given energy E and strength of disorder, the quantum state of the particle $\psi_E(\mathbf{r})$ is either localized or extended, whose envelope is typically characterized by

$$|\psi_E(\mathbf{r})|^2 \propto \begin{cases} \frac{1}{\xi_E^D} e^{-\frac{|\mathbf{r}-\mathbf{r}_0|}{\xi_E}}, & |\mathbf{r} - \mathbf{r}_0| \gg \xi_E, \quad \text{localized,} \\ \frac{1}{\mathcal{V}}, & \text{extended,} \end{cases} \quad (1.6)$$

where D is the dimensionality of the system, \mathbf{r}_0 is the localization center, ξ_E is the localization radius at the energy E , and \mathcal{V} is the volume of the system. The energies in the one-particle spectrum separating the localized and delocalized states are called mobility edges[16], whose locations depend on the type and the strength of disorder. The existence of mobility edges implies transitions between insulating and metallic phases in disordered non-interacting electronic systems, driven by the density and disorder.

For simplicity we assume that there is only one mobility edge E_m in a disordered electronic system: For $E < E_m$ all states are localized. For $E > E_m$ all states are extended. When the Fermi energy E_F of the electrons lies below the mobility edge, that is, $E_F < E_m$, the system is an insulator since no extended state is available in the vicinity of the Fermi level. At finite temperatures, the electrons may gain thermal energies (typically from phonons) to undergo a number of processes[17].

(i) Activation to the mobility edge, which yields $\sigma(T) \propto e^{-(E_m - E_F)/k_B T}$.

(ii) Activation to a neighboring localized state. This gives $\sigma(T) \propto e^{-\Delta_\xi/k_B T}$, where Δ_ξ is the mean level spacing in a localization volume ξ^D .

(iii) Variable range hopping, which is due to the activation to a state localized a distance $R_m \sim \xi(\Delta_\xi/T)^{1/(D+1)}$ away. R_m is obtained by maximizing the probability of hopping between two localized states of spatial separation R and energy mismatch $\Delta_\xi(\xi/R)^D$. This yields the Mott's Law $\sigma(T) \propto e^{-C(T_0/T)^{1/(D+1)}}$, where $C \sim O(1)$ is a dimensionless constant, and $T_0 \sim \Delta_\xi$.

The variable range hopping dominates the electron conduction as long as $R_m \gtrsim \xi$, that is the temperature is low enough so that $T \lesssim T_0$. We note that, for $E_F < E_m$, $\sigma(T) \rightarrow 0$ as $T \rightarrow 0$, and $d\sigma(T)/dT > 0$. Hence, the Anderson localization theory provides a simple explanation for the observation of the low temperature dependence of conductivity in strongly disordered or low-dimensional dirty conductors[4]–[12].

If we increase the density of electrons or decrease the strength of disorder, the Fermi energy E_F and the mobility edge E_m approach each other. At some critical value the Fermi energy may cross the mobility edge, that is, $E_F > E_m$, whereby the system becomes a metal. In this case the conductivity can be well captured by the weak scattering theory.

This type of metal-insulator transition is known as *Anderson transition*[18], which is distinguished from the other mechanisms of metal-insulator transitions, such as the band gaps[19], electron-electron interactions (Mott transition)[20]–[22], and the excitonic mechanism[23], where the disorder can be absent.

In more than half a century of development, the impact of localization has spread throughout all of physics, from condensed matter to wave propagation and imaging[24]. For ex-

ample, electromagnetic waves (light) propagating in a random media can undergo Anderson localization[25], due to the interference of multiply scattered waves.

Anderson’s original argument for the occurrence of complete localization in the presence of sufficiently strong disorder was based on analyzing the convergency of a locator expansion[13]: If t is the magnitude of the hopping matrix element for a particle from each site to its neighbors, and W is the width of the distribution of onsite random energies, starting from a local quantity on some initial site of energy E , a perturbation theory can be developed as a formal series in t/W . For $t/W \lesssim 1$, there are two competing contributions in the locator expansion: (i) On a D -dimensional hypercubic lattice, the number of sites at a distance of $R \gg 1$ (in unit of the lattice constant) is approximately R^D . Therefore, the typical energy mismatch of a distant site decreases with distance like R^{-D} . This leads to small denominators (resonances) in the perturbation series. (ii) Yet the magnitude of the effective hopping to these distant sites decreases exponentially with distance. This results in small numerators. Anderson studied such a locator expansion for the self energy of the particle and argued that, for sufficiently small t/W , the small denominators are compensated for by the small numerators with probability one. Therefore, distant resonances happen with a vanishingly small probability, the series is convergent, and the particle is localized. Otherwise, if t/W is large enough, the distant resonances happen with a finite probability, the series gets divergent, and the particle is delocalized. A mathematical proof of the existence of strongly localized states, at large W , or near the band edge, was given by Fröhlich *et al.*[26].

Much progress in understanding localization was due to the development of an *one-parameter scaling theory* by the “Gang of Four”[27], which was based on the earlier work by Thouless on the quantum conduction in thin wires[28]. The theory describes the flow of the dimensionless conductance $g(L)$ under rescaling:

$$d \ln g(L) / d \ln L = \beta(g), \tag{1.7}$$

where L is the linear size of the system, and $\beta(g)$ is independent of L but depends on the model one studies. This paved the way for the resummation of zero-frequency singularities

in quantum correction for the conductivity near two dimensions[5, 29] and a systematic field-theoretical renormalization group analysis[30]–[32].

The one-parameter scaling theory predicts that, when the time-reversal and spin-rotation symmetries are preserved (in the absence of the magnetic field and spin-orbit coupling), in dimensions $D \leq 2$ all one-particle states are localized, and therefore no mobility edge exists, even if disorder is very weak. In dimensions $D > 2$ mobility edges do exist if the strength of disorder is weak enough, which implies the possibility for Anderson transitions. This one-parameter scaling theory has been confirmed numerically by Mackinnon and Kramer[33, 34] using the technique of finite size scaling. In the presence of spin-rotation coupling, the one-parameter scaling theory predicts the existence of Anderson transitions in two dimensions [35]–[39].

In more general cases, more than one scaling parameters have to be included in the scaling theory. For example, in the theory of the integer quantum Hall effect, not only the longitudinal conductance g [see Eq. (1.7)] but also the Hall conductance, called g_H , appears as a scaling parameter[40]. The scaling theory is crucial for the understanding of the integer quantum Hall effect, mesoscopic fluctuations in small conductors, disorder-driven metal-insulator transitions and some aspects of quantum chaos [24, 41].

The scaling theory does not consider interactions between particles. The observation of a metal-insulator transition on a silicon surface, which is a strongly interacting and weakly disordered two dimensional system in the absence of spin-orbit coupling, was reported in Ref. [42] for the first time, and the transition has been further confirmed in different materials (See Ref. [43] and the references therein). Moreover, the disordered superconductor-insulator transition in two dimensions has recently attracted a lot of attention, due to a series of surprising and puzzling transport experiments, especially on the insulating side of the transition [44]–[48]. Despite many theoretical efforts have been put in these directions (see, for example, Refs. [49]–[62] and the references therein), there is still lack of clear descriptions and interpretations for the natures of these transitions. Full solutions of the above problems require a localization theory which includes the effect of interactions.

1.2 Few-particle systems—Channel competition

One of the possible starting point to incorporate the influence of correlations among particles is to study the localization properties of few interacting particles in a random potential. The main question is: If all one-particle states are localized, does the presence of interaction help to delocalize a few-particle system? This seemingly academic question can be addressed by current techniques with ultracold atoms[63], and is of fundamental importance for solving the more complicated case of many-body systems.

The simplest case of two interacting particles has attracted a lot of studies. The problem was first addressed by Dorokhov[64] in an one-dimensional continuous model with a harmonic attraction between two electrons. It was shown that the disorder-induced coupling between the internal quantization states, which provide the effective transverse channels, might lead to the enhancement of the two-particle localization length, which is a measure for coherent propagation of two bounded particles. The two-particle problem in a one-dimensional chain was later considered by Shepelyansky[65] highlighting the effect of repulsive and short range interaction. It was concluded that, in the weak disorder limit, the two-particle localization length ξ_2 could be much larger than the one-particle localization length ξ_1 .

The basic idea leading to the enhancement effect of the interaction on two-particle localization length is as follows. A short range interaction provides hopping strength in the noninteracting Fock basis. If two particles are launched within a distance of ξ_1 from each other, they may propagate coherently over larger distances. Otherwise, if two particles are launched at a distance much larger than ξ_1 from each other, there is no such enhancement effect due to exponential smallness of the overlap of their wave functions. The delocalization effect of interaction is only related with the former configurations (the fast channel), and the propagating entity is a “pair” of “radius” $\sim \xi_1$. The latter (the slow channel) are irrelevant to interaction effect. More importantly, the fast and slow channels are nearly decoupled (the coupling is proportional to the overlap of the tails of one-particle eigenstates, which is exponentially small). Hence, there is no competition between them.

However, the channel competition is significant in a system with more than two particles. As discussed in Sec. 2.3, there are many parallel but *coupled* channels with parametrically

different transport characteristics (e.g. all particles moving together, or moving in subgroups of fewer particles), which means in the absence of coupling some of them are more delocalized (the fast channel) and the others are more localized (the slow channel). Therefore, a full solution of the few-particle problem requires analyzing the coupling effect of the fast and slow channels.

The principal question in this thesis is raised: If we have coupled fast and slow propagating channels, which one will dominate the localization? If the fast channel dominates, the delocalization effect of interaction is significant, and the Anderson transition is mostly due to the delocalization of the fast channel if approaching the critical point. Otherwise, if the slow channel dominates, the delocalization effect of interaction is much weaker, and the system very possibly stays in strongly localized phase. This type of question arises not only in few-particle systems, but is an important element in the analysis of many-body systems[53], for example, quantum dots[54][66][68]-[70], and quantum wires[55], where few or many excitations have various channels of propagation.

As discussed in Sec. 1.3, the question can be represented by Anderson models for a single hybrid particle, for example, a polariton.

1.3 Anderson localization of polaritons

The problem of competition between a fast channel and a slow channel is raised naturally in studying the localization of linearly mixed hybrid particles, such as polaritons. Polaritons are the result of coherent mixing of the electromagnetic field in a medium (photons in a microcavity for example) and excitations of matter (exciton). In the absence of disorder, photons have a much larger group velocity than excitons, and thus one subsystem is fast and the other is slow. As a special example, quasi-one-dimensional resonators were recently fabricated by confining electromagnetic fields inside a semiconductor rod[72] or to a sequence of quantum wells[73]. In such resonators the dispersion of transverse-quantized photons is quadratic in the small momentum, with an effective mass as small as 10^{-4} of the effective mass of the Wannier-Mott exciton which is of the order of the mass of a free electron.

Disorder is unavoidable in such systems due to the imperfections of the resonator boundary and impurities. In many cases one can consider only one mode of transverse quantization for both the photon and the exciton. Thus a model of two dispersive modes (particles) with parametrically different transport properties arise. Due to the large dipole moment of the exciton these particles are mixed, resulting in avoided mode crossing. On top of that, disorder acts on both of them, whereby its effect on the two channels can be rather different [74, 75]. Therefore, the main question in the thesis can be reshaped in terms of a polariton: What happens to the localization properties when the photon (the fast channel) is coupled to the exciton (the slow channel)? Will the photon dominate the localization of the polariton, or the exciton? Answer to this question will help us to qualitatively understand the channel competition in few- or many-body systems.

1.4 Summary of the results

As discussed in Chap. 3, a polariton propagating in a random potential is described by the Anderson model on two coupled but nonequivalent lattices. We will see that the dimensionality is of particularly importance for understanding the effect of coupling between fast and slow channels. In the present thesis, I study two models which can be solved exactly.

(i) Two-leg Anderson model in one dimension. The *localization lengths* are obtained analytically in the *weak disorder limit*. This solution represents a major technical advance, because for the first time a model, which leads to an extended DMPK equation with non-separable angular and radial variables, is exactly solved.

(ii) Anderson model on two-layer Bethe lattices. This model reflects the properties of infinite-dimensional systems. On these lattices we can write down the recursion relation for the local Green's function, which can be solved efficiently. We study the effect of weak interlattice coupling on the *Anderson transition* at the band center ($E = 0$) of two lattices with equal hopping but different disorder. In contrast to the one-dimensional case, we consider *intermediate or strong disorder*, since in high dimensions ($D > 2$) weak disorder hardly has any effect on localization. More precisely, we want to answer the question: If in the absence of interchain coupling the less disordered lattice (delocalized) is very close to the Anderson transition, and

the more disordered lattice is localized (by definition), will the interlattice coupling push the system to a localized phase or a delocalized phase?

Without going into details the brief results are the following:

(i) In one dimension the physics depends qualitatively on whether the system is close to the resonance energy E_R , which is defined as the energy where the dispersions of the two corresponding decoupled disorder-free chains intersect. Near the resonance, the slow chain dominates. The localization length the ladder is at most by a factor of ≈ 3 larger than the one of slow particles. *Away from the resonance* the wavefunctions stay either mostly on the slow leg, being strongly localized. Or they have their main weight on the fast leg, and hybridize here and there with the slow leg (see Fig. 4.2 and Fig. 4.11). It is this second type of wavefunctions which helps excitations on the slow leg to delocalize due to the presence of the faster leg, even though this happens with small probability far from the resonance. More interesting phenomena are also found such as band edge singularities which strongly affect the large localization length.

(ii) On the Bethe lattices, the physics depends qualitatively on the disorder on the more disordered lattice. If this disorder is not too strong, interlattice coupling may push the system to the delocalized phase. If this disorder is strong enough, the coupling will push the system to the localized phase.

The thesis is organized as follows. In Chap. 2 the problem of few-interacting particle is reviewed. I present a hierarchical structure which is argued to be the fastest channel for the propagation of few particles. Thereby, the problem of coupling between fast and slow channels is formulated. In Chap. 3 the concept of cavity polaritons is introduced and the effect on disorder on photons and excitons is analyzed microscopically. The question of Anderson localization of polarizations is proposed. In Chap. 4 the Anderson localization problem on a two-leg ladder is solved by the Fokker-Planck equation approach. The solution is exact in weak disorder limit at a fixed interchain coupling. We show that the canonical Dorokhov-Mello-Pereyra-Kumar (DMPK) equation is insufficient for this problem. Indeed, the angular variables describing the eigenvectors of the transmission matrix enter into an extended DMPK equation in a non-trivial way, being entangled with the two transmission eigenvalues. This extended DMPK equation is solved analytically and the two Lyapunov exponents are obtained

as functions of the parameters of the disordered ladder. The application of the theoretical results to hybrid particles are discussed in the conclusion. In Chap. 5 the Anderson model on a two-layer Bethe lattice is solved. The recursive relation of the local Green's function is derived and solved numerically by the population dynamics. The phase diagram of the model is presented. In Chap. 6, we discuss the role of dimensionality and possible implications for interacting few-particle problems.

Chapter 2

Localization of few interacting particles

In the presence of interaction it is convenient to formulate a N -body problem in a certain Fock space. Usually the Fock basis contains all the eigenstates of the N -body system in the absence of interaction, which are the permanents (for bosons) or Slater determinants (for fermions) constructed out of the N exact one-particle states. The Hamiltonian in this Fock space takes the form:

$$H_0 + H_1 = \sum_{\alpha} \epsilon_{\alpha} c_{\alpha}^{\dagger} c_{\alpha} + \sum_{\alpha\beta\gamma\delta} Q_{\gamma\delta}^{\alpha\beta} c_{\gamma}^{\dagger} c_{\delta}^{\dagger} c_{\beta} c_{\alpha}. \quad (2.1)$$

Here c_{α}^{\dagger} (c_{α}) is the creation (annihilation) operator of a particle on the one-particle eigenstate $|\alpha\rangle$ with eigenenergy ϵ_{α} . These operators obey the commutation relations for bosons and the anti-commutation relations for fermions. $Q_{\gamma\delta}^{\alpha\beta}$ are the two-body interaction matrix elements given by

$$Q_{\gamma\delta}^{\alpha\beta} = \iint dx dx' Q(x - x') \psi_{\gamma}^{*}(x') \psi_{\delta}^{*}(x) \psi_{\beta}(x) \psi_{\alpha}(x'), \quad (2.2)$$

where $\psi_{\alpha}(x)$ is the amplitude of a particle in the state $|\alpha\rangle$ at the coordinate x , and $Q(x - x')$ is the strength of interaction between two particles at the coordinates x and x' . For the sake of interest we assume that the interaction is local in the real space:

$$Q(x - x') = U\mathcal{V}\delta(x - x'), \quad (2.3)$$

where U is the potential energy per pair of particles, and \mathcal{V} is the volume of the system. The one-particle eigenenergies ϵ_α and the interaction matrix elements $Q_{\gamma\delta}^{\alpha\beta}$ are in general random variables. Their distributions are determined by the statistics of energy levels and eigenfunctions of the one-particle Hamiltonian[76, 77]. Especially, the statistics of the matrix elements $Q_{\gamma\delta}^{\alpha\beta}$ are highly non-trivial. For example, if the underlying one-particle dynamics is diffusive, as in a disordered metal, ballistically chaotic, as in a billiard, or integrable, as in a periodic potential, one obtains different estimates for the magnitude[54, 66].

The presence of the interaction yields two effects: (i) The diagonal matrix elements of $Q_{\gamma\delta}^{\alpha\beta}$ shift the N-body levels, which can yield a rearrangement of the spectrum. This situation has been intensively discussed by Kamimura[78] in the case of Anderson insulators with very small localization lengths. (ii) The off-diagonal elements of $Q_{\gamma\delta}^{\alpha\beta}$ give rise to hopping among certain Fock states, and thus may induce delocalization in the Fock space. In our study below we mainly focus on the limit where the second effect dominates the first. Here we should note that in general the delocalization in the Fock space is not equivalent to the delocalization in the real space. The delocalization in the Fock space characterizes both metals and insulators. The delocalization in real space due to interaction may occur only in insulators, where without interaction all states are localized. This difference has been stressed by an analysis of the sensitivity of the energy levels with respect to a change of boundary conditions in a one dimensional system with two interacting particles[79].

In this section we discuss the localization properties for few interacting particles. Shepelyansky used an analogy between the eigenvalue problem of two particles and that of banded random matrices, and made an assumption on the scaling properties of the interaction matrix elements $Q_{\gamma\delta}^{\alpha\beta}$. Finally, it was concluded that, in the weak disorder limit $\xi_1 \rightarrow \infty$, the two-particle localization length ξ_2 scales with ξ_1 as $\xi_2/\xi_1 \propto \xi_1 U^2$, where U is the strength of the interaction. This result was further supported by Imry in Ref. [80], where the Thouless block scaling argument[28] replaced the banded random matrix analogy. The main idea is to consider a pair of electrons as the entity in the scaling picture. This scaling theory explained the initial approximate results[65] and was further confirmed by an analysis based on the nonlinear supersymmetric σ model[81].

Since the study of two interacting particles is only the first step towards the treatment of realistic many-body systems, it provides motivation to increase the number of particles. We will see that a modest strategy of going from two to three and large numbers of particles can be accomplished by generalizing the scaling theory to more than two particles.

Differently from the study of the low-energy excitations, or in other words, quasi-particles, in many-body systems[51]–[54], we are looking for certain Fock states of a number of bare particles in the bulk of the total energy spectrum, which presumably have the maximum localization length. In general these states lie around the center of the total energy band since the level density is the highest there.

However, we have to point out that our analysis on the few-particle problem is by no means rigorous, since the scaling picture for two or more particles is only qualitatively correct. Improved analyses[82, 83] and direct numerical simulations[84, 85, 94] showed that $\xi_2/\xi_1 \propto \xi_1|U|/(1+|U|)$ in weak disorder limit. In particular, this implies that the enhancement effect occurs for weaker interaction than the previous prediction. Moreover, via different estimations of the interaction matrix elements $Q_{\gamma\delta}^{\alpha\beta}$, several controversial results were obtained. For example, Römer, Schreiber, and Vojta[86] demonstrated that the enhancement effect should be absent completely. Krimer, Khomeriki, and Flach[87] predicted a much weaker enhancement $\xi_2/\xi_1 \propto (\ln \xi_1)^2 U^2$. Despite a number of studies, the two-particle problem remains a complete open question. Nevertheless, we argue that the hierarchical structure obtained by the scaling analysis provides the fastest channel for the delocalization of few particles.

This chapter is organized as follows. In Sec. 2.1 we recall the Thouless block picture[28], which is the basic tool for our analysis on large numbers of particles. In Sec. 2.2 the problem of two interacting particles is discussed. In Sec. 2.3 we generalized the scaling analysis to large numbers of particles and construct the states which very possibly have the largest localization length in the total energy spectrum. At the end we give rise to the problem of coupling effects between many parallel channels with parametrically different localization characteristics, which is one of the motivations to study the exactly solvable models in Chaps. 4 and 5.

2.1 Thouless block picture

Originally, the block picture is developed for non-interacting particles. In order to measure whether a particle at a certain energy is extended or localized the length scale L , we divide the macroscopic system to blocks of linear size L . On one block the averaged one-particle level spacing at the relevant energy is Δ_L . Any two levels on adjacent blocks are coupled by a matrix element V_L . Intuitively, if the levels on one block are dense or the inter-block coupling is strong, that is, $V_L \gg \Delta_L$, a level on one block will couple a large number of levels on the neighbours. Thereby, the particle can propagate easily to the adjacent blocks. It is crucial to introduce the Thouless energy E_c , and the related Thouless number:

$$g(L) = \frac{E_c}{\Delta_L}, \quad (2.4)$$

to characterize this process of a particle hopping among the blocks. The Thouless number is defined by

$$E_c = \frac{1}{2\pi} \frac{\hbar}{\tau_L}, \quad (2.5)$$

where τ_L is the diffusion time of the particle crossing one block. Correspondingly, \hbar/τ_L is the broadening of the energy level due to the inter-block coupling V_L . In this way the Thouless number $g(L)$ is identified with the dimensionless conductance of the block. Furthermore, the diffusion time can be estimated by the Fermi golden rule if the levels in a block are dense enough:

$$\frac{\hbar}{\tau_L} = 2\pi \frac{V_L^2}{\Delta_L}. \quad (2.6)$$

By Eqs. (2.4)-(2.6), we obtain the Thouless number:

$$g(L) = \left(\frac{V_L}{\Delta_L} \right)^2. \quad (2.7)$$

Obviously, each block is metallic if $V_L \gg \Delta_L$ since the conductance $g(L) \gg 1$. More importantly, the one-particle localization length ξ can be estimated by $g(\xi) \simeq 1$.

Although the above scaling analysis was performed for a single particle, we should note that it applies in more general cases. The Thouless number g is a good measure of the entanglement

between two generic quantum systems, namely, A and B . If a state of A with energy E effectively couples the states of B within the energy intervals $[E - E_c/2, E + E_c/2]$, whose width is the Thouless energy E_c , then the Thouless number gives the number of states of B entangled with the state of A . Moreover, if the states carry some charges for transport the Thouless number is identified with the dimensionless conductance.

2.2 Localization of two interacting particles

2.2.1 Two interacting particles in one dimension

Two interacting particles in a one-dimensional chain described by the Hamiltonian (2.1) is the first step towards large numbers of particles. According to the scaling theory[27] all the one-particle states are localized in presence of weak disorder. As shown in Eq. (1.6) a one-particle state with localization length ξ_1 takes the form of $\psi_\alpha(x) \sim c_\alpha/\sqrt{\xi_1} \exp(-|x - x_\alpha|/\xi_1)$ if $|x - x_\alpha| \gg \xi_1$, and $\psi_\alpha(x) \sim c_\alpha \times \text{constant}$ if $|x - x_\alpha| \lesssim \xi_1$, where x_α is the localization center and c_α is a random phase factor. Switching on the interaction H_1 we open scattering channels among two-particle Fock states. In the analysis below we assume $\hbar = 1$ and the length unit is the lattice constant.

In the spirit of Thouless block picture we divide the chain into blocks of size ξ_1 . Statistically, on each block there are ξ_1 number of one-particle states. Thereby, the two-particle Fock space has two propagating channels: (i) The two particles are in different blocks. It is easy to realize that these states are the approximate eigenstates of the total Hamiltonian, since the overlap of two one-particle wave functions is exponentially small, and eventually the interaction are exponentially weak. This part of the Fock space has the same localization properties as these of a single particle. (ii) The two particles are in the same block. The pair-wise interaction may activate the two particles hopping simultaneously from one block to another in neighbor. The hopping strength is given by the typical value of the matrix elements $Q_{\gamma\delta}^{\alpha\beta}$ in Eq. (2.2). This part of the Fock space is relevant to the delocalization effect of interaction. We note that the two subspaces are almost *decoupled*, since the interaction matrix elements between them are exponentially small. Therefore, we can analyze only the interaction-activated subspace.

In the weak disorder limit $\xi_1 \rightarrow \infty$ and for a weak interaction $U \ll B$, on each block the mean level spacing of the Fock states can be estimated as

$$\tilde{\Delta}_2 \sim \frac{B}{\xi_1^2}, \quad (2.8)$$

where B is the one-particle band width. Here we made two crucial simplifications: (i) The magnitude of disorder and the strength of interaction are much smaller than the one-particle band width. (ii) The two-particle levels on each block are uniformly distributed in the two-particle energy band. We have to note that the second simplification is rough. As found in Refs. [82, 83], in a tight binding chain the two-particle density of states are non-uniform and essentially exhibits Van Hove singularities, which is similar as that of a single particle in two dimensions. This modification will improve the original estimation[65, 80], as mentioned later. In order to estimate the typical value of $Q_{\gamma\delta}^{\alpha\beta}$ in Eq. (2.2) we have to know the statistics of the one-particle wave functions. For simplicity we use the very rough approximation of *uncorrelated* one-particle wave functions with amplitude of the order $1/\sqrt{\xi_1}$ on each site on a block and with a random sign. This approximation gives

$$\langle \psi_\alpha(x) \psi_\beta(x') \rangle = \delta_{\alpha\beta} \delta(x - x') / \xi_1. \quad (2.9)$$

As a consequence,

$$\langle (Q_{\gamma\delta}^{\alpha\beta})^2 \rangle \sim U^2 / \xi_1^3. \quad (2.10)$$

This estimation corresponds to a one-particle Hamiltonian belonging to the Gaussian orthogonal ensemble (GOE) in the standard random matrix theory[76, 77].

As pointed out in Ref. [66, 54], this evaluation of the matrix elements only reproduces the zero-mode contribution of a diffusion process. More importantly, a one-dimensional particle actually moves almost ballistically in its localization volume[82, 83], which is far from diffusive. Considering this fact will also help to improve the original results[65, 80]. For simplicity, we use the estimation (2.10).

Based on the two-particle level spacing in Eq. (2.8) and the matrix element in Eq. (2.10) we obtain the two-particle Thouless number on one block:

$$g_2(\xi_1) \sim \frac{\langle (Q_{\gamma\delta}^{\alpha\beta})^2 \rangle}{\tilde{\Delta}_2^2} \sim \left(\frac{U}{B}\right)^2 \xi_1. \quad (2.11)$$

If $g_2(\xi_1) \gg 1$, which means the interaction is not too weak or the one-particle localization length is large enough, the two-particle states can be much more extended rather than a one-particle localization volume. In order to determine the two-particle localization length we assume that the Ohm's law is valid if $g \gg 1$. In one dimension it gives $g(L_1)/g(L_2) \simeq L_1/L_2$ if $g(L_1)$ and $g(L_2) \gg 1$. Therefore, the two particle localization length ξ_2 can be estimated by $g(\xi_2) \sim 1$:

$$\xi_2 \sim g_2(\xi_1)\xi_1. \quad (2.12)$$

In the new length scale ξ_2 the two-particle mean level spacing can be estimated as

$$\Delta_2 \sim \frac{\tilde{\Delta}_2}{g_2(\xi_1)}, \quad (2.13)$$

which will be used when we analyze the problem of four particles in Sec. 2.3.

As we have pointed out, the estimations of the enhancement factor $g_2(\xi_1)$ and the two-particle localization length ξ_2 are only qualitatively correct. More accurate calculations of the two-particle level spacing and the interaction matrix elements based on the Hubbard model with onsite disorder[83] suggest:

$$\frac{\xi_2}{\xi_1} \simeq c(U)\xi_1, \quad c(U) = A \frac{|U|}{1 + |U|}, \quad (2.14)$$

if $\xi_2 \gg \xi_1$. Here the interaction strength U is measured in unit of the one-particle hopping strength, and $A \sim O(1)$ is a numerical constant.

The form of the enhancement factor in Eq. (2.14) was supported by the numerical results in Refs. [84, 85]. Here we have three important observations: (i) $c(U)$ dose not depend on the strength of disorder if disorder is weak enough. This confirms $\xi_2 \propto \xi_1^2$ when ξ_1 is large. (ii) At $U \gg 1$, $c(U)$ gets saturated $c(U) \sim A$. This saturation is easy to understand: When U is larger than the one-particle band width, the Fock space splits into two Hubbard bands,

and the one-particle eigenstates are not preferential basis any more. This splitting makes the interaction less efficient for the delocalization effect. (iii) When $U \gg 1$, $c(U) \propto U$, instead of U^2 in Eq. (2.11) obtained by the Fermi golden rule. This linear- U dependence of the enhancement factor is more subtle. It is due to the van Hove singularity at $E = 0$ in the two-particle density of states, which behaves as $\rho(E) \sim -\ln|E|$, if the amplitude of disorder is much smaller than the one-particle band width[82, 83]. Recently, it was suggested that the enhancement of the two-particle localization length could be much weaker than all analysis above, that is, $\xi_2/\xi_1 \sim U^2(\ln \xi_1)^2$ [87]. Despite a number of studies in the last decade, the problem of two interacting particles still remains an open issue.

Our numerical simulation[88] on the Hubbard model supports the result in Eq. (2.14) and the numerical constant $A \sim 0.22$ is obtained by fitting the data. The method is based on a quantum mechanical time evolution calculation for the wavepackets, which is performed by expanding the time evolution operator by Chebyshev polynomials[89]. The method is so far the most efficient method to simulate the long time evolution of a quantum system.

2.2.2 Two interacting particles in higher dimensions

Naively followed from the block scaling argument, in two dimensions the delocalization enhancement might be exponentially large in the weak disorder limit. Differently from the situation in the one-dimensional case, the number of sites in an one-particle localization volume is proportional to ξ_1^2 . Repeating the scaling analysis in one dimension, we estimate the mean level spacing of two particles on a block and the typical value of interaction matrix elements as

$$\tilde{\Delta}_2 \sim B/(\xi_1^2)^2, \quad \langle (Q_{\gamma\delta}^{\alpha\beta})^2 \rangle \sim U^2/(\xi_1^2)^3, \quad (2.15)$$

which lead to the two-particle Thouless number on a block

$$g_2(\xi_1) \sim \left(\frac{U}{B}\right)^2 \xi_1^2. \quad (2.16)$$

According to the scaling theory in two dimensions[6], in weak disorder limit, we have $e^{cg(L_1)}/e^{cg(L_2)} \simeq L_2/L_1$, where $c \sim O(1)$ is a numerical constant. Thereby, the enhancement

of two-particle localization length is estimated as

$$\xi_2/\xi_1 \sim e^{cg_2(\xi_1)} \sim e^{c(\frac{U}{B})^2 \xi_1^2}. \quad (2.17)$$

Although arbitrarily large for weak disorder, the enhancement is still finite.

However, the numerical analysis of Ref. [90] suggested even that two bosons may delocalize in two dimension, where the critical disorder is $W_c \approx 9.3$ and the critical exponent is $\nu \approx 2.4$ for $U = 1$, even though the mechanism behind this supposed delocalization phenomenon remained unclear. Moreover, delocalization of two spinless fermions, with either short range and long range interactions, was also observed numerically in Ref. [91]. These numerical observations of the delocalization transition of two particles in two dimensions ring the alarm to the naive scaling analysis leading to Eq. (2.17). Yet much more work is needed to confirm whether these transitions do exist. Here note that the author of the present thesis studied two hard core bosons in two dimensions[92]. By constructing a Jordan-Wigner transformation it is argued that the two hard core bosons could very possibly undergo a delocalization transition.

In three dimensions very few works have been done, even though Imry has argued that if there is a mobility edge in the one-particle spectrum the mobility edge for two particles can be much lower by switching on the interaction. The author of the present paper propose that this prediction can be verified numerically even in two dimensions if the spin-orbit coupling effect is included in the one-particle Hamiltonian[35]-[39], which may give rise to mobility edges in the one-particle spectrum. This two-dimensional problem requires less numerical work than the three-dimensional problems.

At the end of this section, we emphasize that the “fast” channel, where two particles are in the same one-particle localization volume, is almost decoupled to the “slow” channel, where the two particles are in different localization volumes. However, in Sec. 2.3 we will see that in the system of large number of particles the fast and slow channels are coupled.

2.3 Localization of N interacting particles in one dimension

How does the interaction-induced delocalization depend on the number of particles is still an open question. There are only a few works in this direction because of both the complication for analytical studies and the limited ability of numerical simulations. Shepelyansky and Shushkov studied three spinless fermions with nearest neighbor interactions by generalizing the scaling analysis on two particles[93]. They suggested that the three-particle localization length might be further strongly enhanced compared to the enhancement of the two-particle localization length in Eq. (2.11). Generalizing the result for three particles they conjectured that the enhancement of the N -particle localization length may increase *exponentially* with the number of particles, that is,

$$\xi_N \sim \left(\frac{U^2}{B^2} \xi_1 \right)^{N-1}, \quad (2.18)$$

if all particles remain in the same one-particle localization volume during their propagation.

Later on Halfpap[94] performed intensive numerical simulations for three and four spinless fermions. It was suggested that the delocalization effect might be even stronger than the prediction in Ref. [93] [see Eq. (2.18)]. Moreover, an hierarchical structure was proposed, which leads to an upper bound for the N -particle localization length:

$$\xi_N \lesssim \xi_1^{2^{N-1}}. \quad (2.19)$$

It was concluded that the localization length might increase *super-exponentially* with the particle number and become arbitrarily large for weak disorder, even though it should not diverge for finite ξ_1 and N .

In the following part we present a 2^n -particle hierarchical structure based on a generalized scaling analysis for two particles, which leads to a much weaker enhancement effect than that proposed in Ref [94], even though the localization length increases *super-exponentially* with the particle number.

What we learned from the two-particle delocalization is that the Fock space can be reorganized to two channels by the one-particle localization length ξ_1 . Briefly, if the distance between the localization centers of the two particles is larger than ξ_1 , the interaction is effectively switched off, and the single-particle localization properties dominate. If the distance is smaller than ξ_1 , however, the interaction is switched on, and the correlation effect enables the two particles to propagate much further than either of the particles. A new localization length, that is, the two-particle localization length ξ_2 , emerges.

Can we generalize this reduction procedure to few particles? As the next step, we study four particles¹. We divide the system to blocks of size ξ_1 and distribute the four particles over the blocks. There are five combination for distributing the four particles, as shown in Fig. 2.1(a)-(e).

(a) Four particles are spread in four different blocks. They do not interact and show one-particle localization properties. (b) Only two of them are in one block and the other two are in other two blocks. As discussed before, the two particles in one block will form a pair, and extend over a domain of size ξ_2 . If one of the other two particles locates in this domain, as shown in (f), it interacts with the pair. By the same consideration for two particles, they may form a cluster and propagate coherently over a larger distance, namely, $\xi_{2,1}$. Continuously, if the last particle interacts with this cluster, a more complicated structure may form, as shown in (i), with localization length $\xi_{2,1,1}$. (c) Two pairs are formed, which means two particles are in one block and the others are in another block. If the two pairs are within the distance ξ_2 , they may form a 2^2 -cluster (see the definition below) and propagating coherently over a distance $\xi_{2,2}$. The configurations in (d), (e), and (h), and the corresponding localization lengths can be characterized by similar considerations.

Now the question is: Which configuration in Fig. 2.1 has the largest localization length? First, we make clear two points: (i) $\xi_1 < \xi_2 < \xi_3 < \xi_4$. This relation is supported by Eq. (2.18),

¹The reason for not considering three particles in the next step has two folds: On the one hand, physically, we are not eventually interested in the localization length for a small number of particles. We are going to find what is the most efficient delocalization mechanism towards large numbers of particles. On the other hand, technically, we will see that $N = 2^n$ particles can be analyzed recursively in a hierarchical way. At the end, the general case for large N can be retrieved by the interpolation $n = \log_2 N$.

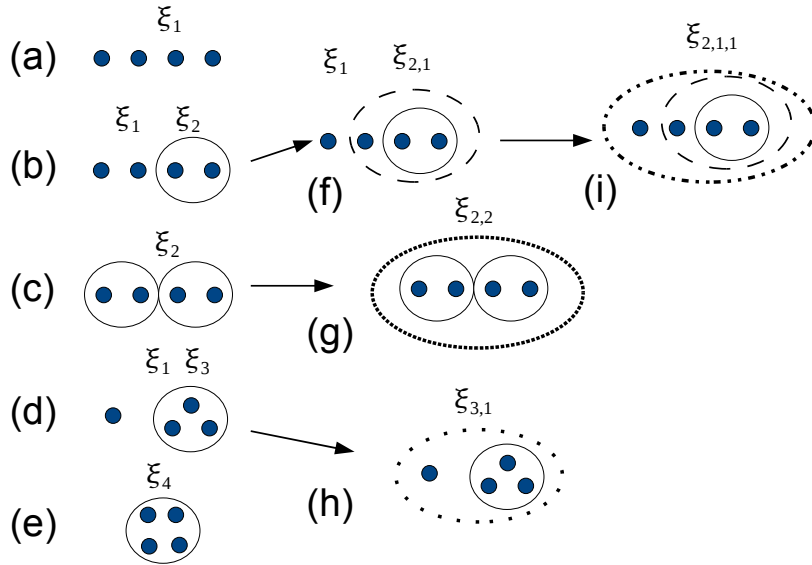


Figure 2.1: Schematic diagrams for the possible configurations of four particles in one dimension. The one-dimensional chain is divided into blocks of size ξ_1 . (a) Four particles are in four different blocks. (b) Only two of the particles are in one block. The other two are spread in other two blocks. (c) Two pairs are formed, where two particles are in one block and the others are in another block. (d) Three of the particles are in one block, and the other one is in another block. (e) All four particles are in one block. (f)-(i) are sequent configurations of (a)-(e), as discussed in the thesis. We are mainly interested in (g), whereby two pairs may coherently propagate further to a localization length $\xi_{2,2}$. We suggest that $\xi_{2,2}$ should be the largest localization length that four particles could have.

which means each particle effectively creates $(U/B)^2/\xi_1$ number of propagating channels for the rest of the particles. Once $(U/B)^2/\xi_1 > 1$, the localization length should be enhanced by increasing the number of particles. (ii) $\xi_{2,1} < \xi_3$. This relation was suggested in Ref. [94]. We consider the three particles which form clusters in Fig. 2.1 (d) and (f). In (d) the delocalization of the pair is induced by the third particle which is as delocalized as the pair, while in (f) the third particle is more localized. The delocalization effect should be stronger in (d). By the same consideration we argue that $\xi_{3,1} < \xi_4$ and $\xi_{2,1,1} < \xi_{2,2}$. Hence, we only need to compare ξ_4 with $\xi_{2,2}$. The value of ξ_4 can be obtained by Eq. (2.18). In the following part, we estimate the value of $\xi_{2,2}$.

We consider the configuration in Fig. 2.1(g). In a volume of size ξ_2 , the pair level spacing Δ_2 is given by Eq. (2.13). Thereby, the four-particle (two-pair) level spacing can be estimated as

$$\tilde{\Delta}_4 \sim \frac{\Delta_2^2}{B} \sim \frac{B}{(\xi_1 \xi_2)^2}. \quad (2.20)$$

Here we assume that the pair band width is of the order of the one-particle band with B , and the four-particle levels on each block are uniform.

Calculating the typical value of the interaction matrix elements among the four-particle levels is subtle. As shown in Fig. 2.2(a), we have to calculate

$$U_4 = \langle P_3, P_4 | H_{int} | P_1, P_2 \rangle = \sum_{\alpha, \beta, \gamma, \delta} Q_{\gamma\delta}^{\alpha\beta} \langle 0 | b_{P_4} b_{P_3} a_{\alpha}^{\dagger} a_{\beta}^{\dagger} a_{\gamma} a_{\delta} b_{P_1}^{\dagger} b_{P_2}^{\dagger} | 0 \rangle, \quad (2.21)$$

where $|0\rangle$ is the vacuum state, $P_{1,2,3,4}$ denote pair states in a volume of size ξ_2 , and

$$b_{P_{1,2,3,4}}^{\dagger} = \sum_{\rho_1, \rho_2} \langle \rho_1, \rho_2 | P_{1,2,3,4} \rangle a_{\rho_1}^{\dagger} a_{\rho_2}^{\dagger} \quad (2.22)$$

are the corresponding creation operators. Substituting Eq. (2.22) in Eq. (2.21) we obtain

$$U_4 = \sum_{\rho_1, \rho_2} \sum_{\rho_3, \rho_4} \sum_{\rho'_1, \rho'_2} \sum_{\rho'_3, \rho'_4} \langle P_3 | \rho_1, \rho_2 \rangle \langle P_4 | \rho_3, \rho_4 \rangle \langle \rho'_1, \rho'_2 | P_1 \rangle \langle \rho'_3, \rho'_4 | P_2 \rangle \quad (2.23)$$

× (all the possible scattering amplitudes in Fig. 2.2(a)).

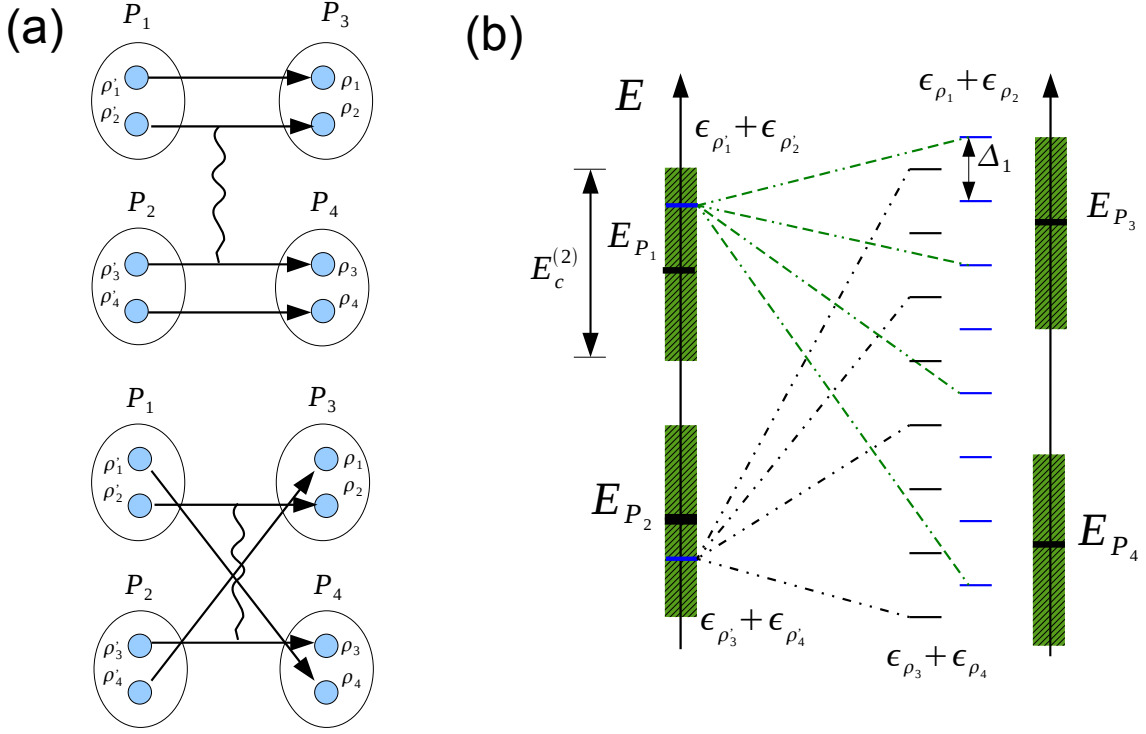


Figure 2.2: The schematic diagrams used for calculating the four particle interaction matrix elements in Eq. (2.23). (a) The leading order interaction between two pairs is only the interaction between two particles belonging to different pairs. (b) In the one-particle localization volume the number of incoming two-pair states is $g_2^2(\xi_1) = (E_c^{(2)}/\tilde{\Delta}_2)^2$. Each incoming pair state can couple to $(E_c^{(2)}/\Delta_1)^2$ number of outgoing states.

In order to evaluate $\langle U_4^2 \rangle$ by Eq. (2.23), following the consideration for the statistics of one-particle wave functions [see Eq. 2.9], we naively assume that the wave functions of pairs are *uncorrelated*, that is,

$$\langle\langle P_1 | \rho_1, \rho_2 \rangle \langle \rho_3, \rho_4 | P_2 \rangle \rangle = \text{Constant} \times \delta_{P_1 P_2} \delta_{\rho_1 \rho_3} \delta_{\rho_2 \rho_4}, \quad (2.24)$$

where the constant is equal to the typical magnitude of a pair state $|P\rangle$ projected on a two-particle Fock state $|\rho_1, \rho_2\rangle$. After this simplification we only need to estimate two quantities

(i) The typical magnitude of a pair state projected on a two-particle Fock state. A $|P\rangle$ state typically extends over $\sim \xi_2/\xi_1 \sim g_2(\xi_1)$ number of blocks of size ξ_1 . In each block, the $|P\rangle$ state can involve the Fock states within an energy interval whose width is the Thouless energy $E_c^{(2)}$, and therefore, only $g_2(\xi_1)$ number of two-particle Fock states are coupled to $|P\rangle$. Consequently, in a pair state $|P\rangle$ the magnitude of a two-particle Fock state is typically

$$|\langle \rho_1, \rho_2 | P \rangle|^2 \sim \frac{1}{g_2(\xi_1) \times g_2(\xi_1)}. \quad (2.25)$$

(ii) The typical number of terms contributing to the summation in Eq. (2.23). It is given by the number of distinguishable scattering events among two-particle Fock states which are components of the incoming pair states $|P_1, P_2\rangle$ and the outgoing pair states $|P_3, P_4\rangle$. Moreover, because the interaction is short range, two pairs interact with each other only if they are in the same block. In a volume of size ξ_2 there are $g_2(\xi_1)$ number of such blocks. In each block, as shown in Fig. 2.2(b), the number of the available incoming states, ($|\rho'_1, \rho'_2\rangle$ and $|\rho'_3, \rho'_4\rangle$), is $g_2^2(\xi_1)$, which are components of $|P_1, P_2\rangle$. For a given incoming state, the outgoing states can only differ in energy by Δ_1 , since the interaction keeps two of the four particles unchanged, as shown in Fig. 2.2(a). Hence, there are $(E_c^{(2)}/\Delta_1)^2$ number of outgoing states which are components of the $|P_3, P_4\rangle$ state. Consequently, the total number of scattering events can be estimated as

$$M_2 \sim g_2 \times g_2^2 \times \left(\frac{E_c^{(2)}}{\Delta_1} \right)^2. \quad (2.26)$$

By Eqs. (2.11) and (2.23)-(2.26) we obtain

$$\langle U_4^2 \rangle \sim \langle U_2^2 \rangle \times (g_2^{-2})^4 \times M_2 \sim \langle U_2^2 \rangle g_2^{-3} \left(\frac{\tilde{\Delta}_2}{\Delta_1} \right)^2. \quad (2.27)$$

By Eqs. (2.20) and (2.27) we obtain the four-particle Thouless energy in a volume of size ξ_2 :

$$E_c^{(4)} \sim \langle U_4^2 \rangle / \tilde{\Delta}_4, \quad (2.28)$$

and the corresponding Thouless number:

$$g_4(\xi_2) \sim \frac{\langle U_4^2 \rangle}{\tilde{\Delta}_4^2} \sim \xi_2^2, \quad (2.29)$$

Finally, we obtain the localization length for the four-particle configuration in Fig. 2.1(g):

$$\xi_{2,2} \sim g_4 \xi_2 \sim \xi_2^3 \sim \left(\frac{U}{B}\right)^6 \xi_1^6. \quad (2.30)$$

The four-particle energy level spacing in the volume of size $\xi_{2,2}$ is

$$\Delta_4 \sim \frac{\tilde{\Delta}_4}{g_4}. \quad (2.31)$$

By Eq. (2.18) the localization length for the configuration in Fig. 2.1(e) is

$$\xi_4 \sim (U/B)^6 \xi_1^4. \quad (2.32)$$

We can realize

$$\xi_{2,2}/\xi_4 \sim \xi_1^2 \gg 1. \quad (2.33)$$

According to our analysis, the configuration shown in Fig. 2.1(g) should be the most efficient channel for the delocalization of four particles.

In order to generalize the above analysis to large number of particles, we adopt the 2^n -cluster terminology, where $N = 2^n$ gives the number of particles. Thereby, a 2^0 cluster is a single particle, a 2^1 cluster is a pair, a 2^2 cluster is a four-particle state in Fig. 2.1(g), and so on. Repeating the above construction for the four-particle states, namely, two 2^2 clusters form a 2^3 cluster and so on, we could analyze the 2^n cluster iteratively.

In this 2^n -cluster terminology, it is convenient to rewrite the notations of the relevant quantities in terms of the hierarchical index n . For a 2^n cluster, the localization length is denoted by ξ_n . In a volume of size ξ_{n-1} , for a 2^n cluster, the mean level spacing is $\tilde{\Delta}_n$, the Thouless energy and the corresponding Thouless number are $E_c^{(n)}$ and g_n . The second moment of the interaction strength of two 2^{n-1} clusters is denoted by $\langle U_n^2 \rangle$. The number of scattering events, which are effectively induced by the the scattering among 2^{n-2} -cluster components, is M_{n-1} .

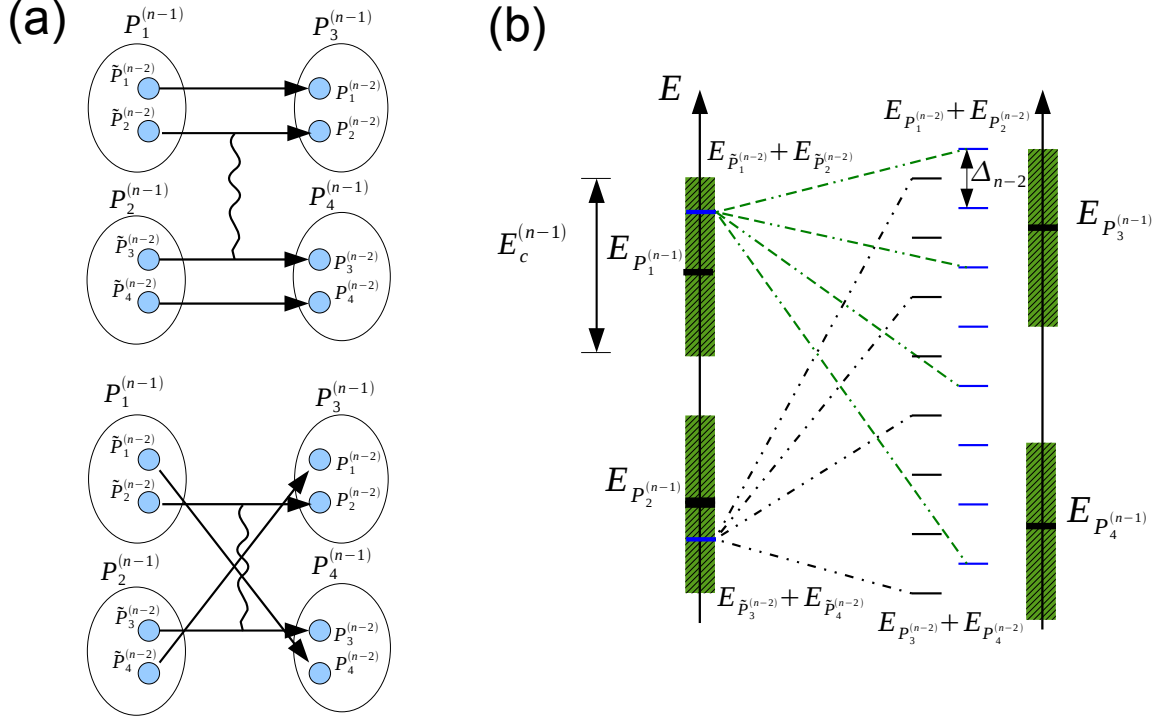


Figure 2.3: The schematic diagrams used for calculating the 2^n cluster interaction matrix elements in Eq. (2.35). (a) The leading order interaction between two 2^{n-1} clusters is only the interaction between two 2^{n-2} clusters belonging to different 2^{n-1} clusters. (b) In the 2^{n-2} cluster localization volume the number of incoming 2^n -cluster states is $g_{n-1}^2(\xi_{n-2}) = (E_c^{(n-1)}/\tilde{\Delta}_{n-1})^2$. Each incoming 2^{n-1} -cluster state can couple to $(E_c^{(n-1)}/\Delta_{n-2})^2$ number of outgoing 2^{n-1} -cluster states.

In a volume of size ξ_n , a 2^n cluster state is denoted by $|P^{(n)}\rangle$, and the mean level spacing is Δ_n . Our goal is to obtain g_n , which characterizes the delocalization of a 2^n cluster.

A 2^n cluster is a pair of 2^{n-1} clusters, each of which is localized in a volume of size ξ_{n-1} . Repeating the same procedure as applied in the case of 2^1 and 2^2 clusters, we divide the system into blocks of size ξ_{n-1} . In each block, the mean level spacing of a 2^{n-1} cluster is

Δ_{n-1} . Therefore, the mean level spacing of non-interacting² two 2^{n-1} -cluster states is

$$\tilde{\Delta}_n \sim \frac{\Delta_{n-1}^2}{B}, \quad (2.34)$$

where we again assume that on a block the 2^n -cluster levels are uniformly distributed. The effective interaction matrix elements among the 2^{n-1} -cluster states can be estimated analogously to the four-particle case. As shown in Fig 2.3, we should calculate

$$\begin{aligned} U_n &= \langle P_3^{(n-1)}, P_4^{(n-1)} | H_{int} | P_1^{(n-1)}, P_2^{(n-1)} \rangle \\ &= \sum_{P_1^{(n-2)}, P_2^{(n-2)}} \sum_{P_3^{(n-2)}, P_4^{(n-2)}} \sum_{\tilde{P}_1^{(n-2)}, \tilde{P}_2^{(n-2)}} \sum_{\tilde{P}_3^{(n-2)}, \tilde{P}_4^{(n-2)}} \\ &\quad \langle P_3^{(n-1)} | P_1^{(n-2)}, P_2^{(n-2)} \rangle \langle P_4^{(n-1)} | P_3^{(n-2)}, P_4^{(n-2)} \rangle \langle \tilde{P}_1^{(n-2)}, \tilde{P}_2^{(n-2)} | P_1^{(n-1)} \rangle \langle \tilde{P}_3^{(n-2)}, \tilde{P}_4^{(n-2)} | P_2^{(n-1)} \rangle \\ &\quad \times (\text{all the possible scattering amplitudes in Fig. 2.3(a)}), \quad n \geq 2. \end{aligned} \quad (2.35)$$

In order to evaluate $\langle U_n^2 \rangle$ in Eq. (2.35), as what we did before, we simply assume that wave functions of a 2^{n-1} cluster are *uncorrelated*, that is,

$$\begin{aligned} &\left\langle \langle P_1^{(n-1)} | P_1^{(n-2)}, P_2^{(n-2)} \rangle \langle P_3^{(n-2)}, P_4^{(n-2)} | P_2^{(n-1)} \rangle \right\rangle \\ &= \text{Constant} \times \delta_{P_1^{(n-1)} P_2^{(n-1)}} \delta_{P_1^{(n-2)} P_3^{(n-2)}} \delta_{P_2^{(n-2)} P_4^{(n-2)}}, \end{aligned} \quad (2.36)$$

where the constant is the typical magnitude of a 2^{n-1} -cluster projected on a 2^{n-2} -cluster state. After this simplification, we can apply a very similar analysis as that for four particles, where a particle is replaced by a 2^{n-2} cluster, and a pair by a 2^{n-1} cluster. We obtain:

(i) The typical magnitude of a 2^{n-1} -cluster state projected on a 2^{n-2} -cluster state is

$$|\langle P^{(n-1)} | P_1^{(n-2)}, P_2^{(n-2)} \rangle|^2 \sim \frac{1}{g_{n-1} \times g_{n-1}}. \quad (2.37)$$

²Here the word ‘‘non-interacting’’ means two clusters do not interact with each other. Nevertheless, either of the clusters is an entity constituted by interacting particles.

(ii) The number of terms in the summation in Eq. (2.27) is

$$M_{n-1} = g_{n-1} \times g_{n-1}^2 \times \left(\frac{E_c^{(n-1)}}{\Delta_{n-2}} \right)^2. \quad (2.38)$$

By Eqs. (2.35)-(2.38) we obtain

$$\langle U_n^2 \rangle \sim \langle U_{n-1}^2 \rangle \times (g_{n-1}^{-2})^4 \times M_{n-1} \sim \langle U_{n-1}^2 \rangle g_{n-1}^{-3} \left(\frac{\tilde{\Delta}_{n-1}}{\Delta_{n-2}} \right)^2. \quad (2.39)$$

Furthermore, by Eq. (2.34) and (2.39) we obtain the Thouless energy of a 2^n -cluster in a volume of size ξ_{n-1} :

$$E_c^{(n)} \sim \frac{\langle U_n^2 \rangle}{\tilde{\Delta}_n}, \quad (2.40)$$

and the corresponding Thouless number

$$g_n \sim \frac{\langle U_n^2 \rangle}{\tilde{\Delta}_n^2}. \quad (2.41)$$

Finally, the 2^n -cluster localization length is

$$\xi_n = g_n \xi_{n-1} \quad (2.42)$$

In a volume of size ξ_n the 2^n -cluster level spacing is

$$\Delta_n \sim \frac{\tilde{\Delta}_n}{g_n}. \quad (2.43)$$

Now we have obtained all the recursive relations, namely, Eqs. (2.34), (2.39), and (2.41)-(2.43). After a short calculation, we obtain decoupled recursive relations for Δ_n , $\tilde{\Delta}_n$, $\langle U_n^2 \rangle$, g_n , and ξ_n :

$$\left\{ \begin{array}{l} \Delta_n \sim \frac{1}{B} \frac{\Delta_{n-1}^4}{\Delta_{n-2}^2}, \quad n \geq 2, \\ \Delta_0 \sim \frac{B}{\xi_0}, \quad \Delta_1 \sim \frac{B}{\xi_0 \xi_1}, \end{array} \right. \quad (2.44)$$

$$\left\{ \begin{array}{l} \tilde{\Delta}_{n+1} \sim \frac{1}{B} \frac{\tilde{\Delta}_n^4}{\tilde{\Delta}_{n-1}^2}, \quad n \geq 2, \\ \tilde{\Delta}_1 \sim \frac{B}{\xi_0^2}, \quad \tilde{\Delta}_2 \sim \frac{B}{(\xi_0 \xi_1)^2}, \end{array} \right. \quad (2.45)$$

$$\left\{ \begin{array}{l} \langle U_{n+1}^2 \rangle \sim \frac{1}{B^2} \frac{\langle U_n^2 \rangle^4}{\langle U_{n-1}^2 \rangle^2}, \quad n \geq 2, \\ \langle U_1^2 \rangle \sim \frac{U^2}{\xi_0^3}, \quad \langle U_2^2 \rangle \sim \frac{U^2}{\xi_0^2 \xi_1^3}, \end{array} \right. \quad (2.46)$$

$$\left\{ \begin{array}{l} g_{n+1} \sim \frac{g_n^4}{g_{n-1}^2}, \quad n \geq 2 \\ g_1 \sim \left(\frac{U}{B}\right)^2 \xi_0, \quad g_2 \sim \xi_1^2, \end{array} \right. \quad (2.47)$$

$$\left\{ \begin{array}{l} \xi_{n+1} \sim \frac{\xi_n^5 \xi_{n-2}^2}{\xi_{n-1}^6}, \quad n \geq 2, \\ \xi_1 \sim \left(\frac{U}{B}\right)^2 \xi_0^2, \quad \xi_2 \sim \xi_1^3. \end{array} \right. \quad (2.48)$$

In order to obtain g_n and ξ_n we only need to solve Eq. (2.47). After defining a new variable

$$a_n = \ln g_n, \quad (2.49)$$

Eq. (2.47) leads to

$$\begin{aligned} a_{n+1} &= 4a_n - 2a_{n-1}, \quad n \geq 2, \\ a_1 &= \ln g_1, \quad a_2 = \ln g_2, \end{aligned} \quad (2.50)$$

which is a second order linear recursion relation with constant coefficients.³ The general solution can be written as

$$a_n = C\lambda_+^n + D\lambda_-^n, \quad (2.51)$$

where

$$\lambda_{\pm} = 2 \pm \sqrt{2}, \quad (2.52)$$

³With a little abuse of symbols, we replace all the “ \sim ” by “ $=$ ”. It should be remembered that all the *calculations* in this notes are essentially *estimations*.

are the characteristic roots of Eq. (2.51), and C and D are constants determined by the initial values of a_1 and a_2 :

$$C = \frac{a_2 - a_1 \lambda_-}{\lambda_+ (\lambda_+ - \lambda_-)} \quad D = \frac{a_1 \lambda_+ - a_2}{\lambda_- (\lambda_+ - \lambda_-)}. \quad (2.53)$$

We can verify that for $g_1 > g_0$, $a_2 > a_1$ and $C, D > 0$. The asymptotic expression of g_n for large n can be obtained:

$$g_n \xrightarrow{n \rightarrow \infty} \exp(C \lambda_+^n). \quad (2.54)$$

Here we notice that $0 < \lambda_- < 1$ and $\lambda_+ > 1$ in Eq. (2.52). Substituting $N = 2^n$ in Eq. (2.54), we can estimate the enhancement factor for any number of particles:

$$g \xrightarrow{N \rightarrow \infty} \exp(C N^\nu) \quad \nu = \log_2 \lambda_+ \simeq 1.77 \quad (2.55)$$

Substituting Eq. (2.54) in Eq. (2.48) we obtain the 2^n -cluster localization length:

$$\xi_n \xrightarrow{n \rightarrow \infty} \xi_0 \exp\left(\frac{C \lambda_+}{\lambda_+ - 1} \lambda_+^n\right). \quad (2.56)$$

Eq. (2.55) implies that in one dimension the enhancement of localization length increases super-exponentially with the number of particles. However, compared to the estimation in Ref. [94] [see Eq. (2.19)], the enhancement effect is much weaker, since the number of the available propagating channels for N particles might be overestimated in Ref. [94].

Here we note that the super-exponentially large enhancement is triggered off by the condition $g_1 > 1$ in Eq. (2.11), which means the delocalization effect of two particles has to be switched on. What happens if $g_1 < 1$? Since two particles are not enough to come over the threshold for the delocalization process, we should consider more particles. Suppose that strength of disorder is fixed and the M -particle Thouless number in a one-particle localization volume is $g_M(U)$ only depending on the interaction strength U . There might be a descending series of strengths of the interaction $\{U_i\}_{i=2}^{M_{\max}}$ with respect to the particle numbers i , so that, if $U_{i+1} < U < U_i$, $g_{i+1}(U) > 1 > g_i(U)$. The upper bond of the particle number M_{\max} depends on the statistics the particles and the size of the one-particle localization volume. This implies that if $U > U_{M_{\max}}$ we could always find a number of particles $M < M_{\max}$ so that $g_M(U) > 1$.

In this case the 2^n -cluster hierarchical structure should be generalized to some M^n -cluster structure. Still much work is needed to clarify this problem.

2.4 Competing channels

Very possibly, our analysis of the 2^n -cluster hierarchical structure is too qualitative. Apart from the handwaving estimations on the mean level spacing and the interaction matrix elements, there is a crucial simplification: We neglect the coupling between different propagating channels. For example, for four particles, as shown in Fig. 2.1, we concluded: The configuration in Fig. 2.1(g) should have the largest localization length if *neglecting* the coupling to the other configurations. This configuration forms the “fast” channel for the propagation of four particles. The localization lengths of the other configurations in Fig. 2.1 is much shorter [cf. Eq. (2.33)], which form the “slow” channel.

However, the coupling between the fast and slow channels are not negligible (e.g. the configuration in Fig. 2.1(g) coupling to (h) via (e)). In order to understand correctly the delocalization of few particles, we have to analyze the competition between the fast and slow channels. Effectively, if the fast channel is hardly affected by the slow channel, the fast channel wins, and the delocalization effect of interaction will be indeed significant. Otherwise, if the fast channel is strong mixed with slow channel, the delocalization effect of interaction is much weaker, and the system very possibly remains in the strongly localized phase. The problem is also of fundamental importance for studying a many-body system, where few or many excitations have various channels of propagation. To clarify the problem of channel competition in interacting particle systems is one of the motivations for analyzing the models in Chaps. 4 and 5.

Chapter 3

Anderson localization of a hybrid particle—Exciton-polariton

In materials the electromagnetic field may strongly couple to excitations which carries electric or magnetic dipole moments. To account for this coupling, it is very useful, especially in the linear regime, to introduce new bosonic quasiparticles, the *polaritons*, which combine the properties of the photons (quanta of the electromagnetic field) and the dipole-carrying excitations. One of the most discussed types of polaritons is the exciton-polariton in direct-gap semiconductors, where photons are strongly coupled to excitons. The importance of exciton-polaritons in the optical properties of semiconductors has been recognized in the late 1950s and early 1960s, with the pioneering works of several authors[96]-[99]. More recently a new directions have been explored for exciton-polaritons[100] using the low-dimensional quantum structures (quantum wells, wires and dots), such as quantum wells embedded in optical microcavities[101], where strong coupling of excitons and photons can be achieved. In these systems the dispersion of transverse-quantized photons is quadratic in the small momentum, with an effective mass as small as 10^4 of that of the Wannier-Mott exciton, which is of the order of the mass of a free electron. In the absence of disorder photons have a much larger group velocity than excitons, and thus one subsystem is fast while the other one is slow. Yet disorder is unavoidable in such systems due to the imperfections of the resonator boundary and impurities. In many cases one can consider only one mode of transverse quantization

for both the photon and the exciton. Thus a model of two dispersive modes (particles) with parametrically different transport properties arise. Due to the large dipole moment of the exciton these particles are mixed, resulting in avoided mode crossing. On top of that, disorder acts on both of them, whereby its effect on the two channels can be rather different [74, 75]. It is easy to see that this system maps one-to-one onto a single particle model of two coupled lattices in the presence of disorder[75]. Ref. [74] solved the coupled Dyson equations for the Green's functions of exciton and cavity phonon in one dimension numerically, focusing on the so-called "motional narrowing" in the reflectivity spectra of normal incidence [102]. However, the issue of localization of cavity polaritons was not raised. The latter was addressed in Ref. [103] and also in Ref. [100]. Ref. [103] analyzed the scattering of electromagnetic waves in a one-dimensional disordered quantum-well structure supporting excitons. The random susceptibility of excitons in each quantum well was shown to induce disorder for the light propagation, and the Dyson equation for the Green's function of the electromagnetic wave was then solved by the self-consistent theory of localization. The author reached the conclusion that the localization length of light with frequencies within the polariton spectrum is substantially decreased due to enhanced backscattering of light near the excitonic resonance. This is in qualitative agreement with our exact and more general study of the coupled disordered two-chain problem in Chap. 4. The latter also finds natural applications in nanostructures and electronic propagation in heterogeneous biological polymers, such as DNA molecules [104].

The main question we are asking is: What happens to the localization properties when a photon is coupled to an exciton? Will the photon dominate the localization of the polariton or the exciton? Here we are only discussing the specific situation of a single polariton in the absence of inelastic scattering. More interesting situations may arise when interacting and non-equilibrium polaritons are approaching Bose-condensation[72]-[109]. The extremely steep dispersion of the confined photon modes results in a typical cavity-polariton mass as small as a photon. Therefore, the polaritons may undergo Bose-Einstein condensation at cryogenic temperatures $\sim 10\text{K}$ [106], which is 10^7 times of the typical condensation temperatures of cold atoms $\sim 10^{-6}\text{K}$ [110].

This chapter is organized as follows. In Sec. 3.1 a short introduction to cavity polaritons in the absence of disorder is presented. In Sec. 3.2 the effects of disorder on polaritons are studied.

The polariton model accounting for quantum-well roughness, which is the main source of disorder on excitons, and fluctuations of the microcavity thickness, which is the main source of disorder on photons, is introduced.

3.1 A short introduction to microcavity polaritons

Before focusing on the disorder effects on polaritons, we give a very short introduction to microcavity polaritons in the absence of disorder. This introduction is only meant to give a brief physical picture of cavity polaritons. A more complete introduction can be found in the text books[111] and the review article[112].

As shown in Fig. 3.1(a), microcavity polaritons are the normal modes resulting from the strong coupling between quantum well excitons and cavity photons. In semiconductor microcavities two Bragg mirrors ¹ are employed to confine the light. Between the Bragg mirrors the cavity light forms a standing wave pattern, which can be described by an approximately quadratic dispersion, $E_{ph}(k) = E_{ph}^0 + k^2/2m_{ph}$, where the effective mass of photons m_{ph} characterizes the curvature of the dispersion at $k = 0$, as shown in Fig. 3.1(b). Excitons are the hydrogen bound states of a conduction band electron and a valence band hole. The relative motion of an electron and a hole in exciton states is usually frozen, and the center of mass motion is characterized by the dispersion $E_{ex}(k) = E_{ex}^0 + k^2/2m_{ex}$ with exciton mass $m_{ex} \simeq 2m_e$, where m_e is the mass of a free electron. The excitons are much heavier than the cavity photons, typically $m_{ph} \sim 10^{-4}m_{ex}$. For this reason the exciton dispersion can be neglected, as shown in Fig. 3.1(b). In microcavities one or multiple quantum wells are in between the mirrors so that excitons are at the antinodes of the confined light waves, which gives rise to strong coupling between the two constituents. In addition the cavity mirrors can be built with a wedge, so as to change the detuning between the relative energy between the photon and the exciton $\delta_e = E_{ex}^0 - E_{ph}^0$. The polariton modes can be found by solving the coupled Schrödinger

¹A Bragg mirror is a set of alternating layers of dielectrics with different refractive indices. The thickness of one layer is quarter of the light wave length.

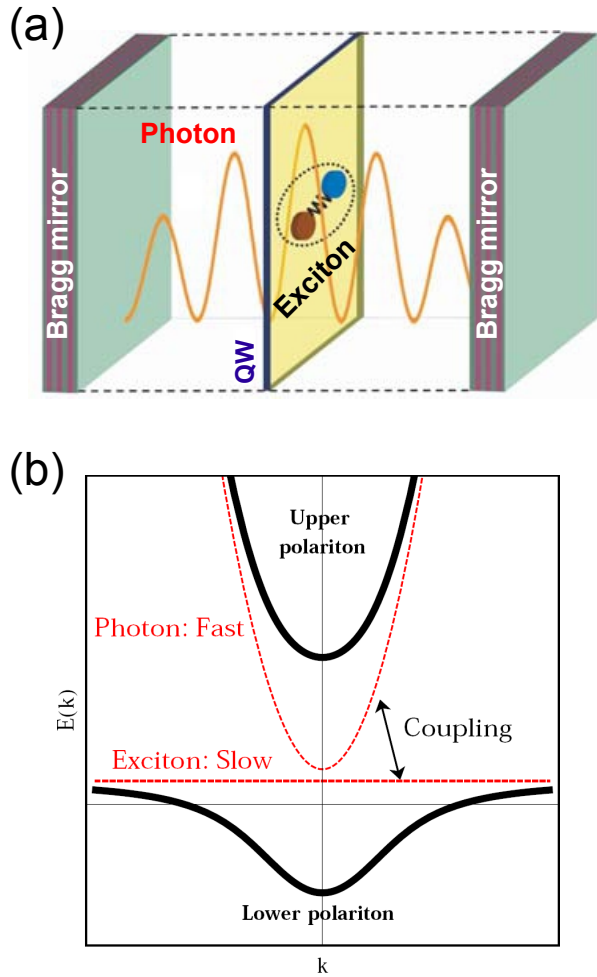


Figure 3.1: Experimental setup of a semiconductor microcavity and energy dispersions of photon, exciton and polariton modes. (a) A microcavity is a Fabry-Perot resonator with quantum wells (QW) embedded in between the two Bragg mirrors. Photons confined in the resonator can strongly couple to excitons confined in the quantum wells. This gives rise to the formation of cavity polaritons, which are linearly mixed exciton-photon states obeying bosonic statistics. (b) Energy dispersions of photon, exciton and polariton modes as functions of the in-plan wavevector. The effective mass of photons (upper dashed curve) are much smaller than that of excitons (lower dashed curve). Hence, the typical group velocity of photons is much larger than that of excitons. The coupling between exciton and photon modes with parabolic dispersions gives rise to lower and upper polariton branches (solid curves) with dispersions featuring an anticrossing typical in the strong coupling regime.

equations for the exciton and photon wave functions, $\psi_{ph,ex} = \psi_{ph,ex}(\mathbf{r})$:

$$H_0 \begin{pmatrix} \psi_{ph} \\ \psi_{ex} \end{pmatrix} = E \begin{pmatrix} \psi_{ph} \\ \psi_{ex} \end{pmatrix}, \quad H_0 = \begin{pmatrix} -\frac{\nabla^2}{2m_C} + E_{ph}^0 & \Omega_R/2 \\ \Omega_R/2 & E_{ex}^0 \end{pmatrix}, \quad (3.1)$$

where Ω_R is the Rabi splitting measuring the strength of photon-exciton (light-dipole) coupling. In general Ω_R is k -dependent and proportional to the dipole moment of the exciton. By the Fourier transform:

$$\psi_{ph,ex}(\mathbf{r}) = \sum_{\mathbf{k}} e^{i\mathbf{k}\cdot\mathbf{r}} \psi_{ph,ex}(\mathbf{k}), \quad (3.2)$$

we obtain the lower ($-$) and upper ($+$) polaritons with dispersions:

$$E_{\pm}(k) = \frac{1}{2} [E_{ex}^0 + E_{ph}(k)] \pm \frac{1}{2} \sqrt{[E_{ex}^0 + E_{ph}(k)]^2 + \Omega_R^2}, \quad (3.3)$$

as shown in Fig. 3.1(b), and eigenstates in the momentum space:

$$\begin{pmatrix} \psi_+(\mathbf{k}) \\ \psi_-(\mathbf{k}) \end{pmatrix} = \begin{pmatrix} \cos \theta_k & \sin \theta_k \\ -\sin \theta_k & \cos \theta_k \end{pmatrix} \begin{pmatrix} \psi_{ph}(\mathbf{k}) \\ \psi_{ex}(\mathbf{k}) \end{pmatrix}, \quad (3.4)$$

with

$$\cos 2\theta_k = \frac{E_{ph}(k) - E_{ex}^0}{\sqrt{(E_{ph}(k) - E_{ex}^0)^2 + \Omega_R^2}}, \quad \theta \in [0, \pi/2]. \quad (3.5)$$

Here we note two points: (i) The group velocity of photons (fast) are much larger than excitons (slow). (ii) At the resonance point, where the dispersion curves of photons and excitons intersect, i.e. $E_{ph}(k) = E_{ex}^0$, polaritons are exactly half-light and half-matter quasiparticles due to $\theta_k = \pi/2$. Far away from the resonance point, however, polaritons are either photon-like or exciton-like.

3.2 Disorder effects on excitons and polaritons

The influence of disorder on cavity polaritons has been investigated for long time. A complete review of this topic can be found in Ref. [75] and the references therein. Here we present a

summary of the basic elements of the theory to see how does disorder enter into Eq. (3.1), and emphasize aspects that are most relevant to the Anderson localization of cavity polaritons.

Disorder on excitons is mainly due to the spatial fluctuation of confinement potentials. In most of quantum wells of average quality bonding energy of the exciton is significantly larger than the strength of the fluctuation of confinement potentials. This suggests that disorder does not influence the electron-hole relative motion in an exciton state. In practice it is also assumed that the perturbation introduced by disorder is not sufficient to produce a transition from the 1s hydrogenic state to high energy states of the relative electron-hole motion. Hence, the exciton stays always in the 1s state and only its center of mass motion is affected by disorder. This “rigid” exciton approximation leads to:

(i) The disorder enters into the effective Schrödinger equation for the center of mass wavefunction as a local random potential $V_{ex}(\mathbf{r})$, which is Gaussian-distributed and characterized by the correlation function

$$\langle V_{ex}(\mathbf{r})V_{ex}(\mathbf{r}') \rangle = f_{ex}(|\mathbf{r} - \mathbf{r}'|), \quad (3.6)$$

where \mathbf{r} are center of mass coordinates of excitons. $f_{ex}(r)$ is finite at $r = 0$ and decay to zero over a correlation length ζ_{ex} . The details of $f(r)$ is determined by the confinement potential fluctuation and the amplitude of the 1s electron-hole hydrogenic wavefunction.

(ii) The disorder does not have influence on the photon-electron coupling. This implies that even in the presence of disorder Ω_R in Eq. (3.1) still capture the photon-exciton coupling sufficiently.

Disorder on photons is largely due to the fluctuation of the cavity-slab thickness, which produces an effective random potential affecting the in-plan motion of the photon. Considering this thickness varies smoothly over lengths comparable with the light wavelength, we can assume that the light field inside the cavity is locally equal to that of an ideal cavity. Within this approximation the disorder on photons can still be modeled by a Gaussian-distributed local random potential $V_{ph}(\mathbf{r})$. It can be characterized in an analogous way to Eq. (3.6):

$$\langle V_{ph}(\mathbf{r})V_{ph}(\mathbf{r}') \rangle = f_{ph}(|\mathbf{r} - \mathbf{r}'|). \quad (3.7)$$

Therefore, the polariton model including the effect of disorder on both excitons and photons is described by the coupled Schrödinger equations similar as Eq. (3.1) but with Hamiltonian replaced by

$$H = H_0 + H_{dis}, \quad H_{dis} = \begin{pmatrix} V_{ph}(\mathbf{r}) & 0 \\ 0 & V_{ex}(\mathbf{r}) \end{pmatrix}, \quad (3.8)$$

where $V_{ph,ex}(\mathbf{r})$ are random potentials applied on excitons and photons characterized by Eqs. (3.6) and (3.7). We note that a polariton propagating in a random potential is described by the Anderson model on two coupled but nonequivalent lattices, in the discrete version of the Hamiltonian (3.8).

Chapter 4

Anderson localization on a two-leg ladder

The simplest example of a disordered propagation problem with competing channels, as discussed in Chaps. 2 and 3, is the Anderson model on two coupled lattices. This is a nontrivial problem, in particular when transport properties of the two lattices are significantly different. Especially for disordered polaritons, the system maps one-to-one onto this model. In this chapter we study the corresponding problem in one dimension, that is, the Anderson model on a two-leg ladder.

Most of the rigorous results on Anderson localization have been obtained in the field of one-dimensional and quasi-one-dimensional systems with uncorrelated disorder. Most of the efforts in this direction were made to obtain the statistics of localized wave functions in strictly one-dimensional continuous systems [114, 115] or tight-binding chains (see the recent work Ref. [116] and references therein). Alternatively, the limit of thick multichannel $N \gg 1$ wires has been studied by the nonlinear supersymmetric σ model[32].

A transfer matrix approach which allows one to consider any number of channels N was suggested by Gertsenshtein and Vasil'ev in the field of random waveguides[117]. This approach has been applied to the problem of Anderson localization by Dorokhov[118] and later on by Mello, Pereyra, and Kumar (DMPK).[119] It is similar in spirit to the derivation of the Fokker-Planck equation (the diffusion equation) from the Langevin equation of motion for a

Brownian particle. However, in the present case an elementary step of dynamics in time is replaced by the scattering off an “elementary slice” of the N -channel wire. As a result, a kind of Fokker-Planck equation arises which describes diffusion in the space of parameters of the scattering matrix \mathbf{M} , in which the role of time is played by the co-ordinate along the quasi-one-dimensional system. Usually the scattering matrix \mathbf{M} is decomposed in a multiplicative way by the Bargmann’s parametrization[119] which separates the “angle variables” of the $U(N)$ -rotation matrices and the N eigenvalues $T_{\rho=1,\dots,N}$ of the transmission matrix. If the probability distribution of the scattering matrix is assumed invariant under rotation of the local basis (*isotropy assumption*), the canonical DMPK equation[118]-[120] may be obtained, which has the form of a Fokker-Planck equation in the space of N transmission eigenvalues. This equation was solved in Ref. [121] for an arbitrary number N of transmission channels.

The isotropy condition is not automatically fulfilled. It is believed that the isotropy condition is valid for a large number $N \gg 1$ of well coupled chains where the “elementary slice” is a macroscopic object and the “local maximum entropy ansatz” applies[119]. It is valid at weak disorder in a strictly one-dimensional chain in the continuum limit $a \rightarrow 0$ or for a one-dimensional chain with finite lattice constant a outside the center-of-band anomaly. In this case the distribution of the only angular variable describing a $U(1)$ rotation, the scattering phase, is indeed flat[116].

However, the case of *few* ($N \gtrsim 1$) coupled chains is much more complicated. As was pointed out originally by Dorokhov[118], and later on by Tartakovski[122]. in this case the angular and radial variables, are entangled in the Fokker-Planck equation. These are the variables determining the eigenvectors and eigenvalues of the transmission matrix, respectively. We refer to this generic Fokker-Planck equation as the *extended* DMPK equation in order to distinguish it from the *canonical* DMPK equation which contains only the radial part of the Laplace-Beltrami operator. The minimal model where such an entanglement is unavoidable, is the two-leg model of $N = 2$ coupled disordered chains.

Motivated by the questions raised in the Chaps. 2 and 3 we are asking : What happens to the localization properties when a fast chain is coupled to a slow one? Will the fast chain dominate the localization length of the ladder? In other words, will the smallest Lyapunov exponent of the two-leg system (the inverse localization length) be similar to the one of the

isolated fast chain, or rather to the one of the isolated slow chain? By intuition one expects the fastest and least disordered chain, this is, the fast chain, to dominate the delocalization. However, our analytical solution of the hybrid two-leg chain shows that in the one-dimensional case, this intuition is not always correct. Instead we find that, when the channels are strongly mixing with each other, it is the largest rate of back scattering, that is, the more disordered chain, which dominates the physics. This may be seen as one of the many manifestations of the fact that in one dimension the localization length is essentially set by the mean free path. Our solution of the two-chain problem furnishes a useful benchmark for approximate solutions in more complex and interacting situations. Nevertheless, we caution that the phenomenology may be quite different in higher dimensions, for example, the situation on the Bethe lattices (infinite dimensions) in Chap. 5. We discuss this further in the conclusion.

The answer to the above questions will be obtained analytically from the exact solution of the two-leg (two-chain) Anderson localization model. This solution represents a major technical advance, because for the first time a model, which leads to an extended DMPK equation with non-separable angular and radial variables, is exactly solved. Without going into details our results are the following:

- (i) The answer depends qualitatively on whether the system is close to the *resonance energy* E_R , which is defined as the energy where the dispersion curves of the two corresponding decoupled disorder-free chains intersect (see Fig. 4.2).
- (ii) *Near the resonance* the presence of the fast leg does not help to substantially delocalize the slow component (see Fig. 4.9). The localization length of a hybrid particle is at most by a factor of ≈ 3 larger than the one of the slow particle [see Eqs. (4.94) and (4.95a)], being parametrically smaller than that of the fast particle. Thus the slow particle dominates the localization properties of the hybrid particle near the resonance energy E_R .
- (iii) A particular case where the resonance happens at all energies is the case of two coupled identical chains subject to different disorder (see Fig. 4.8). In this case the dominance of the more disordered chain extends to all energies, thus pushing the localization length of the ladder sharply down compared to that of the less disordered isolated chain.

(iv) *Away from the resonance* the wave functions stay either mostly on the slow leg, being strongly localized. Or they have their main weight on the fast leg and hybridize here and there with the slow leg [see Fig. 4.2 and Fig. 4.11]. It is this second type of wave functions which helps excitations on the slow leg to delocalize due to the presence of the faster leg, even though this happens with small probability far from the resonance.

(v) A very peculiar behavior occurs *near the band edges* of the slow particle, where the system switches from two to one propagating channels. Just below the band edge the localization length of the hybrid particle decreases dramatically, being driven down by the localization length of the slow chain that vanishes at the band edge (neglecting the Lifshitz tails). Above the band edge the localization length of a hybrid particle sharply recovers, approaching the value typical for the one-chain problem. Thus, near the band edge the localization length of the two-leg system has a sharp minimum, which is well reproduced by direct numerical simulations (see Fig. 4.10).

The chapter is organized as follows. In Sec. 4.1 the problem is formulated and the main definitions are given. In Sec. 4.2 the two-channel regimes is analyzed by the Fokker-Planck equation approach. The extended DMPK equation is derived and the exact solution for the localization lengths is given and the main limiting cases are discussed. In Sec. 4.3 a problem of one propagating channel and one evanescent channel is considered. In Sec. 4.4 numerical results concerning the wave functions in each leg are presented. In Sec. 4.5 another interesting situation where the hopping strength on the slow leg vanishes is studied. The application of the theory to hybrid particles such as polaritons are discussed in the Conclusion. This chapter is based on the published work in Ref. [113].

4.1 Two-leg Anderson model

The Anderson model on a two-leg ladder, as shown in Fig. 4.1 is determined by the tight-binding Hamiltonian

$$H = \sum_{\nu=1,2} \sum_x (\epsilon_{x\nu} c_{x\nu}^\dagger c_{x\nu} - t_\nu (c_{x\nu}^\dagger c_{x+1\nu} + h.c.)) - t \sum_x (c_{x1}^\dagger c_{x2} + h.c.) + \delta e \sum_x c_{x2}^\dagger c_{x2}, \quad (4.1)$$

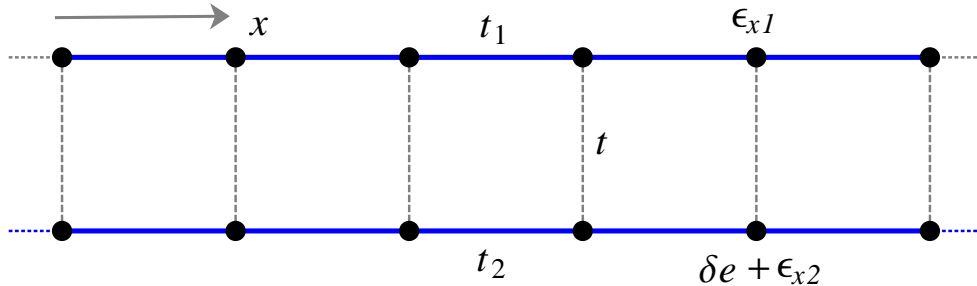


Figure 4.1: Digram for the two-leg Anderson model described by the Hamiltonian (4.1).

where $x \in \mathbb{Z}$ is the co-ordinate along the ladder, and $\nu \in \{1, 2\}$ is the index labeling the two legs. In this model the on-site energies $\epsilon_{x\nu}$ are independently distributed Gaussian random variables with zero mean, and t_ν is the hopping strength between nearest-neighbor sites on the ν -th leg. In general, the two legs will be subject to different random potentials, characterized by the two variances:

$$\sigma_\nu^2 = \overline{\epsilon_{x\nu}^2}. \quad (4.2)$$

We also consider different hopping strengths, for which we assume

$$t_1 \geq t_2. \quad (4.3)$$

The transverse hopping strength between the legs is t . Finally, it is natural to consider a homogeneous potential δe (i.e., a detuning) on leg 2.

The Hamiltonian (4.1) is a generic model describing two coupled, uniformly disordered chains. Moreover, the model can also be adopted as an effective model to describe noninteracting excitations with two linearly mixing channels of propagation in the presence of disorder. An important example is polaritons: the two channels correspond to the photon mode and the exciton mode, respectively.

The model (4.1) has been studied analytically previously in the literature, focusing on the special case $t_1 = t_2$ and $\sigma_1^2 = \sigma_2^2$. The continuous limit was solved long ago by Dorokhov[118]. The tight-binding model was considered later on by Kasner and Weller[123]. Their results will be reference points for our more general study in the present work.

The Schrödinger equation of the Hamiltonian (4.1) at a given energy E has the form

$$\Psi(x-1) + \Psi(x+1) = (\mathbf{h}(E) + \boldsymbol{\epsilon}_x)\Psi(x), \quad (4.4)$$

where $\Psi(x)$ is a single-particle wave function with two components, representing the amplitudes on the leg 1 and 2,

$$\mathbf{h}(E) = \begin{pmatrix} -\frac{E}{t_1} & -\frac{t}{t_1} \\ -\frac{t}{t_2} & -\frac{E-\delta e}{t_2} \end{pmatrix}, \quad (4.5)$$

and

$$\boldsymbol{\epsilon}_x = \text{diag} \left(\frac{\epsilon_{x1}}{t_1}, \frac{\epsilon_{x2}}{t_2} \right). \quad (4.6)$$

The terms $\mathbf{h}(E)$ and $\boldsymbol{\epsilon}_x$ can be considered as the disorder-free and disordered part of the local Hamiltonian at the coordinate x . Notice that the disordered part (4.6) is expressed as an *effective disorder* on the two legs, that is, it is measured in units of the hopping strengths. In the analytical part of the present work, following the Fokker-Planck approach, we solve the problem exactly in the case of small disorder, $\|\boldsymbol{\epsilon}_x\| \ll 1$.

4.1.1 Disorder free part

The disorder-free ladder can easily be solved by diagonalizing $\mathbf{h}(E)$ in Eq. (4.5). Thereby, the Schrödinger equation transforms into

$$\tilde{\Psi}(x-1) + \tilde{\Psi}(x+1) = (\tilde{\mathbf{h}} + \tilde{\boldsymbol{\epsilon}}_x)\tilde{\Psi}(x), \quad (4.7)$$

where

$$\tilde{\mathbf{h}} = \text{diag}(\lambda_1, \lambda_2), \quad (4.8)$$

and the “rotated” disorder potential is given by:

$$\tilde{\boldsymbol{\epsilon}}_x = \begin{pmatrix} \epsilon_{x+} + \epsilon_{x-} \cos \gamma & \epsilon_{x-} \sin \gamma \\ \epsilon_{x-} \sin \gamma & \epsilon_{x+} - \epsilon_{x-} \cos \gamma \end{pmatrix}. \quad (4.9)$$

Both depend implicitly on E via $\lambda_\tau(E)$ and $\gamma(E)$. In Eqs. (4.8) and (4.9) the following definitions are used.

(i) In the disorder-free part (4.8),

$$\lambda_\tau(E) = -\frac{1}{2} \left(\frac{E}{t_1} + \frac{E - \delta e}{t_2} \right) - (-1)^\tau \sqrt{\frac{1}{4} \left(\frac{E}{t_1} - \frac{E - \delta e}{t_2} \right)^2 + \frac{t^2}{t_1 t_2}}, \quad (4.10)$$

where $\tau \in \{1, 2\}$ is the channel or band index. As we see in Eq. (4.15), $\tau = 1$ labels the conduction band, and $\tau = 2$ the valence band of the pure ladder.¹

(ii) In the disordered part (4.9),

$$\epsilon_{x\pm} = \frac{1}{2} \left(\frac{\epsilon_{x1}}{t_1} \pm \frac{\epsilon_{x2}}{t_2} \right) \quad (4.11)$$

are the symmetric and anti-symmetric combination of the disorder on the two legs. The “mixing angle” $\gamma = \gamma(E)$ is defined through

$$\tan \gamma(E) = \frac{\sqrt{2}t\sqrt{t_1^2 + t_2^2}}{(t_1 - t_2)(E - E_R)}, \quad (4.12)$$

with a resonance pole at

$$E_R = \delta e \frac{t_1}{t_1 - t_2}. \quad (4.13)$$

The value of γ is chosen as: $\gamma \in [0, \pi/2]$ if $E \geq E_R$; $\gamma \in [\pi/2, \pi]$ if $E \leq E_R$.

The pure system can be solved easily. In the absence of disorder the eigenfunctions $\tilde{\Psi}(x)$ at energy E are composed of plane waves with momenta k_τ satisfying

$$2 \cos k_\tau = \lambda_\tau. \quad (4.14)$$

$\pm k_\tau$ are degenerate solutions of Eq. (4.14), which is due to the space-inversion symmetry along the longitudinal direction of the pure ladder. Equations (4.10) and (4.14) determine the

¹Note that we are using the semiconductor terminology of valence and conduction band rather loosely to denote the lower and the upper energy band. They will typically not be separated by a gap, but overlap in some energy range, see Fig. 4.2. The latter “two-channel regime” is at the focus of our attention in this paper.

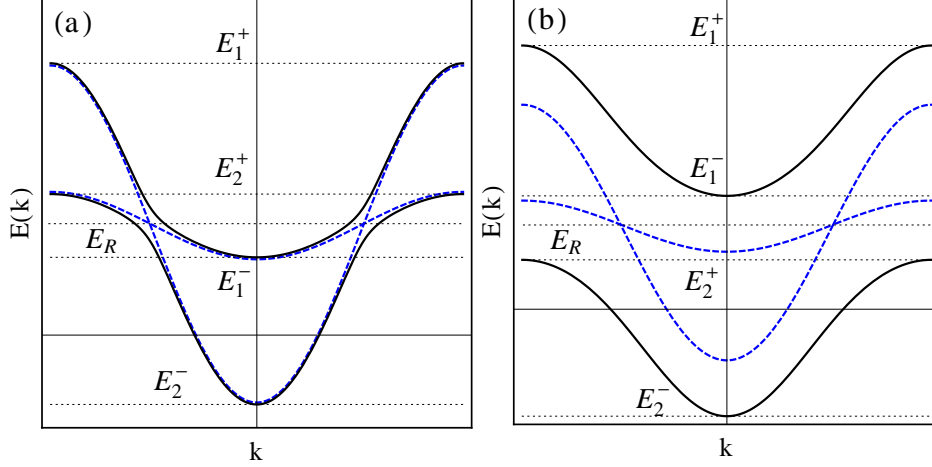


Figure 4.2: Two situations of clean energy dispersions. The dashed and solid curves correspond to decoupled and coupled chains. The decoupled dispersion curves intersect at the resonance energy E_R . (a) *No gap*: $E_1^- \leq E_2^+$. There are two propagating channels at a given energy for $E_1^- \leq E \leq E_2^+$. (b) *Gapped*: $E_1^- > E_2^+$. Apart from a forbidden band, only one propagating channel exists.

energy dispersions of the conduction band and the valance band,

$$E_\tau(k) = -(t_1 + t_2) \cos k + \frac{\delta e}{2} - (-1)^\tau \sqrt{\left[(t_1 - t_2) \cos k + \frac{\delta e}{2} \right]^2 + t^2}. \quad (4.15)$$

Generally, if $t_1 \neq t_2$, the two *decoupled* bands [i.e., $t = 0$ in Eq. (4.15)] cross at the energy E_R (cf. Fig. 4.2), if $|\delta e| \leq 2(t_1 - t_2)$. When the energy E is close to the resonance energy E_R , the two legs mix with almost equal weights, even if we turn on a very small inter-chain coupling t . In the particular case of equal chain hoppings $t_1 = t_2$ and no detuning $\delta e = 0$, there is a resonance at all energies since the two decoupled bands coincide.

The top (+) and bottom (-) edges of the τ band are

$$E_\tau^\pm = \pm(t_1 + t_2) + \frac{\delta e}{2} - (-1)^\tau \sqrt{\left(t_2 - t_1 \pm \frac{\delta e}{2} \right)^2 + t^2}. \quad (4.16)$$

According to Eq. (4.15), there are two cases of energy dispersions, which may arise depending on the choice of the following parameters.

(i) In the case of $E_1^- \leq E_2^+$ [see Fig. 4.2(a)], there is *no gap* between the two bands. This is the case if the detuning δe and the interchain coupling t are both not too large. More precisely, one needs $|\delta e| < 2(t_1 + t_2)$ and $t \leq t_c$, where

$$t_c = \frac{\sqrt{t_1 t_2 [4(t_1 + t_2)^2 - \delta e^2]}}{t_1 + t_2}. \quad (4.17)$$

In the energy interval $E_1^- \leq E \leq E_2^+$, we have two propagating channels; otherwise, at most one propagating channel exists.

(ii) In the opposite case, $E_1^- > E_2^+$ [see Fig. 4.2(b)], there is a *gap* between the two bands. We therefore have at most one propagating channel at any energy.

Moreover, if k_τ is the wavevector of a propagating channel, we call $k_\tau \in (-\pi, \pi]$, and $k_\tau \geq 0$ and $k_\tau < 0$ the *right-* and *left-moving* branches, respectively. From Eq. (4.14) we also define a *rapidity* for each propagating channel as

$$v_\tau \equiv \left| \frac{\partial \lambda_\tau}{\partial k_\tau} \right| = \sqrt{4 - \lambda_\tau^2}. \quad (4.18)$$

4.1.2 Disordered part

The impurity matrix (4.9) contains two ingredients which determine the localization properties of the model. One is $\epsilon_{x\pm}$ [see Eq. (4.11)], which are the equally weighted (either symmetric or anti-symmetric) combinations of *effective disorder* on the two legs. The other is the mixing angle γ [see Eq. (4.12)], which describes the *effective coupling* between the two legs. We refer to γ as the *bare* mixing angle because it is renormalized by disorder. The *renormalized* mixing angle $\tilde{\gamma}$ [see Eq. (4.102)] will be discussed in Sec. 4.2.8. Being functions of these two quantities, the diagonal elements of $\tilde{\epsilon}_x$ are local random potentials applied on the two channels $\tau = 1, 2$, and the off-diagonal elements describe the random hopping between them.

We analyze the model qualitatively in terms of effective disorder and bare mixing angle before carrying out the detailed calculation. As discussed above, either one or two propagating channels are permitted at a given energy. This leads to two distinct mechanisms of localization in the bulk of the energy band:

(i) *Two-channel regime.* In this case, the physics is dominated by the mixing angle γ . If $\gamma \sim 0$ or π , the mixing of the two channels is weak: The magnitudes of off-diagonal elements of matrix (4.9) are much smaller than the magnitudes of the diagonal elements. This means that the two legs are *weakly entangled*, and the transverse hopping t can be treated as a perturbation. A perturbative study of wavefunctions in this regime is presented in Sec. 4.4.2. However, if $\gamma \sim \pi/2$, the magnitudes of the off-diagonal elements are of the same order as the diagonal elements. This implies that the two legs are *strongly entangled*. The localization properties are controlled by the leg with strong disorder, because in Eq. (4.11) it always dominates over the weaker disorder on the other leg.

(ii) *One-channel regime.* The single-channel case has been solved by Berezinskii[114] and Mel'nikov[115] in the case of a single chain. The results they obtained can be applied in our problem by substituting the variance of disorder and rapidity of the propagating channel with the corresponding quantities. However, we have to emphasize here that even if only one channel exists, coupling effects are still present, since both the effective disorder and the rapidity in the remaining channel depend on the transport properties of both legs. In the one-channel regime the second channel is still present, but supports only evanescent modes. We show in Sec. 4.3 that the effect of the evanescent channel on the propagating one is subleading when disorder is weak.

4.2 Two-channel regime

In the two-channel regime, as shown in Fig. 4.2, the Anderson localization problem can be solved by the Fokker-Planck equation approach. The Fokker-Planck approach and its related notations, such as the transfer matrix, the S-matrix, etc., are introduced in detail in Refs. [119] and [120]. We only outline the methodology here. The Fokker-Planck approach to one- or quasi-one-dimensional systems with static disorder at zero temperature is based on studying the statistical distribution of random transfer matrices for a system of finite length. An ensemble of such transfer matrices is constructed by imposing appropriate symmetry constraints. In the present model there are two underlying symmetries: *time-reversal invariance* and *current conservation*, which dramatically reduce the number of free parameters

of transfer matrices. After a proper parametrization, the probability distribution function of these parameters completely describes the ensemble of transfer matrices, and therefore totally determines the statistical distributions of many macroscopic quantities of the system, such as the conductance, etc. In order to obtain the probability distribution function of the free parameters, a stochastic evolution-like procedure is introduced by computing the variation of the probability distribution function of these parameters in a “bulk” system as an extra impurity “slice” is patched on one of its terminals, under the assumption that the patched slice is statistically independent of the bulk. Thereby, we construct a Markovian process for the probability distribution function. This is described by a kind of Fokker-Planck equation in the parameter space of the transfer matrix with the length of the system as the time variable. Essentially, this procedure is analogous to deriving the diffusion equation from the Langevin equation for a Brownian particle. In practice, taking the length to infinity, we can analytically extract asymptotic properties of the model, such as localization lengths, etc., from the fixed-point solution of the Fokker-Planck equation.

4.2.1 Transfer matrix approach

As discussed above, the only microscopic quantity needed in order to write the Fokker-Planck equation of our model Hamiltonian (4.1) is the transfer matrix of an “elementary slice” at any co-ordinate x . The Schrödinger equation (4.7) can be represented in the following “transfer-matrix” form:

$$\tilde{\Phi}(x+1) = \tilde{\mathbf{m}}_x \tilde{\Phi}(x), \quad (4.19)$$

where the four-component wave function $\tilde{\Phi}(x)$ and the 4×4 transfer matrix $\tilde{\mathbf{m}}_x$ is explicitly shown in the 2×2 “site-ancestor site” form:

$$\tilde{\Phi}(x) \equiv \begin{pmatrix} \tilde{\Psi}(x) \\ \tilde{\Psi}(x-1) \end{pmatrix}, \quad \tilde{\mathbf{m}}_x \equiv \begin{pmatrix} \tilde{\mathbf{h}} + \tilde{\boldsymbol{\epsilon}}_x & -\mathbf{1} \\ \mathbf{1} & \mathbf{0} \end{pmatrix}, \quad (4.20)$$

with $\tilde{\Psi}(x)$ and $\tilde{\mathbf{h}}$, $\tilde{\boldsymbol{\epsilon}}_x$ being the two-component vector and 2×2 matrices in the space of channels as defined in Eq. (7).

The transfer matrix $\tilde{\mathbf{m}}_x$ is manifestly *real* (which reflects the time-reversal symmetry) and *symplectic* (which reflects the current conservation):

$$\tilde{\mathbf{m}}_x^T J \tilde{\mathbf{m}}_x = J, \quad (4.21)$$

where J is the standard skew-symmetric matrix:

$$J = \begin{pmatrix} 0 & \mathbf{1} \\ -\mathbf{1} & 0 \end{pmatrix}. \quad (4.22)$$

Note, however, that the transfer matrix $\tilde{\mathbf{m}}_x$ is *not* a convenient representation to construct a Fokker-Planck equation. The reason is simple: Because it is not diagonal without impurities, the perturbative treatment of impurities is hard to perform. The proper transfer matrix \mathbf{m}_x is a certain rotation, which does not mix the two channels of the matrix $\tilde{\mathbf{m}}_x$ but transforms to a more convenient basis within each two-dimensional channel subspace (see Appendix A). The latter corresponds to the basis of solutions to the disorder-free Schrödinger equation $\psi_\tau(x)$ ($\tau = 1, 2$ labeling the channels), which conserves the current along the ladder:

$$j_x = -i [\psi_\tau^*(x)\psi_\tau(x+1) - h.c.] = \text{constant} = \pm 1. \quad (4.23)$$

For propagating modes with real wave vectors k_τ these are the right- and left-moving states

$$\psi_\tau^\pm(x) = e^{\pm i k_\tau x} / \sqrt{2 \sin k_\tau}, \quad (4.24)$$

which obey the conditions

$$\psi_\tau^\pm(x) = (\psi_\tau^\pm(-x))^*. \quad (4.25)$$

For the *evanescent* modes with *imaginary* $k = i\kappa$ the corresponding current-conserving states obeying Eq. (4.25) can be defined, too:

$$\psi_\tau^\pm(x) = \frac{\exp[\mp i\pi/4 - \kappa_\tau x] + \exp[\pm i\pi/4 + \kappa_\tau x]}{\sqrt{4 \sinh \kappa_\tau}} \quad (4.26)$$

In this new basis of current-conserving states, the transfer matrix takes the form (see Appendix A):

$$\mathbf{m}_x = \mathbf{1} + \delta\mathbf{m}_x, \quad \delta\mathbf{m}_x = \begin{pmatrix} -i\boldsymbol{\alpha}_x^* \tilde{\boldsymbol{\epsilon}}_x \boldsymbol{\alpha}_x & -i\boldsymbol{\alpha}_x^* \tilde{\boldsymbol{\epsilon}}_x \boldsymbol{\alpha}_x^* \\ i\boldsymbol{\alpha}_x \tilde{\boldsymbol{\epsilon}}_x \boldsymbol{\alpha}_x & i\boldsymbol{\alpha}_x \tilde{\boldsymbol{\epsilon}}_x \boldsymbol{\alpha}_x^* \end{pmatrix}, \quad (4.27)$$

where the matrix $\boldsymbol{\alpha}_x$ is diagonal in channel space,

$$\boldsymbol{\alpha}_x = \text{diag}(\psi_1^+(x), \psi_2^+(x))_{\text{ch}}. \quad (4.28)$$

Note that it is expressed in terms of the two components of the current conserving states Eqs. (4.24, 4.26) corresponding to the first and the second channels.

In Eq. (4.27), the unit matrix $\mathbf{1}$ is the *pure part* of \mathbf{m}_x , which keeps the two incident plane waves invariant, and $\delta\mathbf{m}_x$ describes the *impurities*, which break the momentum conservation and induce intra- and interchannel scattering. The physical meaning of \mathbf{m}_x can be understood from the scattering processes described below. If there is only one right-moving plane wave in the 1 channel on the left-hand side (l.h.s.) of the slice, which is represented by a four-dimensional column vector with the first component one and the others zero, we can detect four components on the right-hand side (r.h.s.) of the slice, including the evanescent modes. In the case of two propagating channels these four components are right- and left-moving plane waves in the 1 and 2 channels, whose magnitudes and phase shifts form the first row of \mathbf{m}_x . The other rows can be understood in the same manner. In short, the 11-, 12-, 21- and 22- blocks of $\delta\mathbf{m}_x$ represent, respectively, the right-moving forward-scattering, right-moving backward-scattering, left-moving backward-scattering, and left-moving forward-scattering on the slice. In each block, the diagonal elements represent intra-channel scattering and the off-diagonal elements represent interchannel scattering.

It is important that \mathbf{m}_x , Eq. (4.27), fulfills the same constraints regardless of the propagating or evanescent character of the modes [see Appendix A]:

$$\mathbf{m}_x^* = \boldsymbol{\Sigma}_1 \mathbf{m}_x \boldsymbol{\Sigma}_1, \quad \mathbf{m}_x^\dagger \boldsymbol{\Sigma}_3 \mathbf{m}_x = \boldsymbol{\Sigma}_3, \quad (4.29)$$

where $\boldsymbol{\Sigma}_1$ and $\boldsymbol{\Sigma}_3$ are the four-dimensional generalization of the first and third Pauli matrix with zero and unit entries replaced by 2×2 zero and unit matrices in the channels space.

The first condition follows from $\tilde{\mathbf{m}}_x^* = \tilde{\mathbf{m}}_x$, while the second condition is a consequence of the symplecticity Eq. (4.21). Thus these conditions are a direct consequence of the fact that $\tilde{\mathbf{m}}_x$ belongs to the *symplectic group* $\text{Sp}(4, \mathbb{R})$. As is obvious from the choice of the basis (4.23)-(4.26), their physical meaning is the time-reversal symmetry and the current conservation.

The representation Eq. (4.27) of the transfer matrix of an “elementary slice” renders both the physical interpretation and the symmetry constraints very transparent, and it will be seen to be a convenient starting point to construct the Fokker-Planck equation. On the other hand, since $\tilde{\mathbf{m}}_x$ [see Eq. (4.20)] is real and has a relatively simple form, it is more suitable for numerical calculations.

4.2.2 Fokker-Planck equation for the distribution function of parameters

4.2.3 Parametrization of transfer matrices

Once the “building block” (4.27) is worked out, we can construct the Fokker-Planck equation by the blueprint of the Fokker-Planck approach[115, 118, 119, 120]. The transfer matrix of a disordered sample with length L is

$$\mathbf{M}(L) = \prod_{x=1}^L \mathbf{m}_x = \mathbf{m}_L \cdot \mathbf{m}_{L-1} \cdots \mathbf{m}_1, \quad (4.30)$$

which is a 4×4 complex random matrix. It is easy to verify that $\mathbf{M}(L)$ also satisfies the time reversal invariance and current conservation conditions (4.29). It has been proved in Ref. [120] that all the 4×4 matrices satisfying Eq. (4.29) form a group which is identified with the symplectic group $\text{Sp}(4, \mathbb{R})$. By the Bargmann’s parametrization of $\text{Sp}(4, \mathbb{R})$ [119], one can represent $\mathbf{M}(L)$ as

$$\mathbf{M} = \begin{pmatrix} \mathbf{u} & 0 \\ 0 & \mathbf{u}^* \end{pmatrix} \begin{pmatrix} \sqrt{\frac{\mathbf{F}+1}{2}} & \sqrt{\frac{\mathbf{F}-1}{2}} \\ \sqrt{\frac{\mathbf{F}-1}{2}} & \sqrt{\frac{\mathbf{F}+1}{2}} \end{pmatrix} \begin{pmatrix} \tilde{\mathbf{u}} & 0 \\ 0 & \tilde{\mathbf{u}}^* \end{pmatrix}, \quad (4.31)$$

where \mathbf{u} and $\tilde{\mathbf{u}}$ are elements of the unitary group $U(2)$, and statistically independent from each other, and

$$\mathbf{F} = \text{diag}(F_1, F_2), \quad (4.32)$$

with $F_\varrho \in [1, \infty)$ and $\varrho \in \{1, 2\}$. Because $U(2)$ [124] has four real parameters, the group $\text{Sp}(4, \mathbb{R})$ has ten real parameters. Furthermore, it is convenient to parametrize a $U(2)$ matrix by three Euler angles and a total phase angle, that is,

$$\mathbf{u}(\phi, \varphi, \theta, \psi) = e^{-i\frac{\phi}{2}} e^{-i\frac{\varphi}{2}\hat{\sigma}_3} e^{-i\frac{\theta}{2}\hat{\sigma}_2} e^{-i\frac{\psi}{2}\hat{\sigma}_3}, \quad (4.33)$$

in which $\hat{\sigma}_2$ and $\hat{\sigma}_3$ are the second and third Pauli matrix, and the four angles take their values in the range $\phi, \varphi \in [0, 2\pi)$, $\theta \in [0, \pi)$, and $\psi \in [0, 4\pi)$. In matrix form in the channels space, \mathbf{u} can be written as

$$\mathbf{u} = e^{-i\frac{\phi}{2}} \begin{pmatrix} \cos \frac{\theta}{2} e^{-i\frac{\varphi}{2}(\varphi+\psi)} & -\sin \frac{\theta}{2} e^{-i\frac{\varphi}{2}(\varphi-\psi)} \\ \sin \frac{\theta}{2} e^{i\frac{\varphi}{2}(\varphi-\psi)} & \cos \frac{\theta}{2} e^{i\frac{\varphi}{2}(\varphi+\psi)} \end{pmatrix}_{\text{ch}}, \quad (4.34)$$

which is convenient for the perturbative calculation below. The $U(2)$ matrix $\tilde{\mathbf{u}}$ can be parametrized independently in the same form as Eq. (4.34).

The probability distribution function of these ten real parameters determines completely the transfer matrix ensemble of the ladder described by the Hamiltonian (4.1). The goal of the Fokker-Planck approach is to obtain the Fokker-Planck equation satisfied by this probability distribution function, in which the role of time is played by the length L .

From Eq. (4.31) we obtain the transmission matrix

$$\mathbf{t} := (M_{++}^\dagger)^{-1} = \mathbf{u} \left(\frac{\mathbf{F} + \mathbf{1}}{2} \right)^{-1/2} \tilde{\mathbf{u}}, \quad (4.35)$$

by a simple relation between the transfer matrix and its corresponding S matrix²[119, 120].

Due to the unitarity of $\tilde{\mathbf{u}}$, the transmission co-efficients of the two channels are the two

²The transmission matrix \mathbf{t} we calculate here describes transmission from left to right of the sample. Its transpose describes the reverse transmission, as assured by time reversal symmetry. Its element $t_{\tau\tau'}$ denotes the out-going amplitude on the r.h.s of the sample in the τ -channel when there is a unit current incident from the l.h.s in the τ' -channel.

eigenvalues of the Hermitian matrix

$$\mathbf{T} = \mathbf{t}\mathbf{t}^\dagger = \mathbf{u} \left(\frac{\mathbf{F} + \mathbf{1}}{2} \right)^{-1} \mathbf{u}^\dagger, \quad (4.36)$$

which are

$$T_\rho = \frac{2}{F_\rho + 1}, \quad (4.37)$$

where $\rho \in \{1, 2\}$ is the index of the two-dimensional eigenspace of the matrix \mathbf{T} . Now the physical meaning of the parametrization (4.31) becomes clear. The F_ρ 's are related to the *two transmission co-efficients* by the simple form Eq. (4.37). The matrix \mathbf{u} diagonalizing the matrix \mathbf{T} contains the two eigenvectors of \mathbf{T} , describing the polarization of the plane wave eigenmodes incident from the l.h.s. of the sample. For instance, if $\theta = 0$ (\mathbf{u} is a diagonal matrix of redundant phases), the two channels do not mix, and the incident waves are fully polarized in the basis of channels. On the other hand, if $\theta = \pi$, the two channels are equally mixed, and the incident waves are unpolarized. In analogy to spherical co-ordinates, we refer to the F_ρ 's as the *radial* variables, while the angles in \mathbf{u} or $\tilde{\mathbf{u}}$ are called *angular* variables.

In principle, using the “building block” (4.27) and the parametrization (4.31), we can solve the full problem by writing down a Fokker-Planck equation for the joint probability distribution function of all the ten parameters of \mathbf{M} . However, since we are merely interested in the transmission coefficients which are determined by the probability distribution function of \mathbf{T} , instead of manipulating \mathbf{M} , we study

$$\begin{aligned} \mathbf{R} &= \mathbf{M}\mathbf{M}^\dagger \\ &= \begin{pmatrix} \mathbf{u} & 0 \\ 0 & \mathbf{u}^* \end{pmatrix} \begin{pmatrix} \mathbf{F} & \sqrt{\mathbf{F}^2 - \mathbf{1}} \\ \sqrt{\mathbf{F}^2 - \mathbf{1}} & \mathbf{F} \end{pmatrix} \begin{pmatrix} \mathbf{u}^\dagger & 0 \\ 0 & \mathbf{u}^\top \end{pmatrix}. \end{aligned} \quad (4.38)$$

\mathbf{R} is a Hermitian matrix and contains only *six* parameters:

$$\vec{\lambda}(\mathbf{R}) = (F_1, F_2, \theta, \psi, \phi, \varphi). \quad (4.39)$$

The probability distribution function of $\vec{\lambda}$, denoted by $P_L(\vec{\lambda})$, determines the transmission properties of the sample with length L . $P_L(\vec{\lambda})$ is defined by

$$P_L(\vec{\lambda}) = \overline{\delta(\vec{\lambda} - \vec{\lambda}(\mathbf{R}(L)))}, \quad (4.40)$$

where the overline denotes the average over realizations of the random potentials in the sample. It is convenient to introduce the characteristic function of $P_L(\vec{\lambda})$:

$$\tilde{P}_L(\vec{p}) = \int d\vec{\lambda} e^{i\vec{p}\cdot\vec{\lambda}} P_L(\vec{\lambda}) = \overline{e^{i\vec{p}\cdot\vec{\lambda}(\mathbf{R}(L))}}. \quad (4.41)$$

Our main goal in this paper is to calculate the two localization lengths, defined as the inverse Lyapunov exponents of the transfer matrix (4.31):

$$\xi_{1(2)}^{-1} \equiv - \lim_{L \rightarrow \infty} \frac{1}{2} \frac{d}{dL} \langle \ln T_{\max(\min)} \rangle_L, \quad (4.42)$$

in which the subscripts “max” and “min” denote the larger and smaller of the two real values $T_{1,2}$, and the averaging $\langle \cdot \rangle_L$ is earned out with the probability distribution $P_L(\vec{\lambda})$. Therefore, by definition

$$\xi_1 > \xi_2. \quad (4.43)$$

4.2.4 Physical interpretation of ξ_1 and ξ_2

It is worthwhile to visualize how two *parametrically different* localization lengths ($\xi_1 \gg \xi_2$) manifest themselves in transport properties. For instance, let us discuss the dimensionless conductance $g = T_1 + T_2$, a typical behavior of which is shown as a function of the sample length L in Fig. 4.3. If $L \ll \xi_2$, $T_\varrho \approx 1$ and $g \approx 2$ corresponds to a nearly perfect transmission. As L increases, T_ϱ and g decay exponentially. T_2 decays much faster than T_1 since $\xi_1 \gg \xi_2$. As long as $L < \xi_1$ the system still conducts well since g is still appreciable. For $L \sim \xi_1$ it crosses over to an insulating regime. On the other hand, ξ_2 marks the crossover length scale below which $g(L)$ (black curve) decreases as fast as T_2 (blue dashed curve) until the conductance saturates to a plateau $g \approx 1$. For $L > \xi_2$, g decays with the slow rate ξ_1^{-1} , like T_1 (red dotted

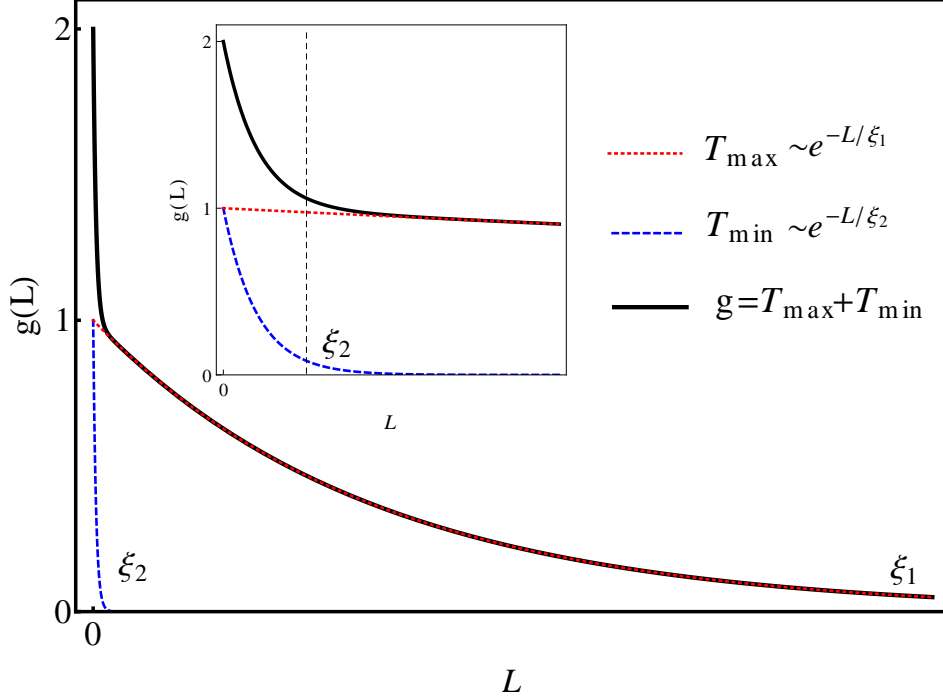


Figure 4.3: Schematic diagram for typical values of dimensionless conductance g as a function of the length L in the case $\xi_1 \gg \xi_2$. A crossover happens at $L \sim \xi_2$. In the region $L < \xi_2$, g decays as fast as T_{\min} (see the insert). Once $L > \xi_2$, g decays as slowly as T_{\max} . The system is well conducting if $L < \xi_1$ and crosses to an insulating regime for $L > \xi_1$.

curve). Therefore, the two parametrically different localization lengths can be identified by two distinct decay rates of g at small and large length scales.

The statistics of transmission eigenvalues and localization lengths of disordered multi-channel micro-waveguides have been visualized in experiments[125]. However, only more or less isotropically disordered cases (identical hopping and disorder strength in each channel) were realized, while a situation where $\xi_1 \gg \xi_2$ is hard to achieve in such systems (see Ref. [125] and references therein). In contrast such anisotropic situations are rather natural in exciton polariton systems.

We see in Sec. 4.4.1 that the two localization lengths ξ_1 and ξ_2 also characterize the spatial variations of the eigenfunctions $\Psi(x)$ on the two legs.

4.2.5 Fokker-Planck equation for the distribution function of $\vec{\lambda}(\mathbf{R})$

Having a disordered sample of length L , whose transfer matrix is $\mathbf{M}(L)$ and adding one more slice, we obtain the transfer matrix of the sample with length $L + 1$:

$$\mathbf{M}(L + 1) = \mathbf{m}_{L+1}\mathbf{M}(L). \quad (4.44)$$

Simultaneously, according to Eqs. (4.38) and (4.27), $\mathbf{R}(L)$ is updated to

$$\mathbf{R}(L + 1) = \mathbf{m}_{L+1}\mathbf{R}(L)\mathbf{m}_{L+1}^\dagger = \mathbf{R}(L) + \delta\mathbf{R}, \quad (4.45a)$$

$$\delta\mathbf{R} = (\mathbf{R}\delta\mathbf{m}_{L+1}^\dagger + h.c.) + \delta\mathbf{m}_{L+1}\mathbf{R}\delta\mathbf{m}_{L+1}^\dagger. \quad (4.45b)$$

Accordingly, $\vec{\lambda}(\mathbf{R}(L))$ is incremented by

$$\vec{\lambda}(\mathbf{R}(L + 1)) = \vec{\lambda}(\mathbf{R}(L)) + \delta\vec{\lambda}. \quad (4.46)$$

According to Eqs. (4.41) and (4.46), we obtain the characteristic function of $P_{L+1}(\vec{\lambda})$:

$$\tilde{P}_{L+1}(\vec{p}) = \overline{e^{i\vec{p}\cdot\vec{\lambda}(\mathbf{R}(L+1))}} = \overline{e^{i\vec{p}\cdot\vec{\lambda}(\mathbf{R}(L))}e^{i\vec{p}\cdot\delta\vec{\lambda}}}. \quad (4.47)$$

We can expand $e^{i\vec{p}\cdot\delta\vec{\lambda}}$ on the r.h.s. of Eq. (4.47) into a Taylor series $e^{i\vec{p}\cdot\delta\vec{\lambda}} = \sum_n^\infty (i\vec{p}\cdot\delta\vec{\lambda})^n$. Using Eqs. (4.45) and (4.46) standard perturbation theory yields an expansion of $\delta\vec{\lambda}$ in powers of the disorder potential as $\delta\vec{\lambda} = \sum_{n \geq 1} \delta\vec{\lambda}^{(n)}$, where $\delta\vec{\lambda}^{(n)}$ is of n -th order in $\tilde{\epsilon}$. With this, the r.h.s. of Eq. (4.47) can be expanded in powers of the disorder potential. In principle, we can proceed with this expansion to arbitrarily high orders. Thereafter, the average over disorder on the slice $L + 1$ can be performed. Equations (4.45)-(4.47) fully define our problem. However, it is impossible to solve it analytically without further simplification.

Progress can be made by considering the *weak disorder* limit. In the two-channel regime, the weak disorder limit implies that *both* of the mean free paths are much larger than the lattice constant. As a first estimation, applying the Born approximation to an “elementary slice”, the inverse mean free paths of the two propagating channels can be expressed as certain linear

combinations of the variances of the effective disorders on the two chains, defined as

$$\chi_\nu^2 = \frac{\sigma_\nu^2}{t_\nu^2}. \quad (4.48)$$

for chain ν . In the weak disorder limit where the smaller of the two localization lengths is much larger than the lattice constant,

$$l \gg 1, \quad (4.49)$$

only the terms proportional to χ_ν^2 on the r.h.s of Eq. (4.47) have to be taken into account. Hence, we calculate $\delta\vec{\lambda}$ perturbatively up to the second order [see Appendix B]. If $L \gg 1$, as we always assume, $\tilde{P}_{L+1} - \tilde{P}_L \simeq \partial_L \tilde{P}_L$. Under these conditions, Eq. (4.47) leads to

$$\partial_L \tilde{P}_L = \overline{i\vec{p} \cdot \delta\vec{\lambda}^{(2)} e^{i\vec{p} \cdot \vec{\lambda}(\mathbf{R}(L))}} - \frac{1}{2} \overline{\left(\vec{p} \cdot \delta\vec{\lambda}^{(1)}\right)^2 e^{i\vec{p} \cdot \vec{\lambda}(\mathbf{R}(L))}}. \quad (4.50)$$

Note that because the random potentials in different slices are *uncorrelated*, the $\delta\vec{\lambda}^{(n)}$ terms can be averaged independently of $e^{i\vec{p} \cdot \vec{\lambda}(\mathbf{R}(L))}$. By the inverse of the Fourier transform defined in Eq. (4.41) we obtain the Fokker-Planck equation for $P_L(\vec{\lambda})$:

$$\partial_L P = - \sum_{i=1}^6 \partial_{\lambda_i} \left[\overline{\delta\lambda_i^{(2)}} P - \frac{1}{2} \sum_{j=1}^6 \partial_{\lambda_j} \left(\overline{\delta\lambda_i^{(1)} \delta\lambda_j^{(1)}} P \right) \right]. \quad (4.51)$$

In Eq. (4.51) the averages are taken over the realizations of random potentials in the slice at $L + 1$.

The Fokker-Planck equation (4.51) can be rewritten in the form of a continuity equation:

$$\partial_L P = - \sum_{i=1}^6 \partial_{\lambda_i} J_i, \quad (4.52)$$

where the generalized current density J_i takes the form:

$$J_i = v_i(\vec{\lambda}) P - \sum_{j=1}^6 D_{ij}(\vec{\lambda}) \partial_{\lambda_j} P, \quad (4.53)$$

with

$$v_i(\vec{\lambda}) = \overline{\delta\lambda_i^{(2)}} + \partial_{\lambda_j} D_{ij}(\vec{\lambda}), \quad (4.54a)$$

$$D_{ij}(\vec{\lambda}) = \frac{1}{2} \overline{\delta\lambda_i^{(1)} \delta\lambda_j^{(1)}}. \quad (4.54b)$$

$v_i(\vec{\lambda})$ and $D_{ij}(\vec{\lambda})$ are a generalized stream velocity and a generalized diffusion tensor, respectively.

4.2.6 Coarse graining

Let us analyze the r.h.s. of Eq. (4.51) qualitatively. From Eqs. (B.10) and (B.12) in the Appendix, it is clear that the coefficients $\overline{\delta\lambda_i^{(1)} \delta\lambda_j^{(1)}}$ and $\overline{\delta\lambda_i^{(2)}}$ are sums of terms carrying phase factors $1, e^{\pm i(k_1 - k_2)L}, \dots$ and so on. These phase factors come from the disorder average of products of two elements of the matrices (4.27). Their phases correspond to the possible wave vector transfers of two scatterings from a slice, similarly as found in the Berezinskii technique [114]. They are thus linear combinations of two or four values of $\pm k_{1,2}$:

$$\begin{aligned} \mathbf{K}_{\text{osc}} = \{ & \pm\Delta k, \quad \pm 2\Delta k, \\ & \pm 2k_{1(2)}, \quad \pm(k_1 + k_2), \quad \pm [3k_{1(2)} - k_{2(1)}], \\ & \pm 4k_{1(2)}, \quad \pm 2(k_1 + k_2), \quad \pm [3k_{1(2)} + k_{2(1)}] \}, \end{aligned} \quad (4.55)$$

where

$$\Delta k = k_1 - k_2. \quad (4.56)$$

Terms with phase “0” do not oscillate. The largest spatial period of the oscillating terms is

$$L_{\text{osc}} = \max_{\delta k \in \mathbf{K}_{\text{osc}}} \delta k^{-1} \quad (4.57)$$

Under the condition that

$$L_{\text{osc}} \ll l, \quad (4.58)$$

a *coarse grained* probability distribution function can be defined as the average of $P_L(\vec{\lambda})$ over L_{osc} . From now on, we use the same symbol $P_L(\vec{\lambda})$ to denote its coarse grained counterpart, which satisfies Eq. (4.51), but neglecting the oscillating terms.

Additionally, at special energies it may happen that an oscillation period becomes commensurate with the lattice spacing, $\delta k = \pi/n$. An important example of this *commensurability* is the situation where $\delta e = 0$, $2(k_1 + k_2) = 2\pi$ at $E = 0$. In this case the terms with the phase factor $e^{\pm 2i(k_1+k_2)L}$ do not average and give anomalous contributions to the non-oscillating coefficients. This effect leads to the so-called center-of-band anomaly in the eigenfunction statistics of the one-chain Anderson model (see Ref. [116] and references therein). While they are not included in our analytical study, the commensurability-induced anomalies can be seen clearly in the numerical results for localization lengths (cf. Figs. 4.7, 4.8, 4.11 and 4.12).

The coarse graining procedure leads to a significant simplification: The coefficients on the r.h.s. of Eq. (4.51) do not depend on L , ϕ , and φ any longer, which renders the solution of Eq. (4.51) much easier. Its nonoscillating coefficients are evaluated in Appendix B. We do not reproduce them explicitly here, since we further transform the Fokker Planck equation below. However, it is worthwhile pointing out a formal property of its coefficients. From Eqs. (B.8), (B.10), and (B.12), it is easy to see that the ingredients for evaluating $\overline{\delta\lambda_i^{(1)}\delta\lambda_j^{(1)}}$ and $\overline{\delta\lambda_i^{(2)}}$ are the disorder-averaged correlators between any two elements of matrices (4.27). During the calculation, three Born cross sections appear naturally, being covariances of the effective disorder variables,

$$V_1 = \frac{1}{4v_1^2} \left(\chi_1^2 \cos^4 \frac{\gamma}{2} + \chi_2^2 \sin^4 \frac{\gamma}{2} \right), \quad (4.59a)$$

$$V_2 = \frac{1}{4v_2^2} \left(\chi_1^2 \sin^4 \frac{\gamma}{2} + \chi_2^2 \cos^4 \frac{\gamma}{2} \right), \quad (4.59b)$$

$$V_3 = \frac{1}{4v_1v_2} (\chi_1^2 + \chi_2^2) \sin^2 \frac{\gamma}{2} \cos^2 \frac{\gamma}{2}, \quad (4.59c)$$

in which $V_{1(2)}$ corresponds to intra channel scattering processes $k_{1(2)} \leftrightarrow -k_{1(2)}$, and V_3 corresponds to interchannel scattering processes $k_{1(2)} \leftrightarrow \pm k_{2(1)}$. Note that the effective disorder variances (4.48) enter into the three Born cross sections, instead of the bare variances (4.2). We will see that the above three Born cross sections completely define the localization lengths and most phenomena can be understood based on them.

We note that the coarse graining, through Eq. (4.58), imposes a crucial restriction on the applicability of the simplified Fokker-Planck equation. According to Eqs. (4.10) and (4.14),

if t is small enough, at $E = E_R$,

$$|\Delta k| \propto t. \quad (4.60)$$

In this case, Eqs. (4.58) and (4.60) require that

$$t \gg \delta E, \quad (4.61)$$

where

$$\delta E \propto l^{-1} \quad (4.62)$$

is the characteristic disorder energy scale (essentially the level spacing in the localization volume). In other words, Eq. (4.61) imposes a “strong coupling” between the two legs, as compared with the disorder scale. However, from the point of view of the strength of disorder, Eq. (4.61) is a more restrictive condition than $\xi_2 \gg 1$ on the smallness of disorder. However, it is automatically fulfilled in the limit $\sigma_\nu \rightarrow 0$ at fixed values of coupling constants t and t_ν . Equation (4.61) restricts the region of applicability of the simplified equation (4.67) which we will derive below. Indeed, we see that by simply taking the limit $t \rightarrow 0$ in the solution of that equation one does not recover the trivial result for the uncoupled chains. This is because the equation is derived under the condition that t is limited from below by Eq. (4.61). The “weak coupling” regime is studied numerically in Sec. 4.2.8 and the crossover to the limit of uncoupled chains is observed at a scale of $t \sim l^{-1}$, as expected.

Since the definition of localization lengths (4.42) only involves the F_ϱ 's, and since the coefficients of Eq. (4.51) do not contain ϕ and φ , we define the marginal probability distribution function

$$W_L(F_1, F_2, \theta, \psi) = \int d\phi d\varphi P_L(\vec{\lambda}). \quad (4.63)$$

Further we change variables to the set

$$\vec{\eta} = (F_1, F_2, u, \psi), \quad (4.64)$$

where

$$u = \cos \theta, \quad u \in (-1, 1]. \quad (4.65)$$

We thus have

$$W_L(\vec{\eta}) = \int d\phi d\varphi P_L(F_1, F_2, \theta(u), \psi, \phi, \varphi). \quad (4.66)$$

Substituting Eq. (4.66) into (4.51), and replacing the differential operators $\partial_\theta \rightarrow -\sqrt{1-u^2}\partial_u$ and $\partial_\theta^2 \rightarrow -u\partial_u + (1-u^2)\partial_u^2$, we obtain the Fokker-Planck equation for $W_L(\vec{\eta})$:

$$\partial_L W = \sum_{i=1}^4 [\partial_{\eta_i} (c_{ii} \partial_{\eta_i} W) + \partial_{\eta_i} (c_i W)] + \sum_{j>i=1}^4 \partial_{\eta_i} \partial_{\eta_j} (c_{ij} W). \quad (4.67)$$

The coefficients c_i, c_{ij} are relatively simple functions of $\vec{\eta}$. They can be obtained from the averages of the matrix elements computed in Appendix B and are given in Appendix C. However, only a small number of them will turn out to be relevant for the quantities of interest to us.

One can see that in Eq. (4.67) the radial variables, F_ρ , are entangled with the angular variables u and ψ . Thus, Eq. (4.67) is more general than the *canonical* DMPK equation[118]-[120], where only radial variables appear. To emphasize the difference we refer to Eq. (4.67) as the *extended* DMPK equation. The derivation of Eq. (4.67) for the two-leg problem is our main technical achievement in the present paper. It allows us to obtain the evolution (as a function of L) of the expectation value of any quantity defined in $\vec{\eta}$ space.

4.2.7 Calculating the localization lengths

It is well-known that in quasi-one-dimensional settings single particles are always localized at any energy in arbitrarily weak (uncorrelated) disorder[27]. The localization length quantifies the localization tendency in real space. In this section we calculate the localization lengths for the present model.

The analytic expression of $\ln T_{\max(\min)}$ in Eq. (4.42) can be written as

$$\ln T_{\max(\min)} = \Theta(\Delta F) \ln T_{2(1)} + \Theta(-\Delta F) \ln T_{1(2)}, \quad (4.68)$$

where $\Theta(z)$ is the Heaviside step function and

$$\Delta F = F_1 - F_2. \quad (4.69)$$

Multiplying both sides of Eq. (4.67) by the r.h.s. of Eq. (4.68) and integrating over all the variables, we obtain from Eq. (4.42)

$$\xi_\rho^{-1} = \lim_{L \rightarrow \infty} \langle (D_1 + D_2) - (-1)^\rho (D_1 - D_2) \text{sgn}(\Delta F) \rangle_L, \quad (4.70)$$

with

$$D_i = \frac{1}{2} \left[\frac{c_{ii}}{(F_i + 1)^2} + \frac{c_i}{F_i + 1} - \frac{\partial_{F_i} c_{ii}}{F_i + 1} \right], \quad i \in \{1, 2\}, \quad (4.71)$$

in which $\rho \in \{1, 2\}$, $\text{sgn}(z)$ is the sign function, and the coefficients c_i, c_{ii} [see App. C] are

$$c_i = (-1)^i 2 \frac{F_i^2 - 1}{\Delta F} \Gamma_6,$$

$$c_{ii} = (F_i^2 - 1) \Gamma_i,$$

with

$$\Gamma_i(u) = V_1 + V_2 + 4V_3 + (-1)^i 2 (V_2 - V_1) u + (V_1 + V_2 - 4V_3) u^2,$$

$$\Gamma_6(u) = V_1 + V_2 - (V_1 + V_2 - 4V_3) u^2.$$

The formula (4.70) for the localization lengths can be further simplified in the limit $L \gg 1$. When L is large, the typical value of $F_{\min(\max)}$ is of the order of $e^{L/\xi_{1(2)}}$, which is exponentially large. Therefore,

$$F_{\max} \gg F_{\min} \gg 1, \quad (4.72)$$

as we assume $\xi_1 > \xi_2$ [see Eq. (4.43)]. The hierarchy (4.72) largely simplifies the coefficients of Eq. (4.67), which leads to

$$\lim_{L \rightarrow \infty} \frac{c_1}{F_1 + 1} = -2\Gamma_6 \Theta(\Delta F), \quad (4.73a)$$

$$\lim_{L \rightarrow \infty} \frac{c_2}{F_2 + 1} = -2\Gamma_6 \Theta(-\Delta F), \quad (4.73b)$$

$$\lim_{L \rightarrow \infty} \frac{c_{ii}}{(F_i + 1)^2} = \Gamma_i, \quad (4.73c)$$

$$\lim_{L \rightarrow \infty} \frac{\partial_{F_i} c_{ii}}{F_i + 1} = 2\Gamma_i. \quad (4.73d)$$

As a result, Eq. (4.70) reduces to

$$\xi_\rho^{-1} = V_1 + V_2 + 2V_3 + (-1)^\rho \left(\frac{1}{2} \langle \Gamma_6 \rangle + |V_1 - V_2| \langle u \rangle \right), \quad (4.74)$$

where $\langle \cdot \rangle \equiv \lim_{L \rightarrow \infty} \langle \cdot \rangle_L$, V_1 , V_2 and V_3 are the Born cross sections defined in Eq. (4.59). The main simplification is that Γ_6 depends only on u , but not on the other parameters of the scattering matrix. Therefore, the localization lengths are fully determined by the marginal probability distribution function of u defined by

$$w_L(u) \equiv \int dF_1 dF_2 d\psi W_L(\vec{\eta}). \quad (4.75)$$

Integrating over F_1 , F_2 , and ψ on both sides of Eq. (4.67), we obtain the Fokker-Planck equation for $w_L(u)$:

$$\partial_L w = \partial_u (c_{33} \partial_u w) + \partial_u (c_3 w), \quad (4.76)$$

where c_3 and c_{33} are derived in Appendix C. It has a fixed-point solution satisfying

$$\partial_u (c_{33} \partial_u w) + \partial_u (c_3 w) = 0. \quad (4.77)$$

In the large L limit the coefficients are given by

$$\lim_{L \rightarrow \infty} c_3 = (|V_1 - V_2| - \partial_u \Gamma_6) (1 - u^2), \quad (4.78a)$$

$$\lim_{L \rightarrow \infty} c_{33} = (V_3 + \Gamma_6) (1 - u^2). \quad (4.78b)$$

From Eq. (4.78) one can see that in the limit (4.72), c_{33} and c_3 do not depend on F_1 , F_2 , and ψ any longer. Therefore, Eq. (4.77) is reduced to an ordinary differential equation with respect to u . By considering the general constraints on a probability distribution function, namely

the non-negativity $w(u) \geq 0$ and the normalization condition $\int duw(u) = 1$, the solution to Eq. (4.77) is unique,

$$w(u) = \begin{cases} w_1(u) = \frac{q_1 \exp\left(\frac{q_1}{q_2} \arctan \frac{u}{q_2}\right)}{2 \sinh\left(\frac{q_1}{q_2} \arctan \frac{1}{q_2}\right) (q_2^2 + u^2)}, & \Delta V \leq 0, \\ w_2(u) = \frac{q_1 \left(\frac{q_2+u}{q_2-u}\right)^{\frac{q_1}{2q_2}}}{2 \sinh\left(\frac{q_1}{2q_2} \ln \frac{q_2+1}{q_2-1}\right) (q_2^2 - u^2)}, & \Delta V \geq 0, \end{cases} \quad (4.79)$$

where

$$q_1 = 2|V_1 - V_2|/|\Delta V|, \quad (4.80)$$

$$q_2 = \sqrt{(V_1 + V_2 + 4V_3)/|\Delta V|}, \quad (4.81)$$

and

$$\Delta V = V_1 + V_2 - 4V_3. \quad (4.82)$$

Equations (4.74) and (4.79) are our main analytical results. The localization lengths are expressed entirely in terms of the three Born cross sections V_1 , V_2 , and V_3 . We recall that we made the assumptions of weak disorder [Eq. (4.49)] and sufficiently strong coupling [Eq. (4.61)].

In Eq. (4.79), $w_2(u)$ is simply the analytical continuation of $w_1(u)$. To show this, we start from $\Delta V > 0$ side and drop the absolute value on ΔV . If ΔV crosses zero from above, namely $\Delta V \rightarrow -\Delta V$, q_1 changes continuously to $-q_1$, and q_2 changes to one of the two branches $\pm i|q_2|$ because of the square root. It can be easily verified that

$$w_1(u; -q_1, \pm i|q_2|) = w_2(u; q_1, |q_2|), \quad (4.83)$$

by the formula $\arctan z = i/2 \ln[(1 - iz)/(1 + iz)]$ for a complex number z .

Given the physical meaning of the parameter u , it is natural to interpret the analytical continuation as describing the *crossover* between two regimes of the polarization, as controlled by the relative strength of the effective disorders. If $\Delta V > 0$ (i.e., $V_1 + V_2 > 4V_3$) the intrachannel scattering is stronger than the interchannel scattering, while $\Delta V < 0$ means the

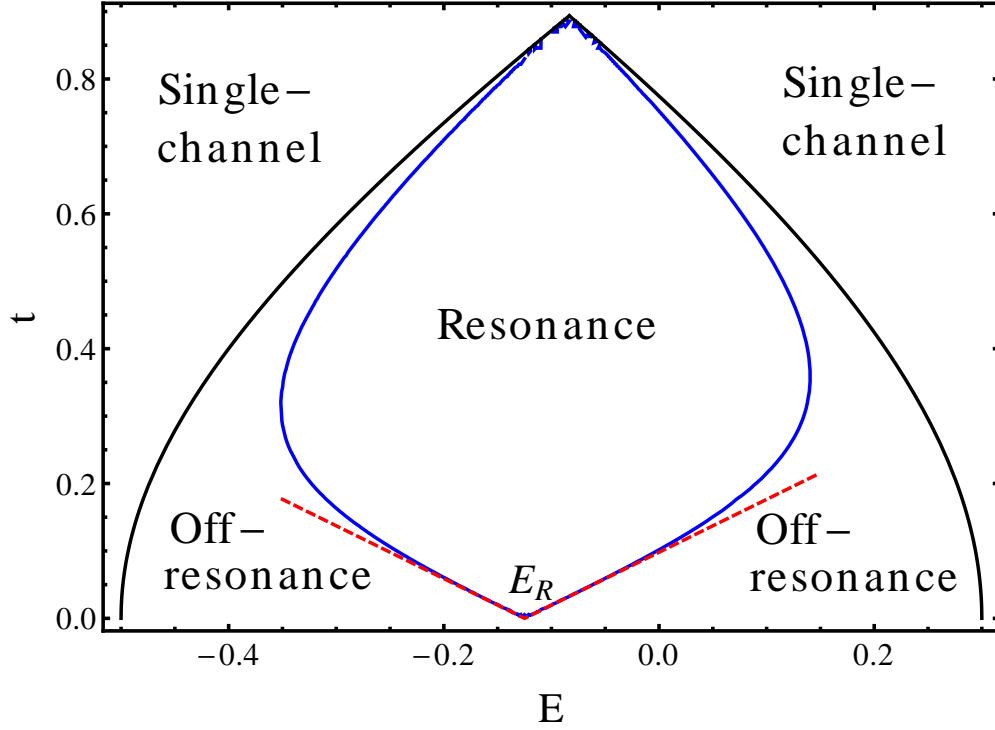


Figure 4.4: The resonant and off-resonant regimes on the $E - t$ plane for $t_1 = 1$, $t_2 = 0.2$, with isotropic disorder $\sigma_1^2 = \sigma_2^2$ and bias $\delta e = -0.1$. The black curve indicates the band edges $E = E_1^-$ and $E = E_2^+$, beyond which only one channel exists. The blue curve marks the crossover line $\Delta V = 0$. At small enough t , $\Delta V = 0$ can be linearized to $t \simeq \kappa|E - E_R|$, cf. Eq. (4.84), which is plotted as the red dashed line.

opposite. The two regimes can be distinguished quantitatively. According to Eq. (4.59), the coefficients in the linear combination of the effective disorder parameters, χ_ν^2 , are determined by the bare “mixing angle” γ and the rapidities, v_τ . Suppose the resonance energy E_R is approached while keeping $t < t_c$ [see Eq. (4.17)]. If E is in the vicinity of E_R , $\gamma \sim \pi/2$, and $\Delta V < 0$. Otherwise, if E is far enough from E_R , $\gamma \rightarrow 0$ or π , and $\Delta V > 0$. Therefore, there must be an energy interval around E_R , in which the physics is similar to that at resonance, $\gamma = \pi/2$. Further away from E_R the physics is similar to the limiting cases $\gamma = 0$ or π . We call $\Delta V < 0$ and $\Delta V > 0$ the *resonant* and *off-resonant* regimes, whose distinct behavior we analyze below.

Resonant and off-resonant regimes

As shown in Fig. 4.4, for fixed t_ν and δe , $\Delta V = 0$ (blue curve) divides the $E - t$ plane into two regions in the two-channel regime (below the black curve). Three important observations are in order.

(i) At *weak coupling* t , more precisely, for $t \ll t_c$, but still within the condition (4.61), the relation $\Delta V = 0$ for the border of the resonance region implies the linear relation (see the red dashed lines in Fig. 4.4)

$$t \simeq \kappa(t_1, t_2) |E - E_R|, \quad (4.84)$$

with

$$\kappa(t_1, t_2) = \frac{t_1 - t_2}{\sqrt{t_1^2 + t_2^2}}. \quad (4.85)$$

The slope $\kappa(t_1, t_2)$ depends on neither σ_ν^2 nor δe .

(ii) If the coupling t is *strong enough*, the resonance energy interval shrinks to zero as $t \rightarrow t_c$ (the top edge of Fig. 4.4). This “re-entrance” behavior is due to the competition between the strong coupling, which pulls γ close to $\pi/2$, and the band edge effect, which reduces the rapidity of one of the channels. We can illustrate this behavior by considering two limiting cases. If t is weak, its effect is of first order on γ , but of second order on the v_τ . Therefore, the coupling wins and the resonance energy interval follows the linear relation (4.84). Alternatively, if the energy is in the vicinity of the band edges $E = E_1^-$ and E_2^+ , one of the rapidities tends to zero. As a consequence, V_1 or V_2 is much larger than V_3 , which gives a large positive ΔV . Therefore,

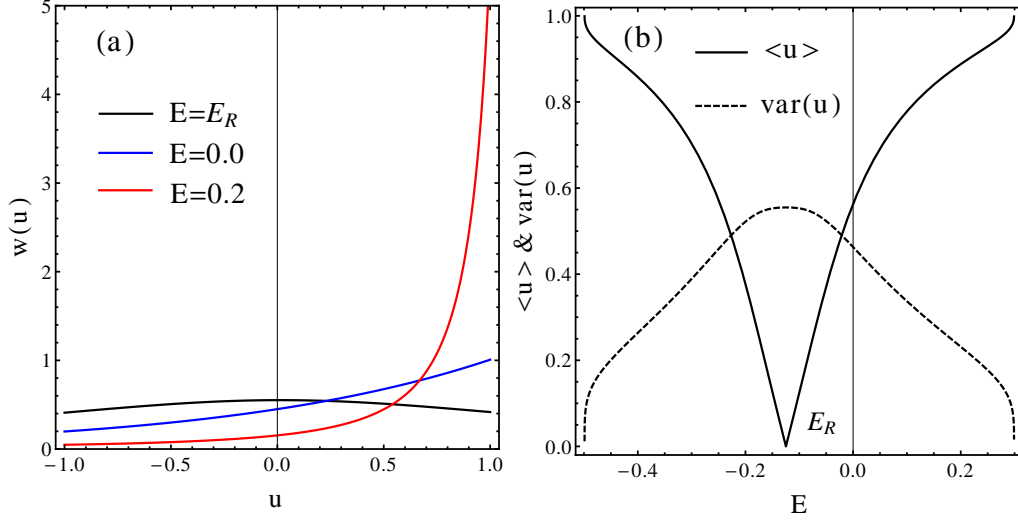


Figure 4.5: Marginal probability distribution for the angular variable $u = \cos(\theta)$, $w(u)$, in different regimes. Here the interchain coupling $t = 0.1$ and the other parameters are the same as in Fig. 4.4. (a) Distributions $w(u)$ for three energies across the resonance and off-resonance regimes, namely, $E = E_R \approx -0.13$ (i.e., resonance energy), $E = 0.2$ (off-resonance), and $E = 0.0$ (crossover). On resonance the distribution is nearly uniform, while it is strongly nonuniform off-resonance (b) The expectation value and variance of u as functions of E .

there is always some region around the band edges (black curves in Fig. 4.4), which is out of resonance. As the crossover line must match the two limits $t \rightarrow 0$ and $t \rightarrow t_c$, it is necessarily re-entrant.

(iii) In the case of a nonzero detuning energy δe the resonant energy interval is slightly *asymmetric* around $E = E_R$.

Fixed point distribution $w(u = \cos \theta)$

Let us now discuss the distribution Eq. (4.79) in different regimes and some of its consequences. For this purpose, we plot in Fig. 4.5 some representative $w(u)$ together with the expectation value and variance of u . We select various values of E across the resonant and off-resonant regime. Two types of behavior can be observed in the two regimes.

(i) *Near the resonance*, $u = \cos \theta$ is distributed relatively uniformly in the interval $(-1, 1]$. Its average value is much smaller than 1, but its variance is large of order $O(1)$. However, the

distribution is definitely not completely uniform. Indeed, the limit of the distribution can be obtained from Eq. (4.79) in the weak coupling limit as $t \rightarrow 0$ as

$$w(u) = \frac{3\sqrt{3}}{\pi(3+u^2)}, \quad (4.86)$$

which is manifestly *nonuniform*. A similar distribution was obtained by Dorokhov [118] in the case of two equivalent chains. We discuss the difference to Eq. (4.86) later.

(ii) *Off resonance*, the distribution function $w(u)$ is strongly peaked at $u = 1$, and its fluctuations are strongly suppressed.

At this point the difference between the canonical DMPK equation [118]-[120], which applies in the case $N \gg 1$, and the extended DMPK equation obtained here for the case $N = 2$, is clear. The isotropy assumption, which allows one to derive the canonical DMPK equation, states that the angular variable distribution $w(u)$ should be uniform, that is, independent of u , in contrast to Eq. (4.86). In order to justify the canonical DMPK equation, we have to have a large number of equal chains. A sufficient condition for obtaining the canonical DMPK equation is that the probability distribution of the transfer matrices of an “elementary slice” is invariant under $U(N)$ rotation. This situation may be achieved in thick wires [119, 120]. However, in few-channel cases the localization lengths are larger, but still of the same order as the mean free path. There is no parametric window between them that permits the emergence of $U(N)$ -invariant ensembles of transfer matrices upon coarse graining.

The qualitative difference in the distribution function $w(u)$ in the two regimes has important implications on the localization lengths. To calculate the localization lengths from Eq. (4.74), we need $\langle \Gamma_6 \rangle$ and $\langle u \rangle$. Using Eq. (4.79) we obtain

$$\langle \Gamma_6 \rangle = \begin{cases} \frac{q_1 q_2 |\Delta V| S_1(q_1, q_2)}{2 \sinh\left(\frac{q_1}{q_2} \arctan \frac{1}{q_2}\right)} - 4V_3, & \Delta V \leq 0, \\ \frac{q_1 q_2 |\Delta V| \tilde{S}_1(q_1, q_2)}{2 \sinh\left(\frac{q_1}{2q_2} \ln \frac{q_2+1}{q_2-1}\right)} - 4V_3, & \Delta V \geq 0, \end{cases} \quad (4.87)$$

and

$$\langle u \rangle = \begin{cases} \frac{q_1 S_2(q_1, q_2)}{2 \sinh\left(\frac{q_1}{q_2} \arctan \frac{1}{q_2}\right)}, & \Delta V \leq 0, \\ \frac{q_1 \tilde{S}_2(q_1, q_2)}{2 \sinh\left(\frac{q_1}{2q_2} \ln \frac{q_2+1}{q_2-1}\right)}, & \Delta V \geq 0, \end{cases} \quad (4.88)$$

where $S_{1(2)}$ and $\tilde{S}_{1(2)}$ are integrals defined by

$$\begin{aligned} S_1(q_1, q_2) &= \int_{-\arctan(1/q_2)}^{\arctan(1/q_2)} dz \sec^2 z e^{\frac{q_1}{q_2} z}, \\ S_2(q_1, q_2) &= \int_{-\arctan(1/q_2)}^{\arctan(1/q_2)} dz \tan z e^{\frac{q_1}{q_2} z}, \\ \tilde{S}_1(q_1, q_2) &= \int_{-1/q_2}^{1/q_2} dz \left(\frac{1+z}{1-z} \right)^{\frac{q_1}{2q_2}}, \\ \tilde{S}_2(q_1, q_2) &= \int_{-1/q_2}^{1/q_2} dz \frac{z}{1-z^2} \left(\frac{1+z}{1-z} \right)^{\frac{q_1}{2q_2}}. \end{aligned} \quad (4.89)$$

Numerical analysis

In order to confirm our analytical results for the localization lengths in Eq. (4.74) we calculated numerically the Lyapunov exponents of the products of transfer matrices in Eq. (4.30). An efficient numerical method, known as the reorthogonalization method, has been developed in the study of dynamical systems[126] and widely spread in the field of Anderson localization[34]. The forthcoming numerical results in Figs. 4.6–4.9, 4.11, and 4.12 are all obtained by this method.

The usefulness of the reorthogonalization method is not restricted to numerical simulations. It also provides the basis for the perturbative analysis about the Lyapunov exponents in the weak disorder limit in Sec. 4.3.1.

4.2.8 Results for the localization lengths

In order to reveal the effects of the transverse coupling t on the localization lengths, we define the two ratios

$$r_\rho = \xi_\rho / \xi_\rho^{(0)}, \quad \rho \in \{1, 2\}, \quad (4.90)$$

where the $\xi_\rho^{(0)}$ s are the localization lengths of the decoupled legs, for which we may assume $\xi_1^{(0)} \geq \xi_2^{(0)}$. For simplicity, we refer to leg 1 and leg 2 as the fast leg and slow leg, respectively. The bare localization lengths $\xi_\rho^{(0)}$ can easily be obtained from Eq. (4.74) by taking $\gamma = 0$, $w(u) = \delta(u - 1)$ and $t = 0$, which yields

$$\xi_\rho^{(0)} = \frac{2v_\rho^2}{\chi_\rho^2}. \quad (4.91)$$

Equation (4.91) coincides with the well-known single-chain result[115].

I. $E = 0$ and $\delta e = 0$: Resonance regime

Consider first the case $\delta e = 0$, in which the resonance energy vanishes $E_R = 0$. From Eqs. (4.12) and (4.18) it follows that the mixing angle is $\gamma = \pi/2$ once $t \neq 0$, and the two rapidities $v_1 = v_2 = v$ are equal to each other:

$$v^2 = 4 - \frac{t^2}{t_1 t_2}. \quad (4.92)$$

Consequently, the three Born cross sections have the same value and are equal to

$$V_1 = V_2 = V_3 = V = \frac{1}{16v^2} (\chi_1^2 + \chi_2^2). \quad (4.93)$$

This gives $q_1 = 0$ and $q_2 = \sqrt{3}$ according to Eqs. (4.80) and (4.82). Evaluating the integrals (4.89), we obtain the two localization lengths

$$\xi_\rho = 8C_\rho v^2 / (\chi_1^2 + \chi_2^2), \quad (4.94)$$

where

$$C_1 = \frac{\pi}{3(\pi - \sqrt{3})} \approx 0.743, \quad (4.95a)$$

and

$$C_2 = \frac{\pi}{\pi + 3\sqrt{3}} \approx 0.377. \quad (4.95b)$$

The corresponding decoupled values ($t = 0$) can easily be obtained from Eq. (4.91),

$$\xi_\rho^{(0)} = \frac{8}{\chi_\rho^2}. \quad (4.96)$$

Therefore, the ratios defined by Eq. (4.90) read

$$r_\rho = C_\rho v^2 \chi_\rho^2 / (\chi_1^2 + \chi_2^2). \quad (4.97)$$

Notice that in the resonant case the Born cross sections (4.59) are dominated by χ_2^2 , which gives rise to the dramatic drop of the localization length of the fast leg: The slow leg is dominating the backscattering rate and thus the localization length.

From Eq. (4.97) we draw several important conclusions below.

A. Statistically identical chains

For two coupled chains, which are statistically identical, one has $\chi_1^2 = \chi_2^2$, and we obtain

$$\begin{aligned} \frac{\xi_1}{\xi_1^{(0)}} &\equiv r_1 = 2C_1 \approx 1.486, \\ \frac{\xi_2}{\xi_2^{(0)}} &\equiv r_2 = 2C_2 \approx 0.754. \end{aligned} \quad (4.98)$$

We note that r_1 is slightly larger than the value obtained by Dorokhov[118] which is $\pi/(\pi-1) \approx 1.467$. The reason is that we have taken into account the *forward-scattering* in the “elementary slice” (4.27), which was neglected in the work by Dorokhov. Moreover, the latter was restricted to $t_1 = t_2$. In Fig. 4.6 we compare our analytical prediction with Dorokhov’s. The effect of forward scattering, which was included in our work, is clearly visible. It is confirmed by the numerical simulation at resonance conditions. However, the value $r_1 \approx 1.776$ obtained by Kasner and Weller[123] deviates significantly from our result.

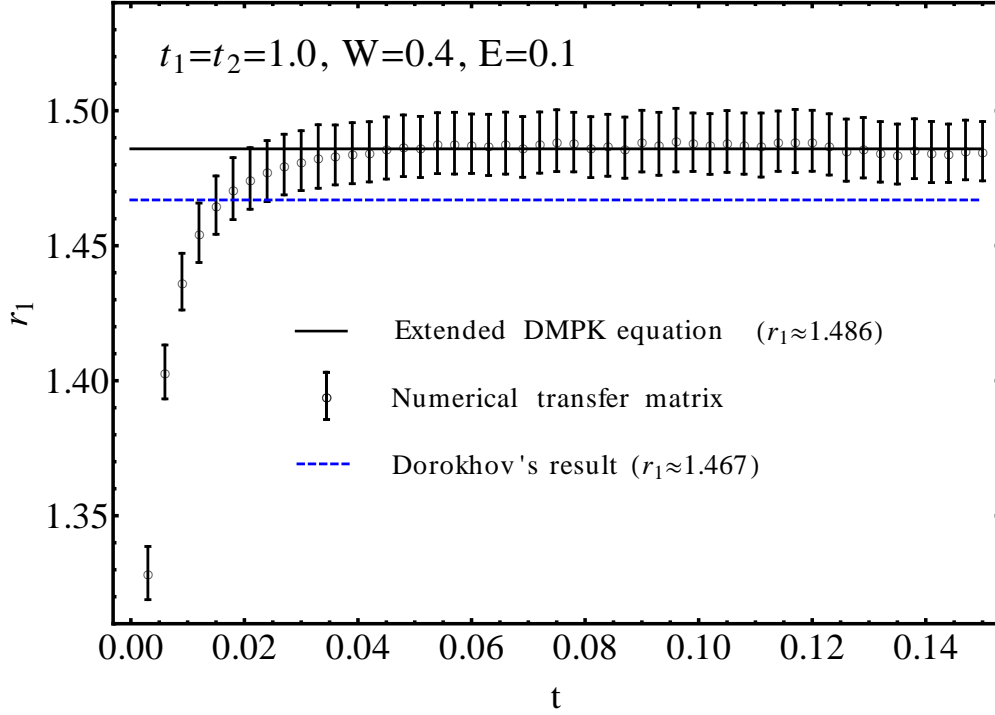


Figure 4.6: Ratio of coupled and uncoupled localization lengths, $r_1 = \xi_1/\xi_1^{(0)}$, for statistically identical chains with $t_1 = t_2 = 1$ and small disorder W . We consider small couplings t , for which any energy is at resonance conditions (here $E = 0.1$). The continuum approximation becomes exact for $W^2 \ll t \ll 1$, as is illustrated by the convergence of the numerical data to the analytical prediction (the agreement is already good for $cW^2 \lesssim t$ with $c \approx 0.25$). For comparison we also plot Dorokhov's prediction [118], which neglected forward scattering in the Fokker-Planck equation. The result of Kasner and Weller[123] ($r_1 \approx 1.776$) is in clear contradiction with these numerics.

B. Parametrically different chains

It is interesting to analyze what happens if the bare localization lengths of the chains are parametrically different $\xi_2^{(0)} \ll \xi_1^{(0)}$. In the resonant regime, for $W^2, |E - E_R| \ll t \ll t_1, t_2$, we obtain

$$\xi_1 \rightarrow 4C_1 \xi_2^{(0)} \approx 2.972 \xi_2^{(0)}, \quad (4.99a)$$

$$\xi_2 \rightarrow 4C_2 \xi_2^{(0)} \approx 1.507 \xi_2^{(0)}. \quad (4.99b)$$

Equation (4.99) is one of the central results in this paper: In the resonant regime, the localization length of the fast leg is *dramatically* dragged down by the slow leg. In contrast, the localization length of the slow leg is increased by the presence of the fast leg, but remains of the same order. As a result both localization lengths become of the order of that for the bare *slow leg*. This is illustrated for two different cases of coupled fast and slow legs in Figs. 4.7 and 4.8. Figure 4.7 shows the effect in the case of legs with equal disorder but different hopping strength, the resonance being at $E = 0$. In Fig. 4.8 the faster leg has the same hopping but weaker disorder. Here the legs are resonant at *every energy* below the band edge E_2^+ .

We note that there is *no* regime where both $r_1 > 1$ and $r_2 > 1$, as this would contradict the equality $\sum_\rho r_\rho / C_\rho = v^2$, which follows from Eq. (4.97). At the band center and $t \rightarrow 0$ one can achieve that both localization lengths do not decrease upon coupling the chains, $r_1 = r_2 = 1$. This happens when $\chi_2^2 / \chi_1^2 = 4C_1 - 1$, which assures that the localization lengths do not change at coupling constants $t \lesssim W^2$ according to the discussion in Sec. 4.2.8 I C.

C. Weak coupling limit

Upon simply taking the $t = 0$ limit,

$$r_\rho = 4C_\rho \chi_\rho^2 / (\chi_1^2 + \chi_2^2), \quad (4.100)$$

one *does not* recover the decoupled values $r_\rho = 1$. This should indeed be expected, as we have discussed in Sec. 4.2.5. The reason traces back to condition (4.61) to obtain Eq. (4.67), namely that t be larger than the disorder energy scale $\delta E \propto W^2$. In order to verify the non-commutativity of $t \rightarrow 0$ and $W \rightarrow 0$, we computed numerically the localization lengths by the transfer matrix approach, and obtained the values of r_ρ down to very small values of

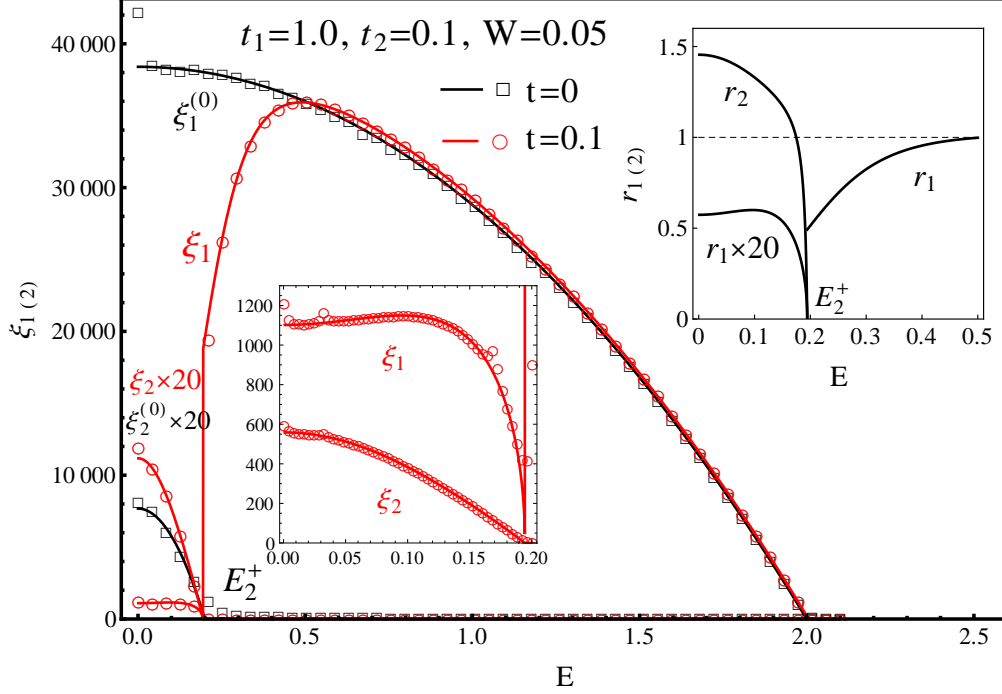


Figure 4.7: Localization lengths for chains with different hopping strengths ($t_1 = 1$ and $t_2 = 0.1$), but equal disorder ($W = 0.05$) as a function of energy at detuning $\delta e = 0$ and intermediate coupling $t = 0.1$. The solid curves are analytical results. Black curves correspond to uncoupled chains; red ones correspond to the coupled chains. The squares and circles are data of the numerical transfer matrix. $\xi_2^{(0)}$ and ξ_2 are amplified 20 times to increase visibility, but $\xi_1 > \xi_2$ always holds. The lower left insert is a magnification in the two-channel region. The upper right inset shows the ratios $r_{1,2}$ of coupled to uncoupled localization lengths. The larger localization length is very significantly suppressed due to the coupling to a slow chain. Note the sharp recovery of the larger localization length beyond the band edge E_2^+ . The analytical results coincide quantitatively with the numerical data anywhere except for specific anomalous energies: In the uncoupled case, $E = 0$ corresponds to the commensurate wave vectors $4k_{1(2)} = 2\pi$. In the coupled case, $E = 0$ and $E \approx 0.03, 0.1$ (very weak) and 0.17 correspond to $2(k_1 + k_2) = 2\pi$, $3k_1 + k_2 = 2\pi$, $4k_1 = 2\pi$, and $3k_2 - k_1 = 2\pi$.

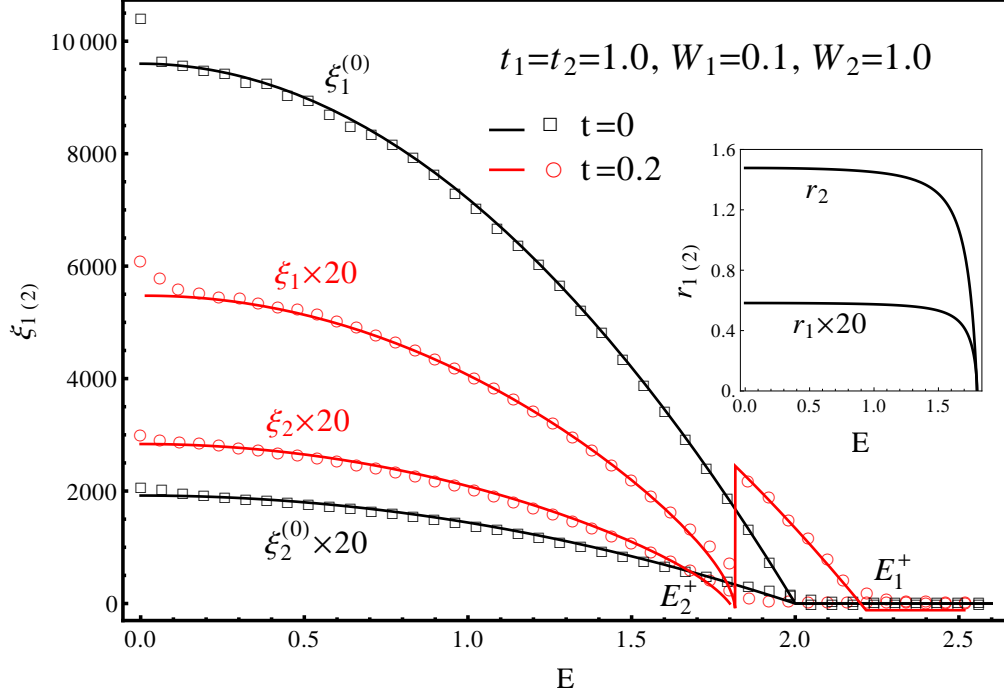


Figure 4.8: Localization lengths for the decoupled ($t = 0$, black) and coupled ($t = 0.2$, red) chains with identical hopping but substantially different disorder ($W_1 = 0.1$ and $W_2 = 1.0$) as a function of energy (detuning $\delta e = 0$). The solid curves are analytical results. The squares and circles are data from the numerical transfer matrix. The values of ξ_1 , $\xi_2^{(0)}$ and ξ_2 are amplified 20 times to increase their visibility. Without coupling $\xi_1^{(0)}/\xi_2^{(0)} \sim 10^2$. In the presence of coupling ξ_1 is substantially reduced, while ξ_2 remains of the same order as its decoupled value. The inset shows the ratios $r_{1,2}$ of coupled to uncoupled localization lengths. Since $t_1 = t_2$ there is resonance at all energies, and thus dominance of the slow chain is expected. Note the sharp recovery of the larger localization length beyond the band edge E_2^+ . There are visible anomalies at $E = 0$ in both the uncoupled and the coupled case, which correspond to the commensurate condition $4k_{1(2)} = 2\pi$ and $2(k_1 + k_2) = 2\pi$. In the coupled case further anomalies exist at the energies corresponding to $3k_1 + k_2 = 2\pi$, $4k_1 = 2\pi$, and $3k_2 - k_1 = 2\pi$. However, they are very close to $E = 0$ and too weak to be observed.

t , (Fig. 4.9). In this simulation, the re-orthogonalization method [34] was used, and length of the ladder is $L = 10^7$ with averaging over 10^3 realizations of disorder. The hopping integral in the fast chain $t_1 = 1$ was taken as the energy unit, and for simplicity, the two legs were taken to be equally disordered. One can see that as the coupling t increases the quantities $r_{1,2}$ evolve and at $t \gg W^2$ approach the limits given by Eq. (4.100).

The insensitivity of the localization lengths to weak couplings $t \ll \delta E$ reflects the fact that the level spacing in the chains is bigger than the coupling between the chains, and thus wavefunctions typically do not hybridize much between the two legs.

Moreover, the two families of curves for different disorder strengths seem to collapse into two universal functions $r_{1,2}(t/W^2)$ (c.f. Fig. 4.9). This scaling shows that at weak disorder $W \ll 1$ and under resonance conditions $E = E_R$, the numerical results approach the analytical ones already at a very small coupling $t \gtrsim W^2$.

We can rationalize the scaling by defining a regularized mixing angle $\tilde{\gamma}$ instead of the bare γ defined by Eq. (4.12). From Eqs. (4.12) and (4.84), we find that

$$\tan^2 \gamma \propto \frac{t^2}{[\kappa(t_1, t_2)(E - E_R)]^2}, \quad (4.101)$$

where $\kappa(t_1, t_2)$ is defined in Eq. (4.85). A natural way of regularizing the above result at resonance conditions is to introduce the disorder-induced “width” $\delta E \propto W^2$ in the form:

$$\tan^2 \tilde{\gamma} \propto \frac{t^2}{[\kappa(t_1, t_2)(E - E_R)]^2 + \delta E^2}, \quad (4.102)$$

where δE scales as in Eq. (4.62).

Using this regularized mixing angle, the resonant regime can be described more precisely by the condition

$$t \gg \max\{\kappa(t_1, t_2)|E - E_R|, \delta E\}, \quad (4.103)$$

or, equivalently, $\tilde{\gamma} \sim \pi/2$. The observed scaling collapse in Fig. 4.9(a) suggests that in the weak coupling one might capture the behavior of localization lengths by replacing γ by $\tilde{\gamma}$ in

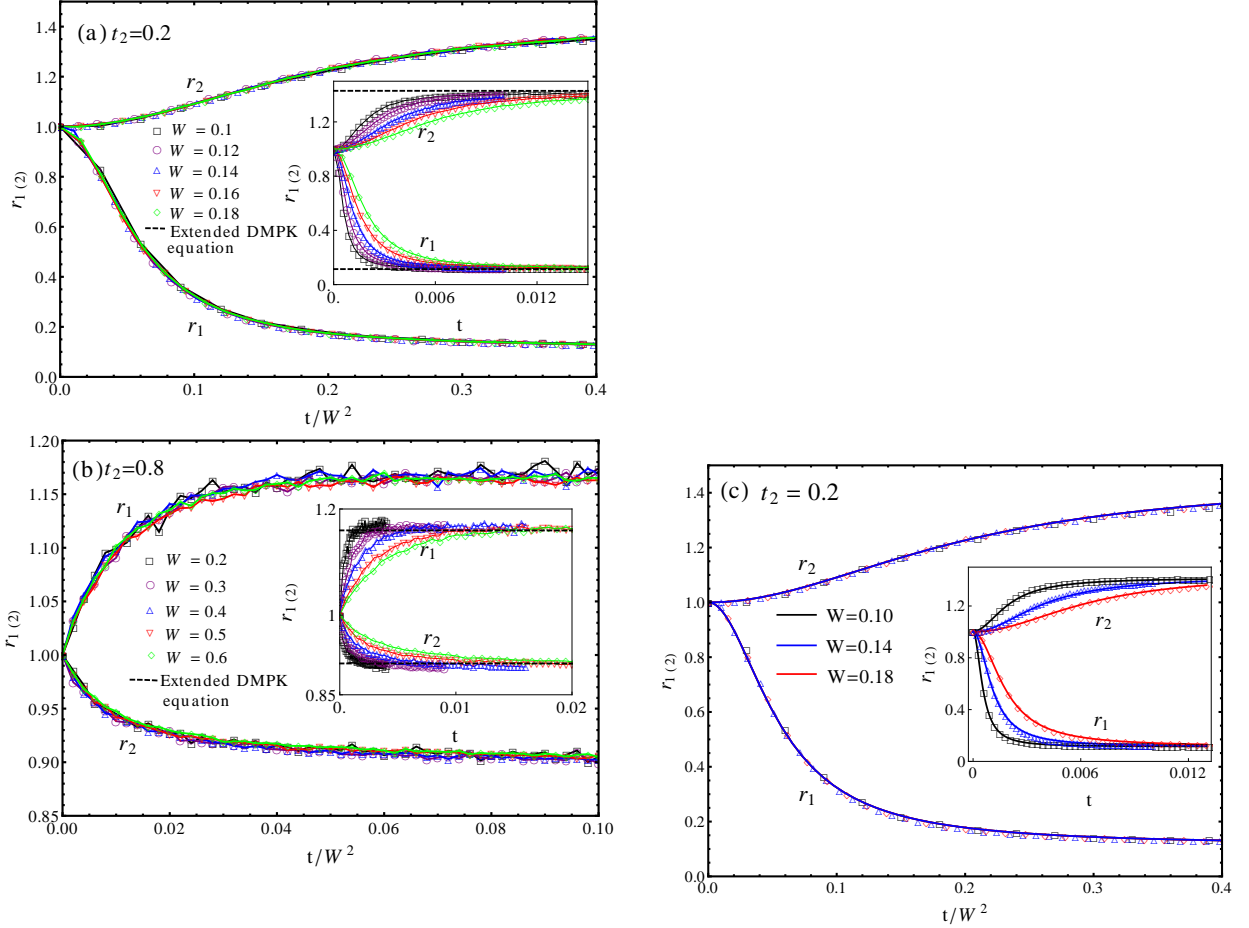


Figure 4.9: The ratio $r_{1,2} = \xi_{1,2}/\xi_{1,2}^{(0)}$ of coupled and decoupled localization lengths, obtained numerically as a function of the coupling constant t at resonant conditions, $E = 0$ and $\delta e = 0$. The two legs are equally disordered with a random potential box distributed in $[-W/2, W/2]$. (a) A slow $t_2 = 0.2$ and a fast $t_1 = 1$ leg: The smaller localization length increases slightly while the larger localization length decreases drastically, being driven down by the slow leg, as the coupling constant t increases. The insert shows the dependence of $r_{1,2}$ on the coupling constant t at different disorder strengths; all the curves collapse to a universal dependence on t/W^2 . The dashed lines in the insert show the analytic result given by Eq. (4.97), which is valid under the assumption $t \gg W^2$ [Eq. (4.61)]. (b) Almost identical legs $t_2 = 0.8$, $t_1 = 1$. In this case the localization length of the slow leg marginally decreases while that of the fast leg marginally increases. (c) Results obtained analytically upon replacing the mixing angle with a renormalized value, $\gamma \rightarrow \tilde{\gamma}$. The parameters are the same as in (a) but with fewer realizations of disorder, and $\delta E/W^2 \approx 0.3$ in Eq. (4.102) was optimized by fitting to the numerical data in (a). The scaling collapse works very well in the weak coupling limit.

Eq. (4.59). This indeed works, as confirmed by Fig. 4.9(c) where we replot the numerical data of Fig. 4.9(a) together with the analytical expressions, where $\tilde{\gamma}$ replaces γ , and the number $\delta E/W^2 \approx 0.3$ was optimized to yield the best fit.

Note that the resonance condition can be broken either by detuning $|E - E_R| \gg t$ or by increasing the disorder $\delta E \gg t$. Our analytic approach is based on the weak-disorder expansion and is therefore valid only in the first regime.

D. Anomalies

One can notice that all our numerical curves for $\xi_{1,2}$ exhibit *anomalies* which are not predicted by the analytical curves: Small “peaks” appear at certain energies on both ξ_1 and ξ_2 . These anomalies of localization lengths are due to the commensurability discussed in Sec. 4.2.6. This is not captured by the extended DMPK equation (4.67). However, we can identify these anomalous energies with commensurate combinations of wave vectors in Eq. (4.56) (see the caption in Figs. 4.7 and 4.8). The anomalies for two chains with identical hopping but different disorder have been observed numerically in Ref. [127]. In this case there are three anomalous energies $E = 0, t/2$ and t , which correspond to commensurate combinations of wave vectors $2(k_1 + k_2) = 2\pi, 3k_1 + k_2 = 2\pi$ and $4k_1 = 2\pi$.

Solution at $E \neq 0$: Off-resonance regime

Without loss of generality the off-resonant regime can be considered at $\delta e = 0$ (for which the resonance is at $E_R = 0$). A non-zero detuning δe merely drives E_R away from zero and induces an asymmetry of the r_ρ as a function of $E - E_R$. However, the mechanism of the crossover from resonance to off-resonance is qualitatively the same as in the case $\delta e = 0$.

Our analytical results for $r_{1,2}$ are presented in Fig. 4.10 as functions of the dimensionless detuning E/t from resonance.

(i) *Small detuning*, $|E| \ll t/\kappa(t_1, t_2) \ll 1$: The resonance conditions are still fulfilled and the localization lengths are close to their corresponding values at $E = 0$. The leading order expansion around $\gamma = \pi/2$ predicts that the ratios of localization lengths, $r_{1,2}$ only depend on E/t , but not on t/t_1 ,

$$|r_\rho - r_\rho(E = 0)| \propto \left(\frac{E}{t}\right)^2, \quad (4.104)$$

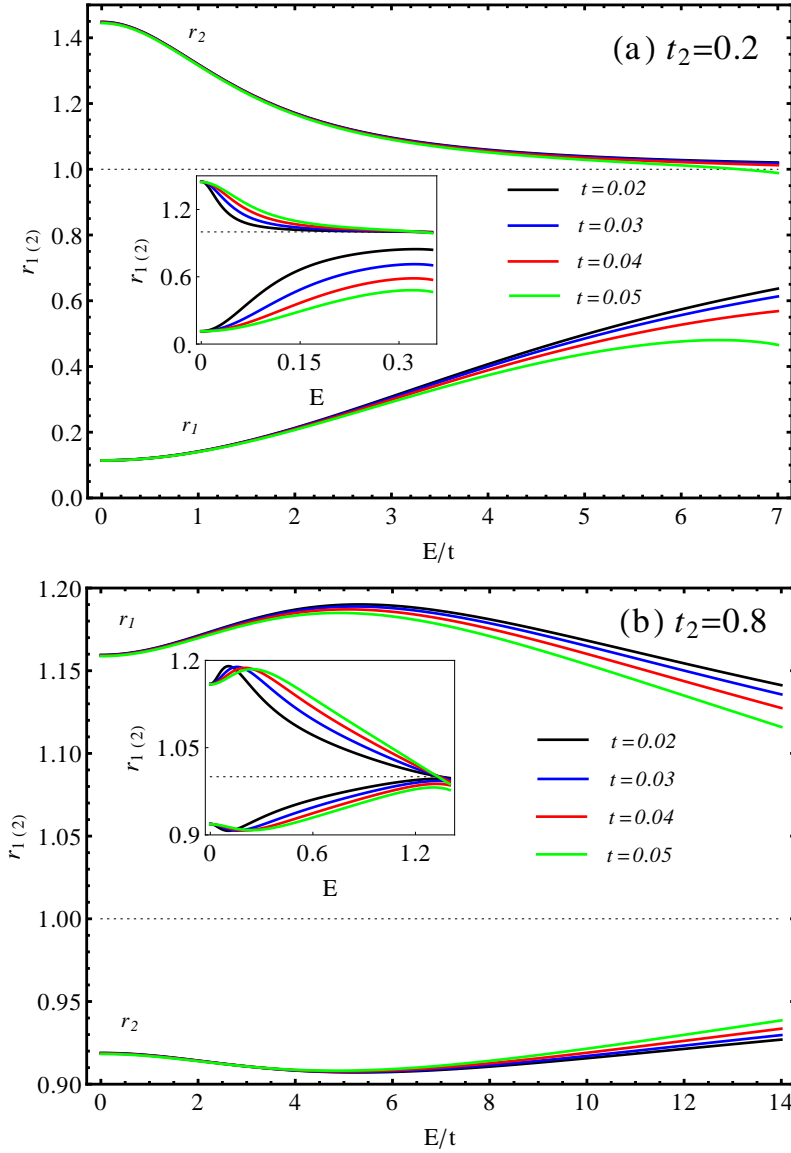


Figure 4.10: Analytical results for $r_{1,2} = \xi_{1,2}/\xi_{1,2}^{(0)}$ as functions of E and E/t obtained from the extended DMPK equation in the weak disorder case $\delta E \ll t$ for detuning $\delta e = 0$. The resonance energy corresponds to $E_R = 0$. (a) $t_2 = 0.2$, $t_1 = 1$. (b) $t_2 = 0.8$, $t_1 = 1$. Close to resonance the r_ρ only depend on the ratio E/t .

as confirmed numerically in Fig. 4.10.

(ii) *Very large detuning*, $|E| \gg t/\kappa(t_1, t_2) \gg 1$, $r_{1(2)}$ approaches 1 from below (above) like

$$|r_\rho - 1| \propto t^2. \quad (4.105)$$

When t is small this result is obtained from the leading order expansion of r_ρ around $\gamma = 0$ or π .

(iii) For chains with *equal hopping*, $t_1 = t_2$, resonance occurs at *any* energy and $r_\rho = 2C_\rho$ is independent of E/t .

Band-edge behavior

Another interesting question to ask is what happens to the localization lengths around the band-edge E_1^- or E_2^+ ? [see Fig. 4.2(a)] Especially, what is the behavior of the localization length of the fast leg once we turn on the coupling t ? The results from the numerical transfer matrix simulation and of the solution (4.74) of the extended DMPK equation [Eq. (4.67)] are compared in Fig. 4.11.

Two remarkable features can be observed in Fig. 4.11.

(i) Near the band edge $E = E_2^+$ where the system switches from one to two propagating channels, the larger localization length ξ_1 (red curves) behaves in a singular way, as obtained from Eq. (4.74). As the energy tends to the band-edge E_2^+ from below, ξ_1 decreases to zero and shows a jump to a finite value for $E > E_2^+$, where only one propagating channel exists. The numerical simulation (black circles) reproduces the same behavior, while the sharp recovering at $E = E_2^+$ is smeared by the finite disorder. This behavior is another drastic example of the dominant effect of the slow channel. It can be understood from the behavior of the Born cross sections Eq. (4.59). As we approach the band-edge from below, the rapidities of the two channels satisfy $v_1 \gg v_2$. As a consequence, the cross sections obey the hierarchy $V_2 \gg V_3 \gg V_1$. Therefore, from Eqs. (4.79) and (4.74), one can see that ξ_1 is dominated by the largest cross section V_2 and shows qualitatively the same behavior as ξ_2 . We emphasize that the mechanism of this suppression is different from that in the resonant regime. In the

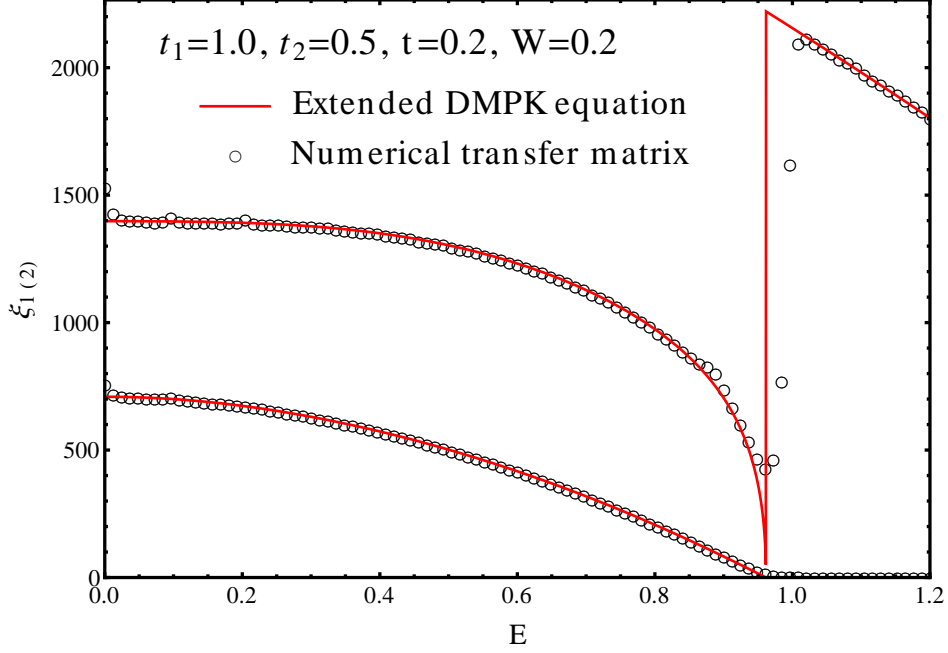


Figure 4.11: Localization lengths as a function of energy near the edge of one of the bands. Here $W = 0.2$, $t_1 = 1$, $t_2 = 0.5$, $t = 0.2$ and $\delta e = 0$. The red curve is the result of the extended DMPK equation, while the black circles are data obtained by the numerical transfer matrix method. The quantitative agreement is significant except for four anomalous energies, for example, $E = 0$ and $E \approx 0.1, 0.2$ and 0.9 . The corresponding commensurate combinations of wave vectors are $2(k_1 + k_2) = 2\pi$, $3k_1 + k_2 = 2\pi$, $4k_1 = 2\pi$, and $3k_2 - k_1 = 2\pi$. Near the termination of the lower band at $E < E_2^+$ the larger localization length is dramatically decreased, driven down by the slow terminating channel. At $E > E_2^+$ the localization length sharply recovers. In numerical simulation the sharpness is smeared by the finite disorder.

latter the suppression is due to $\gamma \sim \pi/2$, which mixes the two effective variances χ_ν^2 equally, while near the band-edge the suppression is due to the vanishing rapidity, which appears in the denominators of the cross sections.

(ii) Anomlies are clearly seen in the numerical data for ξ_1 at energies $E = 0$ and $E \approx 0.1, 0.2$ and 0.9 . The corresponding commensurate combinations of wave vectors are $2(k_1 + k_2) = 2\pi$, $3k_1 + k_2 = 2\pi$, $4k_1 = 2\pi$, and $3k_2 - k_1 = 2\pi$.

4.3 One-channel regime

So far we have discussed the localization lengths in the two-channel regime, where the extended DMPK equation (4.67) applies. In the one-channel regime (see Fig. 4.2) the second channel does not vanish but supports *evanescent* modes. In the presence of disorder a particle in propagating modes can be scattered elastically into these evanescent modes by local impurities. Thus, the evanescent channel is coupled to the propagating channel by random potentials and may influence the transport properties of the system. However, the effect of evanescent modes in the transport properties of 1D disordered systems is scarcely studied.

Bagwell[128] studied in detail the transmission and reflection coefficients in a multi-channel wire with a single δ -function impurity. The evanescent modes renormalize the matrix elements of the impurity potential in the propagating channels. The transmission and reflection coefficients of the propagating channels can be strongly enhanced or suppressed, nevertheless, depending on the strength of the impurity.

The model in Ref. [128] was non-disordered but quite relevant to disordered systems. It is reasonable to argue that in 1D disordered systems the effective disorder in the propagating channels is renormalized by evanescent modes, while the renormalization effect depends upon the strength of disorder.

In the present two-leg Anderson model we specifically analyze the renormalization effect of the evanescent channel in the *weak disorder* limit, which stands on an equal footing with the analysis in the two-channel case. Actually, the special case $t_1 = t_2$ and $\sigma_1^2 = \sigma_2^2$ has been studied analytically early on in Ref. [129]. It was claimed that in the weak disorder limit the effective disorder in the propagating channel is significantly suppressed by the evanescent mode. As a consequence, the localization length defined through the transmission coefficient of the propagating channel is enhanced by a factor ~ 2 compared to the value obtained if the evanescent mode is absent. However, this conclusion was unreliable because the average of the logarithm of transmission eigenvalue was not computed correctly. In contrast, we will prove that the evanescent channel is *decoupled* from the propagating channel to the lowest order in the effective disorder χ_ν^2 defined in Eq. (4.48). The coupling between the two channels becomes relevant only at order χ_ν^4 .

4.3.1 Transfer matrix of an elementary slice

Without loss of generality, we assume that the channel $\tau = 1$ is propagating and $\tau = 2$ is evanescent (the upper branch in Fig. 4.2). A similar analysis applies to the opposite choice (the lower branch in Fig. 4.2). Note first of all that a direct application of the Fokker-Planck equation approach to the transfer matrix given in Eqs. (4.27) and (4.30) would be incorrect. The reason is the following: The weak disorder expansion of the parameters $\vec{\lambda}$, which leads to Eq. (4.51), is ill-defined in the one-channel regime. Note that the amplitude of the evanescent basis $\psi_2(x)$ [see Eq. (4.26)] *grows exponentially* $\sim e^{\kappa_2|x|}$. Likewise, the elements of $\delta\mathbf{m}_x$ [see Eq. (4.27)] with evanescent channel indices also grow exponentially with factors $e^{2\kappa_2|x|}$ or $e^{4\kappa_2|x|}$. Therefore, $\|\delta\mathbf{m}_x/\epsilon\|$ is unbounded in the domain of the coordinate x , and the formal expansion of the parameters $\vec{\lambda}$ in disorder strength is divergent with respect to the length L .³ In order to perform a weak disorder analysis, the basis of the evanescent channel should be chosen as

$$\psi_2^\pm(x) = e^{\mp\kappa_2 x} / \sqrt{2 \sinh \kappa_2}, \quad \kappa_2 > 0, \quad (4.106)$$

which replaces the current-conserving basis Eq. (4.26), and the basis of the propagating channel is the same as Eq. (4.24) even though with $\tau = 1$. In this newly defined basis, the transfer matrix of elementary slice takes the form (see Appendix D)

$$\mathbf{m}_x = \mathbf{m} + \delta\mathbf{m}_x, \quad (4.107)$$

with

$$\mathbf{m} = \text{diag}(1, 1, e^{-\kappa_2}, e^{\kappa_2}), \quad \delta\mathbf{m}_x = \begin{pmatrix} \delta m_1^1 & \delta m_2^1 \\ \delta m_1^2 & \delta m_2^2 \end{pmatrix}, \quad (4.108)$$

whose blocks are

$$\delta m_1^1 = i \frac{\epsilon_{11}}{2 \sin k_1} \begin{pmatrix} -1 & -e^{-i2k_1 x} \\ e^{i2k_1 x} & 1 \end{pmatrix}, \quad (4.109a)$$

³Repeating the perturbative calculation in App. B, we can obtain three cross-sections similar to Eq. (4.59), in which V_2 and V_3 acquire exponential growing factors $e^{4\kappa_\nu|x|}$ and $e^{2\kappa_\nu|x|}$. Thus the obstacle of divergence can be rephrased in this way: The intensities of intra-evanescent-channel and inter-channel scattering (either forward or backward) are amplified exponentially with respect to the coordinate of the elementary slice, which invalidates the weak disorder expansion of $\vec{\lambda}$.

$$\delta m_2^1 = i \frac{\epsilon_{12}}{2\sqrt{\sin k_1 \sinh \kappa_2}} \begin{pmatrix} -e^{-\kappa_2} e^{-ik_1 x} & -e^{\kappa_2} e^{-ik_1 x} \\ e^{-\kappa_2} e^{ik_1 x} & e^{\kappa_2} e^{ik_1 x} \end{pmatrix}, \quad (4.109b)$$

$$\delta m_1^2 = \frac{\epsilon_{21}}{2\sqrt{\sin k_1 \sinh \kappa_2}} \begin{pmatrix} -e^{ik_1 x} & -e^{-ik_1 x} \\ e^{ik_1 x} & e^{-ik_1 x} \end{pmatrix}, \quad (4.109c)$$

$$\delta m_2^2 = \frac{\epsilon_{22}}{2 \sinh \kappa_2} \begin{pmatrix} -e^{-\kappa_2} & -e^{\kappa_2} \\ e^{-\kappa_2} & e^{\kappa_2} \end{pmatrix}, \quad (4.109d)$$

where \mathbf{m} and $\delta\mathbf{m}_x$ are the disorder-free and disordered part of the elementary slice \mathbf{m}_x , respectively. The transfer matrix of a bulk with length L is still defined by the products in Eq. (4.30). Two important points should be emphasized.

(i) Compared with Eq. (4.27) in the two-channel case, the second and third rows and columns of Eq. (4.107) have been simultaneously permuted. The diagonal blocks δm_1^1 and δm_2^2 represent the scattering in the propagating and evanescent channels, respectively, and the off-diagonal blocks $\delta m_{2(1)}^{1(2)}$ represent the scattering between the two channels. In each block, the first and second diagonal elements describe the scattering inside right (+) and left (−) branches respectively, and the off-diagonal elements describe the scattering between the two branches. For instance, δm_{1+}^{2-} labels the 21 element of δm_1^2 and stands for a scattering event from the left evanescent channel to the right propagating channel.

(ii) The disordered part $\delta\mathbf{m}_x$ *does not* contain exponentially growing and/or decaying terms, and hence $\|\delta\mathbf{m}_x/\epsilon\|$ is uniformly bounded for any x . Instead, the disorder-free part \mathbf{m} , which is still diagonal but not unity any more, contains the growing and decaying factor of the evanescent mode per lattice spacing. The exponentially growing and decaying characteristics of evanescent modes are represented in the products of the disorder-free part $\prod_{x=1}^L \mathbf{m}$.

4.3.2 Weak disorder analysis of Lyapunov exponents

In order to calculate the transmission coefficient of the propagating channel, through which the localization length is defined (see Sec. 4.3.3), we have to know the Lyapunov exponents of $\mathbf{M}(L)$ in Eq. (4.30). We are going to determine the Lyapunov exponents by the method introduced in Ref. [126].

The Lyapunov exponents of the present model can be computed via the following recursive relations for the four vectors $V_{i=1,\dots,4}$:

$$V_{1,x+1} = \mathbf{m}_x V_{1,x}, \quad (4.110a)$$

$$V_{i,x+1} = \mathbf{m}_x V_{i,x} - \sum_{j=1}^{i-1} \frac{V_{j,x+1} \cdot (\mathbf{m}_x V_{i,x})}{V_{j,x+1} \cdot V_{j,x+1}} V_{j,x+1}, \quad 2 \leq i \leq 4. \quad (4.110b)$$

Note that the vectors are orthogonalized by Gram-Schmidt procedure after every multiplication by the transfer matrices (4.107). The Lyapunov exponents are extracted from the growing rate of the amplitudes of the respective vectors:

$$\gamma_i = \lim_{L \rightarrow \infty} \frac{1}{2L} \left\langle \ln \frac{|V_{i,L}|^2}{|V_{i,1}|^2} \right\rangle, \quad 1 \leq i \leq 4, \quad (4.111)$$

in which $\langle \cdot \rangle$ is the average over realizations of disorder along the strip. Moreover, $\{\gamma_i\}$ are in descending order:

$$\gamma_1 \geq \gamma_2 \geq \gamma_3 \geq \gamma_4. \quad (4.112)$$

The initial vectors $V_{i,1}$ of the recursive relations (4.110) can be randomly chosen but must be *linearly independent*. In the absence of specific symmetry constraints the Lyapunov exponents are non-degenerate in the presence of the disordered part of \mathbf{m}_x . Additionally, because of the symplecticity of $\tilde{\mathbf{m}}_x$ represented in Eq. (4.21) the Lyapunov exponents are related by

$$\gamma_3 = -\gamma_2, \quad \gamma_4 = -\gamma_1, \quad (4.113)$$

which is proved in App. D. Therefore, only the first two recursions in Eq. (4.110) are needed.

In the absence of disorder the four Lyapunov exponents take the values:

$$\gamma_1|_{\epsilon=0} = \kappa_2, \quad \gamma_2|_{\epsilon=0} = \gamma_3|_{\epsilon=0} = 0, \quad \gamma_4|_{\epsilon=0} = -\kappa_2, \quad (4.114)$$

in which the two Lyapunov exponents corresponding to the propagating channel are *degenerate*. Therefore, we make an *ansatz* on the first two vectors, which separates their “moduli”

and “directions,”

$$V_{1,x} = v_{1,x} \begin{pmatrix} s_1(x) \\ s_2(x) \\ s_3(x) \\ 1 \end{pmatrix}, \quad V_{2,x} = v_{2,x} \begin{pmatrix} p(x) \\ q(x) \\ t_3(x) \\ t_4(x) \end{pmatrix}, \quad (4.115)$$

in which

$$s_{1,2,3}(x), t_{3,4}(x) \sim O(\epsilon), \quad (4.116)$$

$|s_{1,2,3}(x)/\epsilon|$ and $|t_{3,4}(x)/\epsilon|$ are bounded for all x , and

$$|p(x)|^2 + |q(x)|^2 = 1. \quad (4.117)$$

Eventually, the Lyapunov exponents are determined by the growth rate of $\{v_{i,x}\}$, which is easy to be realized from Eqs. (4.111) and (4.115). The initial vectors of Eq. (4.115) are chosen as the eigenvectors of the disorder-free part of the transfer matrix \mathbf{m} (see Eq. (4.108)):

$$V_{1,1} = \begin{pmatrix} 0 \\ 0 \\ 0 \\ 1 \end{pmatrix}, \quad V_{2,1} = \begin{pmatrix} p(1) \\ q(1) \\ 0 \\ 0 \end{pmatrix}, \quad (4.118)$$

with some $p(1)$ and $q(1)$ satisfying $|p(1)|^2 + |q(1)|^2 = 1$.

Note that the ansatz (4.115) is reasonable in the sense of a perturbative analysis. Consider the final vectors after L iterations of Eq. (4.110) with the initial condition Eq. (4.118). In the absence of disorder, it is easy to obtain $V_{1,L} = e^{\kappa_2 L} V_{1,1}$ and $V_{2,L} = V_{2,1}$. On top of it weak enough disorder will induce perturbative effects: The direction of $V_{1,L}$ will deviate from $V_{1,1}$ *perturbatively* in the strength of disorder. This is characterized by the smallness of $s_{1,2,3}(L)$. In other words, the exponential growth of $|V_{1,L}|$ is dominated by \mathbf{m} . Simultaneously, the degeneracy of the second and third exponents are lifted perturbatively. As a consequence, $\gamma_2 > 0$ and $v_{2,L}$ become exponentially large because of the constraint in Eq. (4.113). $p(L)$ and $q(L)$ are, in general, very different from their initial values $p(1)$ and $q(1)$, while $t_{3,4}(L)$ will be shown to remain small quantities of order ϵ .

The orthogonality between $V_{i,x}$ in Eq. (4.115) gives

$$t_4(x) + s_1^*(x)p(x) + s_2^*(x)q(x) + s_3^*(x)t_3(x) = 0, \quad (4.119)$$

in which the first three terms $\sim O(\epsilon)$ and the last term $\sim O(\epsilon^2)$. Up to the first order in disorder strength, the recursion (4.110a) gives

$$v_{1,x+1} = v_{1,x} [e^{\kappa_2} + \delta m_{2-}^2 + O(\epsilon^2)], \quad (4.120a)$$

$$v_{1,x+1}s_1(x+1) = v_{1,x} [s_1(x) + \delta m_{2-}^{1+} + O(\epsilon^2)], \quad (4.120b)$$

$$v_{1,x+1}s_2(x+1) = v_{1,x} [s_2(x) + \delta m_{2-}^{1-} + O(\epsilon^2)], \quad (4.120c)$$

$$v_{1,x+1}s_3(x+1) = v_{1,x} [e^{-\kappa_2}s_3(x) + \delta m_{2+}^2 + O(\epsilon^2)]. \quad (4.120d)$$

The recursion (4.110b) gives

$$v_{2,x+1} \begin{pmatrix} p(x+1) \\ q(x+1) \end{pmatrix} = v_{2,x} \left[(1 + \delta m_1^1) \begin{pmatrix} p(x) \\ q(x) \end{pmatrix} + O(\epsilon^2) \right], \quad (4.121a)$$

$$v_{2,x+1}t_3(x+1) = v_{2,x} [e^{-\kappa_2}t_3(x) + \delta m_{1+}^{2+}p(x) + \delta m_{1-}^{2+}q(x) + O(\epsilon^2)], \quad (4.121b)$$

$$v_{2,x+1}t_4(x+1) = -v_{2,x} [s_1^*(x+1)p(x) + s_2^*(x+1)q(x) + O(\epsilon^2)]. \quad (4.121c)$$

It can be verified that the higher-order terms $\sim O(\epsilon^2)$ *do not* involve exponentially growing factors, which is guaranteed by the Gram-Schmidt re-orthogonalization procedure in the recursive relations (4.110).

We draw two important observations from Eqs. (4.120) and (4.121):

(i) The ansatz (4.115) is consistent with the perturbative expansion of the recursions (4.110). Here the consistency means that $|s_{1,2,3}(x)/\epsilon|$ and $|t_{3,4}(x)/\epsilon|$ are uniformly bounded after any number of iterations, and the first two Lyapunov exponents can be extracted from $v_{j,x}$.

(ii) Up to linear order in disorder strength, the recursion (4.120a), which determines the first Lyapunov exponent γ_1 , is decoupled from the recursion relation (4.121a), which determines the second Lyapunov exponent γ_2 . However, the coupling terms are present in higher-order

terms. This implies that to the leading order effect in disorder the evanescent and propagating channels evolve independently, the entanglement between the two channels being a higher-order effect.

From Eq. (4.120a) one can easily calculate the first Lyapunov exponent to linear order in the effective variances χ_ν^2 ,

$$\begin{aligned}\gamma_1 &= \lim_{L \rightarrow \infty} \frac{1}{L} \left\langle \ln \prod_{x=1}^L |e^{\kappa_2} + \delta m_{2-}^{2-}(x)| \right\rangle \\ &= \kappa_2 + \left\langle \ln \left| 1 + \frac{\epsilon_{22}}{2 \sinh \kappa_2} \right| \right\rangle \\ &\simeq \kappa_2 - \frac{1}{8 \sinh^2 \kappa_2} \left(\chi_1^2 \sin^4 \frac{\gamma}{2} + \chi_2^2 \cos^4 \frac{\gamma}{2} \right) + O(\chi_\nu^4),\end{aligned}\tag{4.122}$$

in which γ is the mixing angle defined in Eq. (4.12). The minus sign of the leading order corrections implies that the first Lyapunov exponent is *reduced* in the presence of weak disorder.

Equation (4.121a) is exactly the same as in a single chain Anderson model, for which the Lyapunov exponents are already known.[115] The second Lyapunov exponent takes the value

$$\gamma_2 \simeq 2V_1 + O(\chi_\nu^4),\tag{4.123}$$

where V_1 is the Born cross-section given in Eq. (4.59).

Equations (4.122) and (4.123) are our main results for the one-channel case, yielding the localization length and the renormalized decay rate of evanescent waves.

4.3.3 Localization length and evanescent decay rate

The two Lyapunov exponents calculated above can be identified in transport experiments. In general a two-probe experiment has the geometry of the form “lead–sample–lead,” in which the two leads are semi-infinite. The current amplitudes (not the wave amplitudes) are measured in leads. In the propagating channels both right (+) or left (–) modes exist in both of the leads. However, the situation is rather different in the evanescent channels: There are only growing modes (–) in the left lead, and only decaying modes (+) in the right lead. These

modes *do not* carry current at all.[128, 130] Hence the current transmission and reflection coefficients are only defined in propagating channels regardless of the wave amplitudes in evanescent channels. In terms of the transfer matrix $\mathbf{M}(L)$, this restriction on the evanescent channel implies that

$$\begin{pmatrix} a_1^+(L) \\ a_1^-(L) \\ a_2^+(L) \\ 0 \end{pmatrix} = \begin{pmatrix} M_1^1 & M_2^1 \\ M_1^2 & M_2^2 \end{pmatrix} \begin{pmatrix} a_1^+(1) \\ a_1^-(1) \\ 0 \\ a_2^-(1) \end{pmatrix}. \quad (4.124)$$

From the scattering configuration (4.124) one can derive an effective transfer matrix for the propagating channel. The evanescent amplitude $a_2^-(1)$ can be expressed in terms of the propagating amplitudes as

$$a_2^-(1) = -\frac{1}{M_{2-}^{2-}} [M_{1+}^{2-} a_1^+(1) + M_{1-}^{2-} a_1^-(1)]. \quad (4.125)$$

Substituting Eq. (4.125) into Eq. (4.124) we obtain

$$\begin{pmatrix} a_1^+(L) \\ a_1^-(L) \end{pmatrix} = \mathbf{X}(L) \begin{pmatrix} a_1^+(1) \\ a_1^-(1) \end{pmatrix}, \quad (4.126)$$

in which the elements of $\mathbf{X}(L)$ take the form

$$X_+^+ = M_{1+}^{1+} + \Delta M_{1+}^{1+}, \quad \Delta M_{1+}^{1+} = -\frac{M_{2-}^{1+} M_{1+}^{2-}}{M_{2-}^{2-}}, \quad (4.127a)$$

$$X_-^+ = M_{1-}^{1+} + \Delta M_{1-}^{1+}, \quad \Delta M_{1-}^{1+} = -\frac{M_{2-}^{1+} M_{1-}^{2-}}{M_{2-}^{2-}}, \quad (4.127b)$$

$$X_+^- = X_-^{+*}, \quad X_-^- = X_+^{+*}. \quad (4.127c)$$

$\mathbf{X}(L)$ is the effective transfer matrix for the propagating channel. Note that its elements are modified from the values in the absence of the evanescent channel. One can easily verify that $\mathbf{X}(L)$ satisfies time-reversal invariance and current conservation conditions as (4.29) in the single chain case:[119, 120]

$$\mathbf{X}^* = \sigma_1 \mathbf{X} \sigma_1, \quad \mathbf{X}^\dagger \sigma_3 \mathbf{X} = \sigma_3. \quad (4.128)$$

However, $\mathbf{X}(L)$ does not evolve multiplicatively with the length L any more. The transmission coefficient is determined through $\mathbf{X}(L)$ in the usual way[120, 119]

$$T(L) = |X_+^+|^{-2}, \quad (4.129)$$

where X_+^+ is defined in Eq. (4.127a).

Equations (4.127) and (4.129) determine exactly the transmission coefficient of the propagating channel. A full solution requires extensive calculations. However, if the disorder strength is weak, as analyzed in Sec. 4.3.2, the coupling between the two channels is small, so that the contribution of the evanescent channel, ΔM_{1+}^{1+} is negligible. Indeed, from Eqs. (4.110) and (4.115), using initial vectors $V_{1,1} = \begin{pmatrix} 0 & 0 & 0 & 1 \end{pmatrix}^T$ and $V_{2,1} = \begin{pmatrix} 1 & 0 & 0 & 0 \end{pmatrix}^T$, respectively, we can extract the various matrix elements of $\mathbf{M}(L)$, in particular

$$\frac{\Delta M_{1+}^{1+}(L)}{M_{1+}^{1+}(L)} = \frac{s_1(L)t_4(L)}{p(L)} \sim O(\epsilon^2). \quad (4.130)$$

This proves that the contribution of the evanescent channel is subleading at weak disorder. To leading order the transmission coefficient is simply given by the propagating channel as

$$T(L) \simeq |M_{1+}^{1+}|^{-2} \simeq |v_{2,L} p(L)|^{-2}. \quad (4.131)$$

From this the localization length is obtained,

$$1/\xi = - \lim_{L \rightarrow \infty} \frac{1}{2L} \langle \ln T(L) \rangle \simeq 2V_1 + O(\chi_\nu^4). \quad (4.132)$$

Equation (4.132) implies that to leading order in χ_ν^2 the localization length in the propagating channel equals the inverse of the second Lyapunov exponent obtained in Eq. (4.123).

Similarly to Eq. (4.90), we can introduce the localization length enhancement factor

$$r = \xi / \xi_1^{(0)}, \quad (4.133)$$

in which $\xi_1^{(0)}$ is the localization length of the leg 1 (with the larger hopping) in the absence of inter-chain coupling.

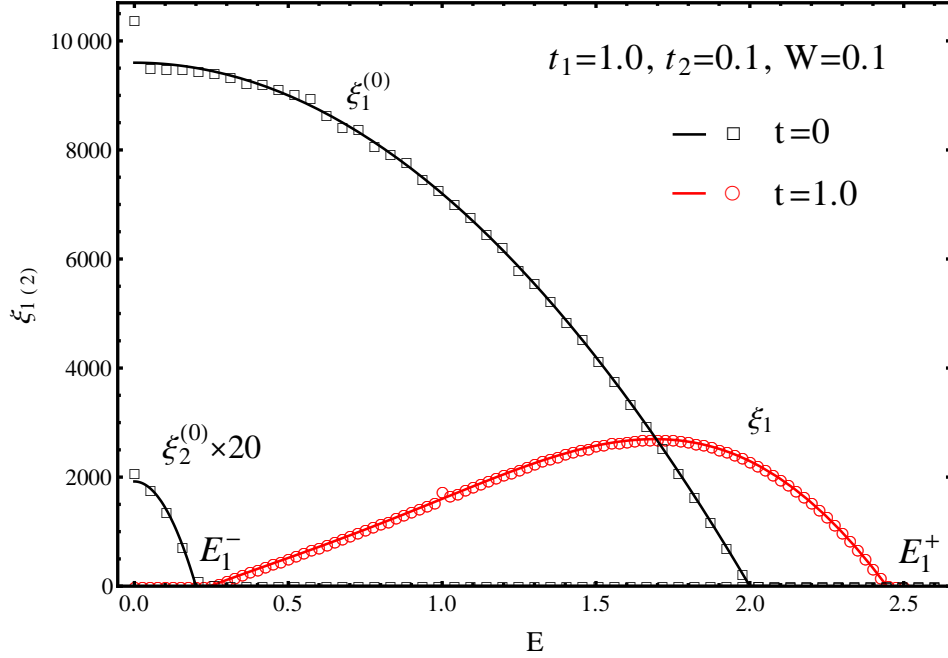


Figure 4.12: Localization length as a function of energy in the one-channel case. Here $t_1 = 1$, $t_2 = 0.1$, $\delta e = 0$ and the amplitude of disorder is $W = 0.1$. The solid curves are analytical results. Black curves correspond to uncoupled chains. The red one corresponds to the upper polariton (conduction) band (propagating channel) for strong coupling $t = 1$, which is obtained by omitting the lower polariton (valence) band (evanescent channel). The squares and circles are data of the numerical transfer matrix. The quantitative agreement is significant except for the anomalous energy $E \simeq 1.0$, which corresponds to the commensurate combination of wave vectors $4k_1 = 2\pi$. The coincidence between analytics and numerics confirms that the evanescent channel is decoupled to the propagating channel in weak disorder limit.

On the other hand, the inverse of the first Lyapunov exponent in Eq. (4.122) should be associated with the evanescent decay rate which is slightly modified by disorder.

The analytical results (4.132) and/or (4.133) are compared with numerics in Figs. 4.7, 4.11, and 4.12. Figures 4.7 and 4.11 correspond to the weak coupling case $t < t_c$ [see Fig. 4.2(a)] and Fig. 4.12 corresponds to the strong coupling case $t > t_c$ [see Fig. 4.2(b)]. The remarkable agreement confirms the weak disorder analysis developed in this section.

We specifically analyze the typical behavior of the enhancement factor $r_1(E)$ close to the band-edge E_2^+ in the case of $t < t_c$, where the system switch from one to two propagating channels. From Eqs. (4.12) and (4.18) it is not hard to obtain: at the band edge E_2^+ , when

coupling is weak $r_1(E_2^+)$ deviates from 1 like

$$1 - r_1(E_2^+) \propto \left(\frac{t}{E_2^+}\right)^2. \quad (4.134)$$

If E is away from E_2^+ , $r_1(E)$ increases linearly, i.e.,

$$r_1(E) - r_1(E_2^+) \propto t^2(E - E_2^+), \quad (4.135)$$

with a fixed but weak coupling t . A typical curve for $r_1(E)$ is shown in the upper right inset in Fig. 4.7.

4.4 Shape and polarization of the wave functions

In certain applications, such as exciton-polaritons, the two linearly coupled types of excitations (represented by the two chains) are very different in nature. This makes it, in principle, possible to probe the original excitations separately from each other. For a two-leg atomic chain one can imagine probing the amplitude of wave function on each of the spatially separated legs. For polaritons the analog would be a separate probing of cavity photons or excitons, for example, by studying the 3D light emitted due to diffraction of cavity photons at surface roughnesses or by studying the exciton annihilation radiation or the electric current of exciton decomposition provoked locally. Therefore it is of practical interest to be able to manipulate the strength of localization of one of the original excitations by coupling them to the other.

4.4.1 Numerical analysis

With this goal in mind we have carried out a numerical study of the amplitude of wave functions on either of the chains in each of the distinct parameter regimes discussed above. We numerically diagonalized the Hamiltonian (4.1) [see Fig. 4.13], choosing $t_1 = 1$, $t_2 = 0.2$, $W = 0.4$, $t = 0.04$. The length of the ladder was taken to be $L = 10^3$ and periodic boundary conditions were used. With the above parameters the localization lengths of the decoupled legs were of the order of $\xi_1^{(0)} \sim 10^3$ and $\xi_2^{(0)} \sim 10$, for energies close to the band-center. In

Fig. 4.13 the black curves depict the amplitudes of eigenfunctions on the fast leg 1, while the red curves show the corresponding amplitudes on the slow leg 2.

Our main findings are as follows.

- (i) $E_2^+ < E < E_1^+$. The energy is far from resonance, and only *one channel* exists. As shown in Fig. 4.13(a), most of the weight is on the fast leg. The amplitude on the slow leg is small but the spatial extension of the component ψ_2 is the same as that of ψ_1 on the fast leg, which is almost unaffected by the chain coupling. Thus, the coupling can create a nonzero amplitude on the chain 2, in the energy region where the decoupled chain 2 cannot support any excitations. The spacial extension is controlled by the localization properties of the leg 1.
- (ii) $t/\kappa(t_1, t_2) < E < E_2^+$. The energy is in the *two-channel, off-resonant regime*. The wave-function components ψ_1 and ψ_2 are characterized by *both* localization lengths ξ_1 and ξ_2 . However, the relative weights of the parts of the wavefunction with the smaller and the larger localization lengths fluctuate very strongly from eigenstate to eigenstate. This is shown in Figs. 4.13(b) and 4.13(c), with two *adjacent* energy levels, which were properly selected. In Fig. 4.13(b), ψ_2 consists almost entirely of a component with the smaller localization length, while the fast leg clearly shows contributions of both components. In Fig. 4.13(c), both ψ_1 and ψ_2 consist almost entirely of a component with the larger localization length. In brief, the former can be thought of as a state on leg 2, which weakly admixes some more delocalized states on leg 1, while the latter wave function is essentially a state of leg 1 which admixes several more strongly localized states on leg 2.

We have checked in specific cases that this interpretation is indeed consistent (see Sec. 4.4.2): In the off-resonant regime the wave functions can be obtained perturbatively in the coupling t , confirming the picture of one-leg wave functions with small admixtures of wave functions on the other leg. Off resonance, the perturbation theory is controlled even for appreciable t , since the matrix elements that couple wave functions of similar energy are very small due to significant cancellations arising from the mismatched oscillations of the wave functions ($k_1 - k_2 > \xi_2^{(0)}$) on the two legs. Resonance occurs precisely when at a fixed energy $k_1 - k_2$ becomes too small, so that the modes on both legs start to mix strongly. A closer analysis of the perturbation theory in special cases shows that the perturbative expansion is expected to break down at the resonant crossover determined further above.

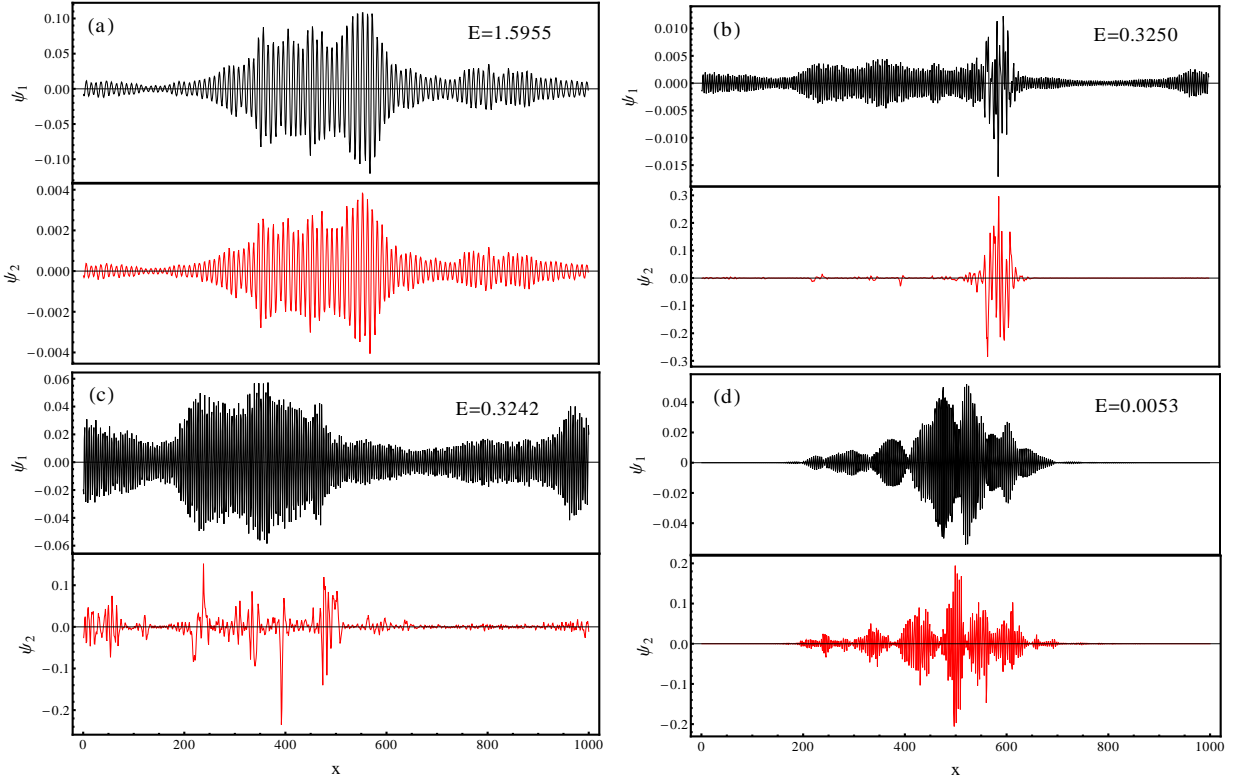


Figure 4.13: Typical wave functions in different regimes. Pay attention to the varying scales for the amplitudes in the various cases. Parameters are $t_1 = 1$, $t_2 = 0.2$, $W = 0.4$, $t = 0.04$, while E selects the regime. The length of the ladder is $L = 10^3$ with periodic boundary condition. The black(red) curves are the amplitudes on the 1(2) leg. (a) $E = 1.5955$, at which only one channel exists. (b), (c) Off-resonant regime: $E = 0.3250$ and $E = 0.3242$ are a pair of adjacent levels of “opposite type.” (d) $E \simeq 0$, which is within the resonant regime.

(iii) $|E| < t/\kappa(t_1, t_2)$. If the energy is in the *resonant regime*, the two localization lengths are of the same order $\xi_1 \sim \xi_2 \sim \xi_2^{(0)}$ and the spatial extension of both wave function components is governed by the localization length $\xi_2^{(0)}$ of the decoupled slow chain. This is illustrated in Fig. 4.13(d).

4.4.2 Perturbative analysis

The properties of eigenstates at different energy regimes can be explained by applying a perturbative analysis on the coupling t . First, we define the relevant quantities of decoupled legs as follows. The eigenstate of the ν leg with eigenenergy $E_{\nu n}$ is $\psi_{\nu n}(x)$. The corresponding

localization length is $\xi_\nu^{(0)}$, where we assume $\xi_1^{(0)} \gg \xi_2^{(0)}$ in order to reveal the resonance-off-resonance crossover. The mean level spacing inside the localization volume is Δ_ν . Because in one dimension a particle is nearly ballistic in its localization volume, which means its wave vector is nearly conserved and its amplitude is almost uniform, we introduce a simple “box” approximation on the eigenstates as the following. Inside the localization volume,

$$\psi_{\nu n}(x) \sim \frac{1}{\sqrt{\xi_\nu^{(0)}}} e^{ik_\nu x}, \quad (4.136)$$

up to a random phase, in which $\xi_\nu^{(0)}$ and k_τ are the localization length and the wave vector at the energy $E_{\nu n}$. Outside the localization volume $\psi_{\nu n}(x) = 0$.

Now we turn on a weak enough coupling t and calculate the deviation of an energy level E_{1n} on the 1 leg. Up to second order in t , the deviation is

$$\delta E_{1n}^{(2)} = t^2 \sum_m \frac{|\int dx \psi_{1n}^*(x) \psi_{2m}(x)|^2}{E_{1n} - E_{2m}}. \quad (4.137)$$

In order to estimate the value of $\delta E_{1n}^{(2)}$ by the r.h.s. of Eq. (4.137) we have to make clear three points.

- (i) The summation is dominated by the terms with the smallest denominators, whose typical value is the mean level spacing Δ_2 .
- (ii) The typical value of the integral on the numerator can be estimated by the “box” approximation introduced above, which gives

$$\int dx \psi_{1n}^* \psi_{2m} \sim \int_0^{\xi_2^{(0)}} dx \psi_{1n}^* \psi_{2m} \sim \left[(k_1 - k_2) \sqrt{\xi_1^{(0)} \xi_2^{(0)}} \right]^{-1}. \quad (4.138)$$

- (iii) We should consider more carefully how many dominant terms there are in the summation. We can easily realize that a state $\psi_{1n}(x)$ on the 1 leg can couple to about $\xi_1^{(0)}/\xi_2^{(0)}$ states $\psi_{2m}(x)$ on the 2 leg. However, the value of the summation is different from a naive deterministic evaluation because the random signs of the denominators. If we neglect the correlation of

these random signs, according to the central limit theorem, the fluctuation of $\delta E_{1n}^{(2)}$ is

$$\left| \delta E_{1n}^{(2)} \right| \sim \sqrt{\frac{\xi_1^{(0)}}{\xi_2^{(0)}}} \times \frac{t^2}{\xi_1^{(0)} \xi_2^{(0)} (k_1 - k_2)^2 \Delta_2}. \quad (4.139)$$

The validity of the perturbation analysis is guaranteed if

$$\left| \delta E_{1n}^{(2)} \right| < \Delta_1, \quad (4.140)$$

which means there is no level crossing in the localization volume of the 1 leg. To estimate the relevant quantities in Eq. (4.140), for simplicity we assume $t_1 \gg t_2$ and $\sigma_1^2 = \sigma_2^2$. If the energy $E = E_{1n}$ is close to the resonant energy E_R , according to Eq. (4.10) and (4.14), we obtain

$$|k_1 - k_2| \sim |E - E_R| (t_1 - t_2) / t_1 t_2. \quad (4.141)$$

The mean level spacings are

$$\Delta_\nu \sim t_\nu / \xi_\nu^{(0)}, \quad (4.142)$$

and the localization lengths satisfy

$$\xi_1^{(0)} / \xi_2^{(0)} \sim t_1^2 / t_2^2. \quad (4.143)$$

Substituting Eqs. (4.141), (4.142) and (4.143) to Eq. (4.140) we obtain the condition

$$t < |E - E_R| (t_1 - t_2) / t_1, \quad (4.144)$$

which is consistent with the result of Eq. (4.84) with $t_1 \gg t_2$. Therefore, Eq. (4.140) is essentially equivalent to the criterion for being off resonant ($\Delta V > 0$) at weak coupling t .

4.5 Limit of vanishing hopping on the “slow” leg

In the present work we are particularly interested in the case that the localization lengths of the uncoupled legs are parametrically different $\xi_1^{(0)} \gg \xi_2^{(0)}$. Accordingly, we refer to the

two legs as the “fast” and the “slow” one, respectively. So far we have analyzed the model extensively in the weak disorder limit $\xi_\nu^{(0)} \gg 1$ where the disorder is weak for *both* of the two legs and thus $\xi_\nu^{(0)} \gg 1$.

Another interesting situation is the case where the hopping strength on the slow leg vanishes $t_2 = 0$ or weak enough. This is experimentally relevant for polariton systems in which the exciton hopping is weak as compared to the disorder potential. In this case the dimensionless disorder parameter which we introduced previously diverges $\chi_2^2 \rightarrow \infty$, and formally $\xi_2^{(0)} = 0$ even if the disorder strength on the 2-leg is arbitrarily small. For this reason the perturbative analysis in χ_ν^2 breaks down. Nevertheless, this limit case can be solved exactly, too, but requires a different treatment which is beyond the weak disorder analysis.

If $t_2 = 0$ the second leg is composed of mutually nonconnected sites, which form a comb structure together with the first leg. The Schrödinger equation (4.4) takes the form

$$\begin{pmatrix} -t_1 & 0 \\ 0 & 0 \end{pmatrix} [\Psi(x+1) + \Psi(x-1)] = \begin{pmatrix} E - \epsilon_{x1} & t \\ t & E - \delta e - \epsilon_{x2} \end{pmatrix} \Psi(x), \quad (4.145)$$

where

$$\Psi(x) = \begin{pmatrix} \psi_1(x) \\ \psi_2(x) \end{pmatrix}, \quad (4.146)$$

describes the amplitudes on the two legs, respectively. We can obtain the effective Schrödinger equation for $\psi_1(x)$ by eliminating $\psi_2(x)$ in Eq. (4.145):

$$-t_1 [\psi_1(x+1) + \psi_1(x-1)] = (E - \tilde{\epsilon}_{x1})\psi_1(x-1), \quad (4.147)$$

where

$$\tilde{\epsilon}_{x1} = \epsilon_{x1} + \frac{t^2}{E - \delta e - \epsilon_{x2}}. \quad (4.148)$$

Note that $\tilde{\epsilon}_{x1}$ has the meaning of an effective disorder potential on the 1-leg. Furthermore, if $|\epsilon_{x2}| \ll |E - \delta e|$ Eq. (4.148) can be expanded as

$$\tilde{\epsilon}_{x1} \simeq \frac{t^2}{E - \delta e} + \left[\epsilon_{x1} + \frac{t^2}{(E - \delta e)^2} \epsilon_{x2} \right] + O(\epsilon^2). \quad (4.149)$$

The first term on the r.h.s. of Eq. (4.149) is a homogeneous potential shift, and the second term is an effective disorder potential of mean-zero.

Equations (4.147) and (4.149) present a single-chain problem, which can be solved exactly. The dispersion relation of the disorder-free part is determined by

$$-2t_1 \cos k + \frac{t^2}{E - \delta e} = E, \quad (4.150)$$

which gives the two nonoverlapping bands

$$E_\tau(k) = -t_1 \cos k + \frac{\delta e}{2} - (-1)^\tau \sqrt{\left(t_1 \cos k + \frac{\delta e}{2}\right)^2 + t^2}. \quad (4.151)$$

Of course, this coincides with Eq. (4.15) for $t_2 = 0$. Using the result for a single-chain Anderson model[115] we obtain the localization length as

$$1/\xi = \frac{\chi_1^2 + \tilde{\chi}_2^2 \tan^2 \gamma}{8 \sin^2 k} + O(\chi_1^4, \tilde{\chi}_2^4), \quad (4.152)$$

Here, the disorder on the leg 2 is measured by the dimensionless ratio

$$\tilde{\chi}_2 = \frac{\sigma_2^2}{t_1^2}, \quad (4.153)$$

γ is the mixing angle defined in Eq. (4.12) with $t_2 = 0$. Comparing the result (4.152) with Eq. 4.132, which describes the one-channel case in the weak disorder limit ($W_2 \ll t_2$), one sees that the two limits do not commute. This is similar to the non-commutativity of the limits of weak disorder and weak inter-chain coupling in the resonant case. As in Eq. (4.62) the characteristic disorder energy scale is the mean level spacing in the localization volume when $t_2 = 0$, which can be estimated as

$$\delta \tilde{E} \sim t_1/\xi \sim \max\{\sigma_1, \sigma_2\}/t_1. \quad (4.154)$$

A perturbative analysis in t_2 is valid only if $t_2 \ll \delta \tilde{E}$. We expect a crossover to the regime of strong hopping on the slow leg when $t_2 \sim \delta \tilde{E}$.

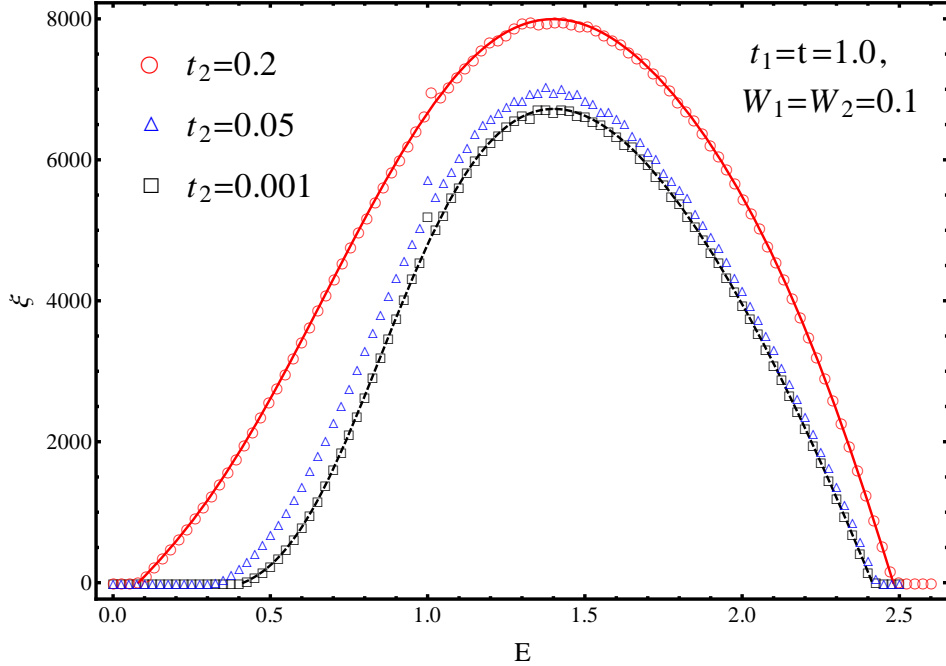


Figure 4.14: Localization length as a function of energy for three values of t_2 for three values of t_2 . $t_1 = t = 1$ and $W_1 = W_2 = 0.1$ are kept fixed. $t_2 = 0.2, 0.05,$ and 0.001 capture the weak disorder limit, the intermediate regime and the limit of a nearly disconnected slow leg, respectively. The symbols are data of numerical transfer matrix. The solid and the dashed curve are the analytical results in Eqs. (4.132) and (4.152). The agreement with numerics in the limiting cases is very good. The localization length increases monotonically with t_2 for a fixed energy. An anomaly due to the commensurate wave vector $4k = 2\pi$ appears at $E \approx 1.0$.

The non-commutativity of the two limits is illustrated in Fig. 4.14 where we compare the two analytical limits with numerical simulations at fixed disorder $W_1 = W_2 = 0.1$ and hoppings $t_1 = t = 1$. Three values of t_2 are selected to cover the crossover from the weak disorder limit ($t_2 \gg W_2$) to the limit of a slow leg with disconnected sites ($t_2 \rightarrow 0$). Equations (132) and (152) are indeed seen to capture the two limits very well. Note that the localization length increases monotonically with t_2 for a fixed energy, as one may expect.

4.6 Possible application to polaritons

The most important potential application of our theory is in the realm of polaritons in quasi-one-dimensional semiconductor structures [72, 73]. Here the fast chain corresponds to the

electromagnetic modes (“light”) confined in a one-dimensional structure and therefore having a parabolic dispersion with a very small mass (large t_1) at small wave vectors. The slow chain corresponds to the Wannier-Mott excitons, an electron-hole pair coupled by Coulomb attraction. The mass of the exciton is typically 10^4 times larger than that of “light”. Surface roughness of the one-dimensional structure and impurities therein produce a disorder potential acting on both excitons and “light” [74, 75]. Experimentally, one can easily probe the intensity of the “light” component by measuring the intensity of three-dimensional photons that emerge due to diffraction from the surface roughness. The amplitude of the wave function of the exciton’s center of mass is more difficult to access, but, in principle, still possible, for example, via stimulated or spontaneous exciton recombination and the related radiation. Another application is related with one-dimensional structures in cold-atom traps. By this technique one can construct and study coupled one-dimensional chains in the same way as it was recently done for a single chain [131, 132].

While all possible regimes can be achieved in a system of cold atoms, the most relevant regime for one-dimensional cavity polaritons is that described in Fig. 4.2(b), where for each band (the lower and the upper polariton bands) only one channel exists. This is because the exciton-light coupling is typically stronger than the narrow bandwidth $t_2 \sim 1/m_{\text{exc}}$ of the excitons. The localization length in the case relevant for the upper exciton-polaritons is shown in Fig. 4.12.

As expected, the localization length tends to zero near the bottom and the top of the band, due to the vanishing rapidity. Note that in the context of polaritons the upper band edge does not exist, since the light has an unbounded continuous spectrum. In our model the top of the band appears merely due to the discreteness of the lattice. In the center of the band the localization length is of the order of the localization length for the uncoupled “light” component. More important is the distribution of amplitudes of “light” and “exciton” wave functions which are similar to Fig. 4.13(a), with “light” being represented by the wave function ψ_1 on the fast leg and the “exciton” part being represented by the wave function ψ_2 on the slow leg. One can see that the coupling to light makes the exciton wave function spread over a distance $\xi \sim \xi_1^{(0)}$ of the order of the localization length of light. This is much larger than the maximum exciton localization length $\xi_2^{(0)}$ in the absence of coupling. The price for the “fast transit” is that the amplitude of the exciton wave function is small. This means that

the transfer of a locally created exciton to distances of order $\xi_1^{(0)}$ is possible, but occurs with reduced probability.

In the long search for light localization (see the paper by Lagendijk, van Tiggelen, and Wiersma in Ref. [24]) the crucial point was to achieve a smaller localization length of light. Our results show that this can also be achieved by coupling light to excitons near the bottom of the upper polariton band.

We would like to emphasize that the model considered above does not take into account an important property of polaritons, namely their finite lifetime due to recombination of excitons, and the out-coupling of the light from the waveguide. This limits the coherence of polaritons and inhibits Anderson localization. More precisely, the effects of Anderson localization are relevant only if the time to diffuse up to the scale of the localization length (which by Thouless' argument is of the order of the inverse level spacing in the localization volume) is smaller than the life time of the excitons. Further crucial aspects are interactions among polaritons at finite density and the related possibility of interaction-induced delocalization and Bose condensation of polaritons[107]. A complete theory of localization of hybrid particles like polaritons should take into account all these issues.[109]

Chapter 5

Anderson localization on two-layer Bethe lattice

One of the most significant results obtained in the case of two coupled chains in Chap. 4 is that there are two regimes: (i) The resonance regime, where the slow chain dominates the localization length of the ladder [see Figs. (4.7), (4.8), and (4.13)]. This slow-chain dominance is a manifestation of the fact that in one dimension the *backscattering* rate determines the localization properties of a coupled system, since the localization length is of the order of the mean free path. (ii) The off-resonance regime, where the fast chain helps to delocalize the slow chain, although with low efficiency [See Figs. (4.10) and (4.13)]. In both cases disorder is the smallest energy scale, which is characterized by Eqs. (4.49) and (4.61). There is also the special case when the disorder is larger than the intrachain coupling for the slow chain. The extreme case of $t_2 = 0$ has been discussed in Sec. 4.5. From Eq. (4.148) we obtain: (i) For $|\epsilon_{x2}| \rightarrow \infty$, there is no effect of the slow chain on the fast chain. (ii) As long as $|t^2/\epsilon_{x2}|$ is comparable with $|\epsilon_{x1}|$ the disorder on the fast chain starts to be enhanced by the slow chain, while the slow is not much affected by the fast.

In high dimensions $D > 2$, weak disorder does not have significant effect on localization. Hence, we are restricted to consider intermediate or strong disorder in order to address the question of the role of interchain coupling. In the meanwhile, since the disorder is compa-

rable with or stronger than the intra- and interchain coupling, the resonance conditions are impossible. In the *absence* of resonance there are only two possible regimes:

(i) The less disordered channel promotes the more disordered one (delocalization), when the disorder on the more disorder one is not too strong. This can be verified by studying how a nearly delocalized (fast) channel reacts to the coupling with a more disordered (slow) channel, and establish that the coupling will pushed the system into a delocalized phase (cf. Regime A in Fig. 5.4).

(ii) The less disordered channel becomes more localized without substantially delocalizing the more disordered one, when the disorder on the more disordered one is extremely strong. This can be verified by studying a critical channel coupled to a strongly localized one and to observe it becoming localized, without substantial variation of the localization properties of the strongly localized channel (cf. Regime B in Fig. 5.4).

In this chapter we study two coupled Bethe lattices whose transport characteristics are different, which can be viewed as the limit of infinite dimensions $D \rightarrow \infty$ of the problem, and to contrast the results with the two-chain (one-dimensional) case. The model provides a very useful indication for high ($D > 2$) but finite-dimensional cases, since it is still simple enough to be studied exactly.

Form the point of view of mathematics, the Bethe lattice is an infinitely large Cayley tree, that is, a graph without loop where each vertex has the same coordination number $K + 1$. The main difference between the two is that a Cayley tree contains the boundaries whereas the Bethe lattice does not. The boundary of a Cayley tree contains a large number of sites, which is of the order of the number of sites of the entire tree. Hence, the boundary effect on a Cayley is significant. Alternatively, the Bethe lattice can be considered as the large-size limit of a random $K + 1$ -regular graph, that is, a graph where each site connects to other randomly and uniformly chosen $K + 1$ sites. It is known that any finite portion of such a graph is a tree, with probability going to one as the size tends to infinity. The advantage of the random-graph construction is the absence of the boundary effect. It can be viewed as regular trees wrapped to themselves.

Statistical models on the Bethe lattice[133, 134] have attracted a lot of studies, because they admit exact solutions and reflect essential features of the systems in sufficiently high spatial dimensions. In particular, the Anderson model on the Bethe lattice was first introduced and solved exactly by Abou-Chacra, Anderson, and Thouless in Refs. [135, 136], where the existence of the Anderson transition was proved and the location of a mobility edge was found. It proved that localization is possible in the *absence* of loops in the lattice. Their method is based on a study of the self-consistent equation for the onsite self energy, which leads to a nonlinear integral equation for the probability distribution function of the self energy. The transition from the localized phase to the delocalized phase is characterized by the instability of the real solution of the self energy with respect to inserting an infinitesimal imaginary energy shift. Physically, the latter describes an infinitesimally weak coupling to a dissipative bath, e.g., photons. The stationary distribution function of the self energy can be found numerically based on the population dynamics, also called the “pool” method[135]. This original work has inspired a number of studies in both the physics[137]–[140] and the mathematics[141]–[145] communities.

For two coupled Bethe lattices, Following Abou-Chacra *et al.*[135, 136], we derive a recursive relation for the local Green’s functions, which are in the form of a 2×2 matrix, and study the effect of interlattice coupling on the Anderson transition at the band center ($E = 0$) in the case of two lattices with identical hopping but different disorder. The existence of the two regimes proposed above is verified.

This chapter is organized as follows. In Sec. 5.1 we introduce the Anderson model on two coupled Bethe lattices and derive the recursion relation for the local Green’s functions. In Sec. 5.2 we briefly present the algorithm of the population dynamics, which is used to study the statistics of the self energy. In Sec. 5.3 we show the phase diagram and explain it by a perturbative analysis.

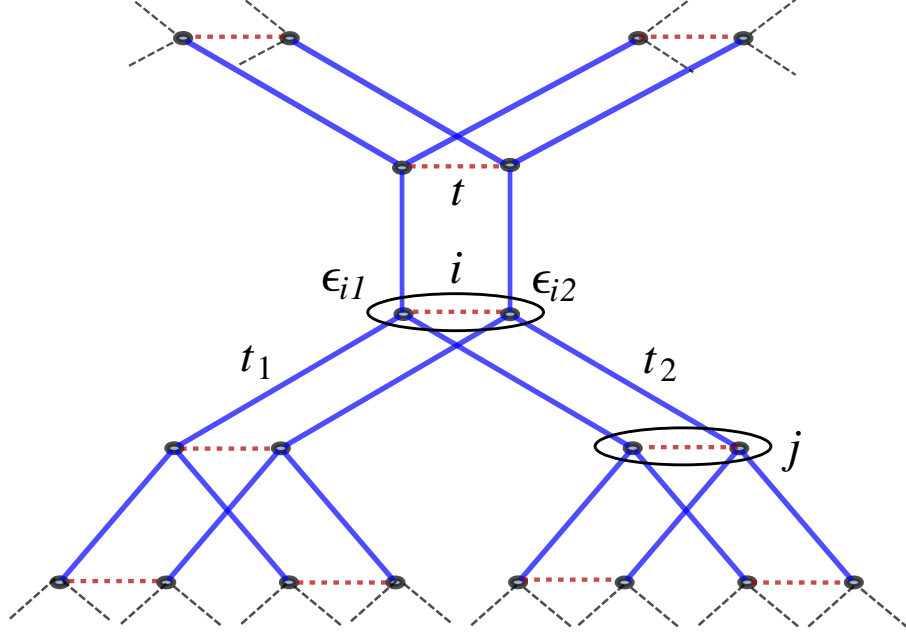


Figure 5.1: Diagram for the Anderson model on the two-layer Bethe lattice ($K = 2$) described by the Hamiltonian (5.1).

5.1 Anderson model and the recursion relation for the local Green's functions

Analogous to the two-chain model in Eq. (4.1), the Hamiltonian of the Anderson model on a two-layer Bethe lattice, as shown in Fig. 5.1, takes the form

$$H = \sum_{\nu=1,2} \left(\sum_i \epsilon_{i\nu} c_{i\nu}^\dagger c_{i\nu} - t_\nu \sum_{\langle i,j \rangle} (c_{i\nu}^\dagger c_{j\nu} + h.c.) \right) - t \sum_i (c_{i1}^\dagger c_{i2} + h.c.), \quad (5.1)$$

where i is the coordinate of a site on the Bethe lattice with coordination number $K + 1$, $\nu \in \{1, 2\}$ is the index labeling the two layers, and $\langle i, j \rangle$ denotes two nearest-neighbor sites i and j . In the model, the on-site energies $\epsilon_{i\nu}$ are independently distributed Gaussian random variables with zero mean, t_ν is the longitudinal hopping strength between nearest-neighbor sites on the ν th layer, and t is the transverse hopping strength between the two layers. In general, the two layers will be subject to different random potentials, characterized by two

probability distribution functions $p_\nu(\epsilon)$. For convenience we assume they are box distributed:

$$p_\nu(\epsilon) = \begin{cases} 1/W_\nu, & \epsilon \in [-W_\nu/2, W_\nu/2], \\ 0, & \text{otherwise.} \end{cases} \quad (5.2)$$

The longitudinal hopping strengths t_ν 's can also be different.

Our aim is to study the effect of weak interlattice coupling on the Anderson transition of the system. In the present thesis we only consider the case of $t_1 = t_2$, $\delta e = 0$, and $W_1 \neq W_2$. This parallels with the case of two resonant chains described in Fig. 4.8. However, as shown in Sec. 5.3, the parameter range under discussing is $W_{1,2} \gtrsim t, t_{1,2}$, which is contrasted with the weak disorder limit in the two-chain problem [see Eqs. (4.49) and (4.61)], and resonance between the two lattices is not possible.

The retarded Green's function at the energy E is defined by

$$G_{i\mu,j\nu}(E) = \langle i, \mu | \frac{1}{E + i\eta - \hat{H}} | j, \nu \rangle, \quad |i, \nu\rangle \equiv c_{i\nu}^\dagger |\text{Vacuum}\rangle, \quad (5.3)$$

where η is a positive and infinitely small real number, representing an infinitesimally weak coupling to a dissipative bath, for example, phonons. We introduce 2×2 matrices \hat{H}_i , \hat{G}_i , and \hat{T} , whose elements are

$$\langle \mu | \hat{H}_i | \nu \rangle = \langle i, \mu | \hat{H} | i, \nu \rangle, \quad (5.4a)$$

$$\langle \mu | \hat{G}_i | \nu \rangle = G_{i\mu,i\nu}, \quad (5.4b)$$

$$\langle \mu | \hat{T} | \nu \rangle = \delta_{\mu\nu} t_\mu. \quad (5.4c)$$

On can prove that $\hat{G}_i = \hat{G}_i(E)$ satisfies the following equation:

$$\hat{G}_i = \frac{1}{E + i\eta - \hat{H}_i - \hat{T} \sum_{j \in \partial i} \hat{G}_j^{(i)} \hat{T}}, \quad (5.5a)$$

where ∂i denotes the set of neighbors of i , and $\hat{G}_j^{(i)}$ contains the Green's functions at the coordinate j in the absence of the bonds between i and j . $\hat{G}_j^{(i)} = \hat{G}_j^{(i)}(E)$ satisfies the recursive

relation

$$\hat{G}_j^{(i)} = \frac{1}{E + i\eta - \hat{H}_j - \hat{T} \sum_{k \in \partial j|i} \hat{G}_k^{(j)} \hat{T}}, \quad (5.5b)$$

where $\partial j|i$ denotes the set of neighbors of j excluding i . \hat{G}_i and $\hat{G}_j^{(i)}$ are complex and symmetric matrices. In order to obtain \hat{G}_i 's, we first solve the recursion relation (5.5b), and then substitute the solution in Eq. (5.5a).

The self energies are defined by the diagonal matrix elements of $\hat{G}_j^{(i)}$'s, that is, $G_{j,\nu\nu}^{(i)}$ ($\nu = 1, 2$) via

$$S_{j\nu}(E) = E + i\eta - \epsilon_{j\nu} - 1/G_{j,\nu\nu}^{(i)}, \quad \Gamma_{j\nu}(E) \equiv \text{Im}S_{j\nu}(E), \quad (5.6)$$

where the imaginary part $\Gamma_{j\nu}(E)$ defines the ‘‘decay rate’’ of the state $|j, \nu\rangle$ at the energy E . The characteristics of the stationary distributions of the decay rate $\Gamma_{j\nu}$, defined in Eq. (5.6), with respect to the recursions (5.5a) and (5.5b), determines whether the system is in the localized phase or in the delocalized phase[13, 135, 136, 53]:

$$\lim_{\eta \rightarrow 0} \lim_{\mathcal{N} \rightarrow \infty} P(\Gamma_1 > 0 \text{ or } \Gamma_2 > 0) = \begin{cases} 0, & \text{localized,} \\ > 0, & \text{delocalized,} \end{cases} \quad (5.7)$$

where \mathcal{N} is the number of sites of the lattice. Here we note: (i) The thermodynamic limit, $\mathcal{N} \rightarrow \infty$, and the limit of vanishing dissipation, $\eta \rightarrow 0$, do not commute, since in a finite system, whose spectrum is discrete, $\eta \rightarrow 0$ always leads to a zero decay rate. (ii) The values of the decay rate on the two sublattices $\Gamma_{\nu=1,2}$ are statistically dependent in the presence of coupling. (iii) The average value of Γ_ν , namely $\langle \Gamma_\nu \rangle$, *can not* be used to indicate the Anderson transition, because in the localized phase an infinitesimal dissipation η leads to appearance of long tails in the distribution function of Γ_ν . Instead, the typical value of Γ_ν , which is defined by the geometric average

$$\Gamma_{\text{typ},\nu} = e^{\langle \ln \Gamma_\nu \rangle}, \quad (5.8)$$

can determine the transition in such a way that

$$\lim_{\eta \rightarrow 0} \lim_{\mathcal{N} \rightarrow \infty} \Gamma_{\text{typ}, \nu} = \begin{cases} 0, & \text{localized,} \\ > 0, & \text{delocalized.} \end{cases} \quad (5.9)$$

5.2 Anderson transition and population dynamics

A precise way to determine the mobility edge by Eqs. (5.5a) and (5.5b) was proposed in Ref. [135, 136]. It is based on analyzing the stability of the real solution of Eq. (5.5b) at the energy E with respect to the insertion of an infinitesimal imaginary energy shift $i\eta$. In the localized phase the real solution is stable, which means the typical value of the decay rate vanishes $\Gamma_{\text{typ}}(E + i\eta) \rightarrow 0$ as $\eta \rightarrow 0$. In the delocalized phase, however, the solution has a finite imaginary part with probability one, which means $\Gamma_{\text{typ}}(E + i\eta) \neq 0$ as $\eta \rightarrow 0$. The physical interpretation of this procedure is: For a finite but large tree, if the boundary sites are coupled to a bath with a dissipation rate η , we test whether the dissipation at the root of the tree, measured by $\Gamma_{\text{typ}}(E)$, is vanishing or not as the tree size tends to infinity. If E is in the localized regime, particle transport is absent at large scale and there is no dissipation at the root. In contrast, in the delocalized regime we do observe a finite dissipation. This procedure is consistent with the criterion for the Anderson transition in Eq. (5.7). This stability analysis can be realized by the population dynamics as follows.

The population dynamics, also called the “pool” method, is a numerical recipe to solve the random recursive relation Eq. (5.5b). A complete description of the algorithm can be found in Refs. [135], [138]-[140]. The basic idea is to simulate the distribution of a random variable X by the empirical distribution of a large population of representants $\{X_\alpha\}_{\alpha=1}^{\mathcal{N}}$. Here the random variable X is the symmetric 2×2 matrix $\hat{G}_j^{(i)}$. For simplicity, we denote $\hat{G}_j^{(i)}$ by \hat{G} , and the population by $\{\hat{G}_\alpha\}_{\alpha=1}^{\mathcal{N}}$. We choose the initial condition of the population $\{\hat{G}_{\alpha,0}\}_{\alpha=1}^{\mathcal{N}}$ whose matrix elements are

$$(\hat{G}_{\alpha,0})_{\nu\nu} = (E - \epsilon_{\alpha\nu} + i\eta)^{-1}, \quad \nu \in \{1, 2\}, \quad (5.10)$$

where $\epsilon_{\alpha\nu}$ are randomly and independently drawn from the probability distribution in Eq. (5.2), and η is a small positive number, and

$$(\hat{G}_{\alpha,0})_{12} = (\hat{G}_{\alpha,0})_{21} = 0. \quad (5.11)$$

Essentially, this initial condition describes \mathcal{N} uncoupled sites subject to a random potential and a small dissipation. The simulation consists of a number of sweeps of the population. After the n_s th ($n_s \in \mathbb{N}$) sweep, we denote the population as $\{\hat{G}_{\beta,n_s}\}_{\alpha=1}^{\mathcal{N}}$. For the n_s th sweep we update the matrices \hat{G}_{α,n_s-1} 's one by one from $\alpha = 1$ to $\alpha = \mathcal{N}$. For updating the β th matrix \hat{G}_{β,n_s-1} , we do the follows. (i) Choose K matrices randomly and uniformly from the population $\{\hat{G}_{\alpha,n_s-1}\}_{\alpha=1}^{\mathcal{N}}$, and call them $\{\hat{G}_{\alpha_1,n_s-1}, \dots, \hat{G}_{\alpha_K,n_s-1}\}$. (ii) Generate $2K$ random numbers according to the probability distribution function in Eq. (5.2), and call them $\{\epsilon_{1\nu}, \dots, \epsilon_{K\nu}\}$ with $\nu = 1, 2$. (iii) Substitute the quantities obtained in (i) and (ii) on the right hand side of Eq. (5.5b) with $\eta = 0$, and thereby, obtain a new matrix \hat{G}_0 on the left hand side. (iv) Replace \hat{G}_{β,n_s-1} by \hat{G}_0 .

After the n_s th sweep we calculate the values of the decay rate in the population $\{\hat{G}_{\beta,n_s}\}_{\alpha=1}^{\mathcal{N}}$ by Eq. (5.6), and call them $\{\Gamma_{\alpha,\nu}^{(n_s)}\}$ where $\nu = 1, 2$. Thereby, we calculate the typical values of the decay rate in the population by

$$\ln \Gamma_{\text{typ},\nu}^{(n_s)} = \frac{1}{\mathcal{N}} \sum_{\alpha=1}^{\mathcal{N}} \ln \Gamma_{\alpha,\nu}^{(n_s)}, \quad (5.12)$$

In order to determine the system is localized or delocalized, we calculate the *growth rate* of $\Gamma_{\text{typ},\nu}^{(n_s)}$ under sweeps, that is,

$$\lambda_{n_s} = \ln \Gamma_{\text{typ},\nu}^{(n_s)} - \ln \Gamma_{\text{typ},\nu}^{(n_s-1)}. \quad (5.13)$$

Here we note two important properties of λ_{n_s} .

(i) As long as $\Gamma_{\text{typ},\nu}^{(n_s)}$ is sufficiently small, statistically, $\Gamma_{\text{typ},\nu}^{(n_s)}$ grows *linearly* under sweeps. As a consequence, λ_{n_s} fluctuates about a steady value, and the magnitude of the fluctuation is proportional to $1/\sqrt{\mathcal{N}}$ according to the central limit theorem.

(ii) In this linear regime, as long as the two lattices are coupled, the statistics of λ_{n_s} is *independent* of the lattice index ν .

These properties can be understood as follows. As shown in Ref. [135], if $\Gamma_{j\nu}$'s are small enough, the recursion relation (5.5b) leads to a *linear homogeneous* equation for $\Gamma_{j\nu}$. The growth of the typical value of $\Gamma_{j\nu}$ under sweeps is dominated only by the *largest* eigenvalue of the linearized recursion relation.

The average growth rate of $\Gamma_{\text{typ},\nu}^{(n_s)}$ over $N_s \gg 1$ sweeps is defined by

$$\bar{\lambda}(N_s) = \frac{1}{N_s} \sum_{n_s=1}^{N_s} \lambda_{n_s}, \quad (5.14)$$

and the variance is

$$\delta\lambda(N_s) = \sqrt{\frac{1}{N_s} \sum_{n_s=1}^{N_s} (\lambda_{n_s} - \bar{\lambda})^2}. \quad (5.15)$$

which reflects the finite size effect and is proportional to $1/\sqrt{N}$. In the thermodynamic limit $\mathcal{N} \rightarrow \infty$, $\delta\lambda \rightarrow 0$, and the criterion (5.9) indicates that

$$\bar{\lambda} = \begin{cases} < 0, & \text{localized,} \\ > 0, & \text{delocalized.} \end{cases} \quad (5.16)$$

In our simulations of the model (5.1), we took $\mathcal{N} = 10^7$, $\eta = 10^{-15}$ ($t_1 = t_2 = 1$), and $N_s = 200$. Two points are worthwhile to mention.

(i) We started to collect samples of λ_{n_s} after about 50 sweeps of the population, when λ_{n_s} started to fluctuate about a steady value. We find that in this way the η -dependence of $\bar{\lambda}$ and $\delta\lambda$ is very weak, as long as η is small enough ($\lesssim 10^{-10}$).

(ii) Comparing the results of $\bar{\lambda}$ and $\delta\lambda$ for $\mathcal{N} = 10^7$ with those for $\mathcal{N} = 10^6$, we find that the finite size effect on $\bar{\lambda}$ is very weak, but the variance $\delta\lambda$ for $\mathcal{N} = 10^6$ is about 2.5 times of that for $\mathcal{N} = 10^7$, which coincides with the prediction of the central limit theorem.

5.3 Phase diagram

In this section we study the effect of the interlattice coupling t on the Anderson transition at the band center $E = 0$ of the system described by the model (5.1) in the case of two lattices with identical hopping ($t_1 = t_2$) but different disorder ($W_1 \leq W_2$). Our goal is to verify the two possible regimes proposed at the beginning of this chapter. Here we note that the effect of weak coupling $t \lesssim t_{1,2}$ is considered, which guarantees that in the absence of disorder the energy band is not substantially changed by the coupling, and therefore, the mobility edge first appears at the band center $E = 0$.¹

In Sec. 5.3.1 we present the numerical results of the population dynamics, where two cases are studied: (i) Two statistically identical lattices, that is, $W = W_1 = W_2$. We find that the critical disorder is enhanced by the interlattice coupling. (ii) Parametrically different lattices ($W_1 < W_2$). We focus on the case that in the absence of coupling the 1 lattice is critical and the 2 lattice is localized. We find: For a fixed coupling t , there exists a critical disorder strength of the 2 lattice, $W_{2,c}$, so that for $W_2 < W_{2,c}$ the system is delocalized, and for $W_2 > W_{2,c}$ the system is localized. If $W_2 \rightarrow \infty$, the two lattice are effectively decoupled. In Sec. 5.3.2, we present a perturbative analysis to explain the numerical results.

5.3.1 Numerical results

I. Statistically identical lattices ($W_1 = W_2$)

We first analyze two statistically identical lattices, which is analogous to two identical chains in one dimension. In Fig. 5.2 we compute $\bar{\lambda}$ and $\delta\lambda$ at $E = 0$ as functions of the disorder strength $W = W_1 = W_2$ for uncoupled and coupled ($t = 1$) lattices, where we take $K = 2$, and $t_1 = t_2 = 1$. The transition point is determined by the criterion in Eq. (5.16). For uncoupled lattices we find the critical disorder $W_c(t = 0) \approx 17.3$, which is coincident with the result obtained in Ref. [140]. For coupled lattices with $t = 1.0$, the critical order strength is $W_c(t = 1.0) \approx 20.7$.

¹As in the two-chain problem, if t is strong enough we reach the one-channel regime, where there is a gap between the two subbands. In this case the energy where we obtain the largest localization length is not at the band center any longer [See Figs. 4.12 and 4.14]. The similar situation may happen on two Bethe lattices: If the coupling is too strong, the mobility edge first appears at $E \neq 0$.

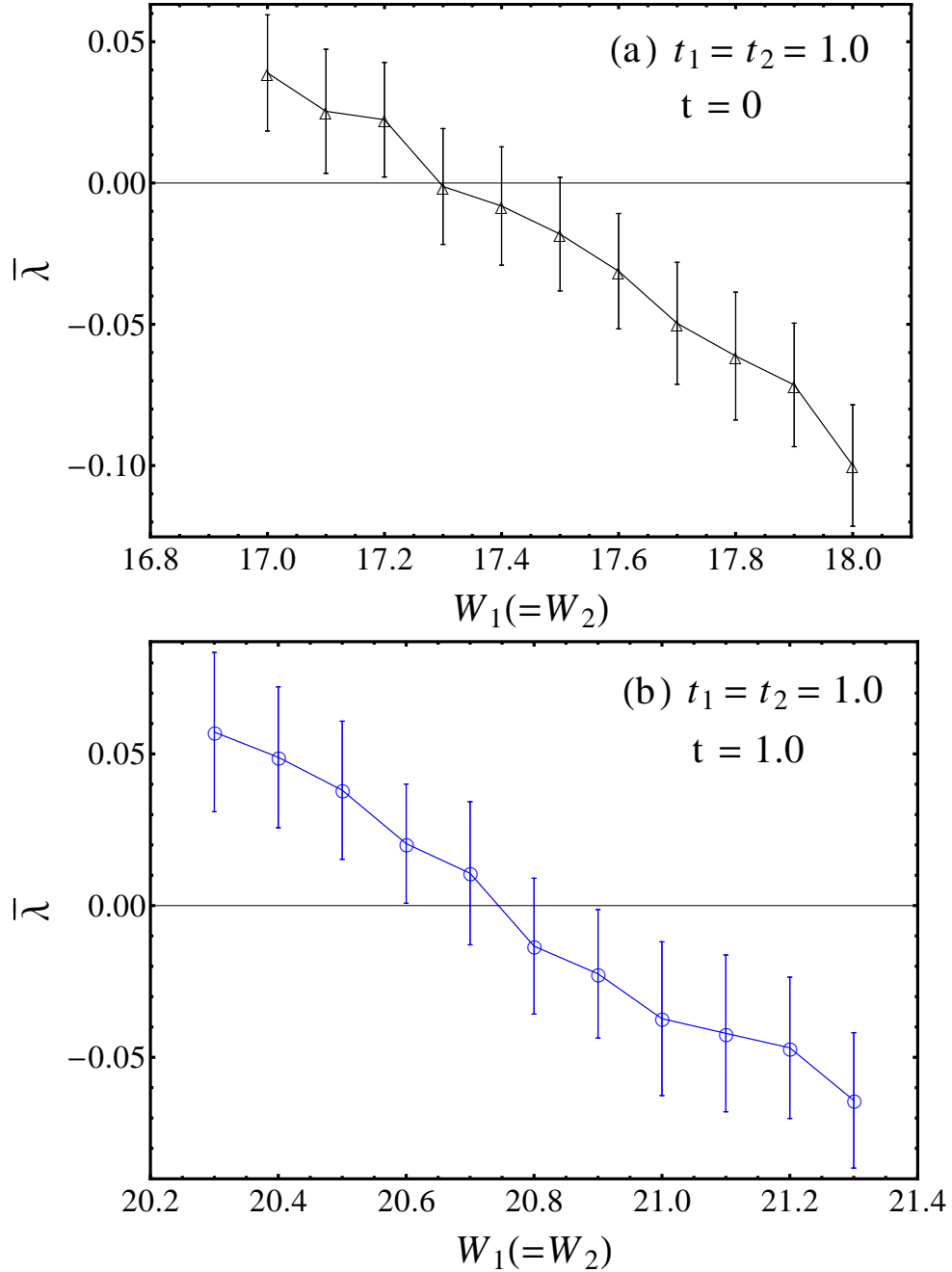


Figure 5.2: Numerical results for the growth rate of the typical values of the decay rate for the uncoupled and coupled *statistically identical* Bethe lattices as functions of disorder strength. The results were obtained for $K = 2$, $t_1 = t_2 = 1$, $E = 0$. The error bars indicate the variances $\delta\lambda$ obtained from Eq. (5.15), which reflect the finite size effect. (a) For the uncoupled lattices we find the critical disorder strength $W_c(t = 0) \approx 17.3$, which is very close to the result obtained in Ref. [140]. (b) For the coupled lattices with $t = 1.0$, the critical disorder strength is $W_c(t = 1, 0) \approx 20.7$.

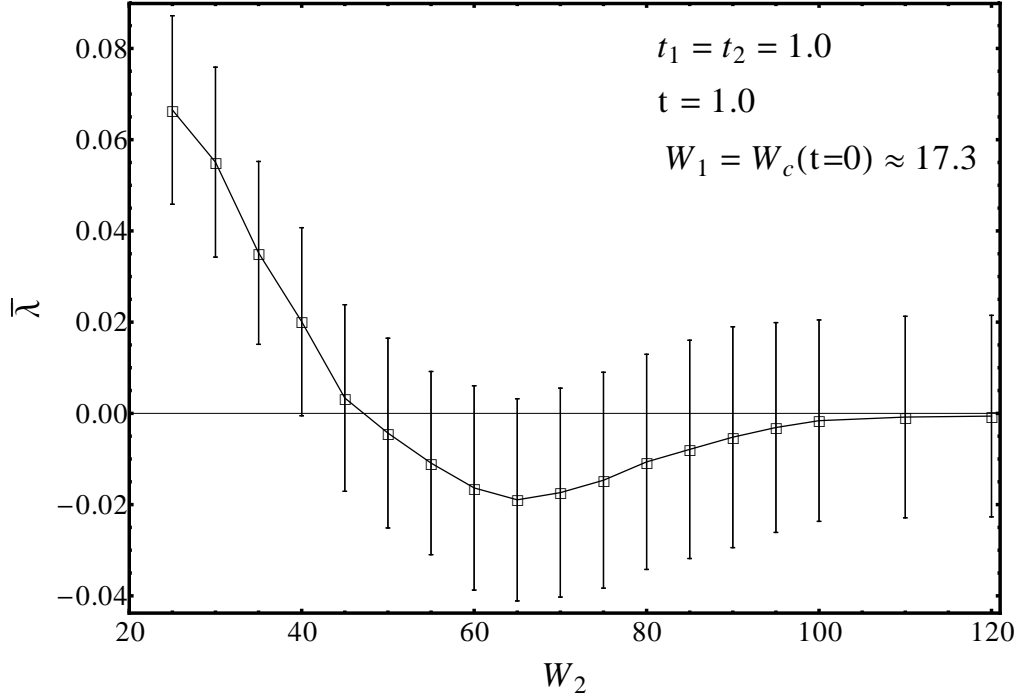


Figure 5.3: Numerical results for the growth rate of the typical values of the decay rate for the coupled Bethe lattices with *identical hopping but different disorder* as a function of the disorder strength on the 2 lattice. The disorder strength on the 1 lattice is fixed at $W_1 = W_c(t = 0) \approx 17.3$ and the interlattice coupling is $t = 1$. The other parameters are the same as in Fig. 5.2. There is a critical value of W_2 , $W_{2,c} \approx 47$, so that, for $W_2 < W_{2,c}$ the system is delocalized, and for $W_2 > W_{2,c}$ the system is localized. When W_2 is large enough, the system is infinitely close to the transition point from the localized phase.

We conclude that the critical disorder is enhanced by coupling the two lattices, that is, $W_c(t \neq 0) > W_c(t = 0)$. This implies that if two decoupled lattices are in the localized phase but close enough to the critical point, switching on the coupling may drive the system to a delocalized phase.

II. Parametrically different lattices ($W_1 \neq W_2$)

Let us now study what happens for two Bethe lattices with identical hopping but different disorder. More precisely, we couple the 1 lattice, which is *critical*, to the 2 lattice, which is *localized*, and analyze the coupling will push the system to a localized phase or a delocalized phase. As shown in Fig. 5.3, we fix $W_1 = W_c(t = 0) \approx 17.3$ and $t = 1$, and compute $\bar{\lambda}$ and $\delta\lambda$ as functions of W_2 . Two remarkable features are observed.

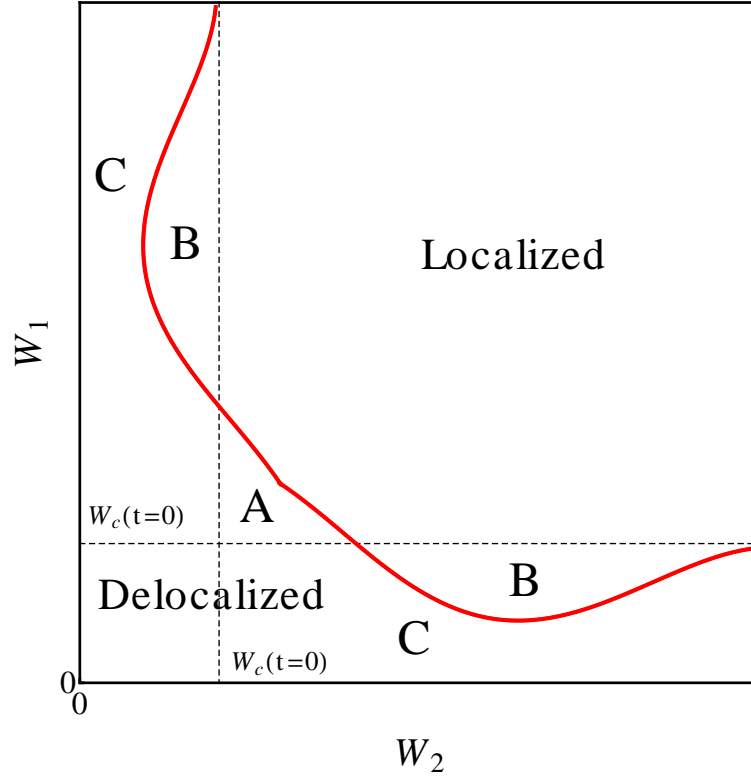


Figure 5.4: Schematic phase diagram for the coupled Bethe lattices with identical hopping but different disorder obtained from the results in Figs. 5.2 and 5.3. The red curve separates the $W_1 - W_2$ plane to the localized and delocalized regimes. For a guide to the eye we indicate the critical disorder for the uncoupled lattices $W_c(t=0) \approx 17.3$ by the dashed lines.

(i) Anderson transition happens at $W_2 = W_{2,c} \approx 47$. For $W_2 < W_{2,c}$ the system is delocalized, and for $W_2 > W_{2,c}$ the system is localized.

(ii) When $W_2 \rightarrow \infty$, the system infinitely tends to the transition point but still in the localized phase.

According to the results obtained in Figs. 5.2 and 5.3, the schematic phase diagram for two coupled disordered Bethe lattices with identical hopping is shown in Fig. 5.4. There are three regimes strongly affected by the interlattice coupling.

(i) Regime *A*. In the absence of coupling the two lattices are both localized but close enough to transitions. The coupling pushes the two nearly delocalized lattices to the delocalized phase.

(ii) Regime *B*. In the absence of coupling the less disordered lattice is delocalized but very close to the transition point, and the more disordered lattice is strongly localized. The coupling pushes the system to the localized phase.

(iii) Regime *C*. The less disordered lattice is deep in the delocalized phase, and the more disordered lattice is strongly localized. The coupled system is delocalized.

5.3.2 Perturbative analysis

The regime B in the phase diagram (see Fig. 5.4) can be explained qualitatively by applying a perturbative analysis in the limit of $W_2 \rightarrow \infty$. There are two competing effects on the 1 lattice due to coupling to the 2 lattice: The nearest neighbor hopping strength is enhanced, but the magnitude of the onsite energies is enhanced as well. Up to second order in $1/W_2$, the correction for the hopping strength between nearest neighbor sites $|i, 1\rangle$ and $|j, 1\rangle$ is

$$\delta t_{1,ij} = t^2 t_2 / (\epsilon_{i2} - \epsilon_{j2})^2 \sim t^2 t_2 / W_2^2, \quad (5.17)$$

and the correction for the random potential on site $|i, 1\rangle$ is

$$\delta \epsilon_{i1} = t^2 / (\epsilon_{i1} - \epsilon_{i2}) \sim t^2 / W_2. \quad (5.18)$$

It is easy to see that for $t_1 = t_2$, $W_2 \gg W_1$ leads to $\delta t_{1,ij}/t_1 \ll \delta \epsilon_{i1}/W_1$, which means that the enhancement of the disorder is much stronger than that of the hopping. Therefore, the more disordered lattice, which is strongly localized, may drive the less disordered lattice, which is delocalized but very close to the transition point, to the localized phase.

Chapter 6

Discussion

The work in this thesis is motivated by the problem of localization of interacting particles. The qualitative investigation of Thouless-type arguments in Chap. 2 lead us to consider the question of competition between alternative propagation channels, a question which we studied in great detail in the form of a single particle problem with two parallel, coupled channels. The theory also naturally applies for the Anderson localization of hybrid particles such as polaritons. These systems have a common feature: Two or more propagating channels with parametrically different transport properties are coupled and compete with each other.

The principal question is: What happens to the localization properties when a less localized lattice is coupled to a more localized one? Will the less localized lattice dominate the localization of the system or the more localized? The qualitative answer to this question depends on the dimensionality of the system. Correspondingly, we exactly solved the Anderson models on a two-leg ladder ($D = 1$) and on a two-layer Bethe lattice (formally $D = \infty$).

In one dimension, weak disorder has a strong localization effect. In the *weak disorder limit* we have found that under *resonance* conditions the localization lengths of two coupled chains are of the order of the localization length of the more localized, uncoupled leg. We may interpret this phenomenon as a manifestation of the fact that in one dimension the mean free path is the relevant length scale that sets the localization length. It is not surprising that the backscattering rate, and thus the “worst” leg of the chains determines the localization properties of a coupled system. If away from resonance the two legs are hardly affected

by each other. However, the close relation (proportionality) between mean free path and localization length is special for one-dimensional systems.

On coupled Bethe lattices, weak disorder is irrelevant to localization. The localization effect is significant only if the disorder is intermediate or strong. Therefore, resonance conditions, which require weak disorder as compared to the hopping, can not be achieved. In general, we found that the less disordered lattice is not affected much by the more disordered lattice in the presence of coupling, except in the case where the less disordered (delocalized) lattice is very close to the transition and the more disordered lattice is strongly localized, in which case the more disordered lattice can push the less disordered lattice to a localized phase. We believe that these trends persist in high dimensions ($D > 2$) where the metal-insulator transition takes places at strong disorder.

In two dimensions, the localization length becomes parametrically larger than the mean free path at weak disorder. However, since the proliferation of weak-localization and backscattering leads to complete localization (in the absence of special symmetries), we expect that a well propagating channel becomes more strongly localized upon resonant coupling to a more disordered channel, similarly as in one dimension. It might be interesting to investigate this numerically.

Investigating the localization properties of few- or many-particle systems is more complicated. First, we should map an interacting Hamiltonian to the Anderson model in the few- many-particle Fock space [cf. Eq. 2.1]. Thereby, the interaction provides effective hopping among the Fock states. This hopping in Fock space can be organized into channels with rather different propagation characteristics [e.g. Fig. 2.1 for four particles], namely, faster channels and slower channels. According to our analysis, the slow channel dominates only if it is *resonantly* coupled to the fast channel. If the two channels are away from resonance, the fast channel essentially dominates the localization properties. For the few-particle problems discussed in Chap. 2 we expect that the fast channel, that is, the hierarchical structure we predicted, dominates the delocalization of the interacting particles, since the resonance between the fast and slow channels should be an exception rather than a rule. At this stage, this remains a conjecture which needs to be tested further.

Appendix A

Transfer matrix of an “elementary slice” in the current-conserving basis Eqs. (4.24) and (4.26)

In this appendix we derive Eqs. (4.27) and (4.29). In Eqs. (4.19) and (4.20), $\tilde{\mathbf{m}}_x$ is a *symplectic* matrix which by definition satisfies

$$\tilde{\mathbf{m}}_x^T J \tilde{\mathbf{m}}_x = J, \quad (\text{A.1})$$

$$\tilde{\mathbf{m}}_x = \tilde{\mathbf{m}}_x^*, \quad (\text{A.2})$$

where

$$J = \begin{pmatrix} 0 & \mathbf{1} \\ -\mathbf{1} & 0 \end{pmatrix}, \quad (\text{A.3})$$

and $\tilde{\mathbf{m}}_x^T$ is the matrix obtained from $\tilde{\mathbf{m}}_x$ by transposition.

Define the new matrix \mathbf{m}_x

$$\mathbf{m}_x = \mathbf{U}_{x+1}^{-1} \tilde{\mathbf{m}}_x \mathbf{U}_x, \quad (\text{A.4})$$

where the rotation matrix is

$$\mathbf{U}_x \equiv \begin{pmatrix} \boldsymbol{\alpha}_x & \boldsymbol{\alpha}_x^* \\ \boldsymbol{\alpha}_{x-1} & \boldsymbol{\alpha}_{x-1}^* \end{pmatrix}, \quad (\text{A.5})$$

with $\boldsymbol{\alpha}_x$ defined by Eq. (4.28). The corresponding inverse matrix is given by

$$\mathbf{U}_x^{-1} = \frac{1}{\Delta} \begin{pmatrix} \boldsymbol{\alpha}_{x-1}^* & -\boldsymbol{\alpha}_x^* \\ -\boldsymbol{\alpha}_{x-1} & \boldsymbol{\alpha}_x \end{pmatrix} \quad (\text{A.6})$$

where Δ is the diagonal matrix

$$\Delta = \boldsymbol{\alpha}_x \boldsymbol{\alpha}_{x-1}^* - \boldsymbol{\alpha}_x^* \boldsymbol{\alpha}_{x-1}. \quad (\text{A.7})$$

The crucial point is that by current conservation Eq. (4.23), Δ is independent of coordinates and is proportional to the unit matrix in channel space:

$$\Delta = i \mathbf{1}. \quad (\text{A.8})$$

Note also that, by construction, the rotation matrix \mathbf{U}_x obeys the disorder-free Schrödinger equation Eq. (4.19):

$$\mathbf{U}_{x+1} = \tilde{\mathbf{m}}_x|_{\tilde{\epsilon}=0} \mathbf{U}_x. \quad (\text{A.9})$$

It follows immediately from Eqs. (A.9) and (A.4) that in the absence of disorder $\mathbf{m}_x = \mathbf{1}$. In the presence of weak disorder the matrix \mathbf{m}_x acquires a small coordinate-dependent correction proportional to $\tilde{\epsilon}_x$ which is given by Eq. (4.27).

Next, by inverting Eq. (A.4) and plugging into Eq. (A.2) one obtains:

$$\boldsymbol{\Sigma}_{x+1}^{(1)} \mathbf{m}_x \boldsymbol{\Sigma}_x^{(1)*} = \mathbf{m}_x^*. \quad (\text{A.10})$$

Using the definition of $\boldsymbol{\alpha}_x$ Eq. (4.28) one can readily show that

$$\boldsymbol{\Sigma}_x^{(1)} \equiv (\mathbf{U}_x^*)^{-1} \mathbf{U}_x = \boldsymbol{\Sigma}_1 \quad (\text{A.11})$$

is real and independent of x . This immediately reduces the time-reversal symmetry condition Eq. (A.10) to the form in Eq. (4.29).

The same procedure applied to the symplecticity relation Eq. (A.1) results in the following constraint (using $\tilde{\mathbf{m}}_x^T = \tilde{\mathbf{m}}_x^\dagger$):

$$\mathbf{m}_x^\dagger \Sigma_{x+1}^{(3)} \mathbf{m}_x = \Sigma_x^{(3)}, \quad (\text{A.12})$$

where

$$\Sigma_x^{(3)} \equiv \mathbf{U}_x^\dagger J \mathbf{U}_x = -\Delta \Sigma_3 = -i \Sigma_3 \quad (\text{A.13})$$

is independent of coordinate due to current conservation. Thus, we obtain the current conservation condition in Eq. (4.29).

Appendix B

Perturbative calculation of $\delta\vec{\lambda}$ up to second order

Equations (4.38), (4.45), and (4.46) fully determine the variation of the eigen-system of the Hermitian matrix \mathbf{R} . It is given by $\delta\vec{\lambda}$, which characterize the “perturbation” $\delta\mathbf{R}$. We can therefore use standard perturbation theory to expand $\delta\vec{\lambda}$ into powers of disorder on the additional slice. In this appendix we calculate $\delta\vec{\lambda}$ up to the second order, which is necessary to derive the Fokker-Planck equation (4.51).

We introduce some quantities which are convenient to present the results. Analogously to α_x , defined by Eq. (4.28), we define

$$\beta_x = \alpha_x \mathbf{u}, \tag{B.1}$$

where \mathbf{u} is the unitary matrix in Eq. (4.34). Since α_x describes the propagation in the plane-wave basis on the individual chains, and \mathbf{u} is the “polarization” matrix, we can consider β_x as describing clean propagation in the “polarized” plane-wave basis. Furthermore, analogously to the blocks in Eq. (4.27), we can define two quantities on the “polarized” basis, related with the forward- and back-scattering of the right-moving particle off the slice:

$$\begin{aligned} \Lambda_x &= i\beta_x^\dagger \tilde{\epsilon}_x \beta_x, \\ \Sigma_x &= i\beta_x^\dagger \tilde{\epsilon}_x \beta_x^*, \end{aligned} \tag{B.2}$$

which are 2×2 matrices. It is easy to realize that $\mathbf{\Lambda}_x$ is *anti-Hermitian* and $\mathbf{\Sigma}_x$ is *symmetric*. The corresponding left-moving quantities are complex conjugates of them. The perturbative series of $\delta\vec{\lambda}$ are functions of elements of $\mathbf{\Lambda}_x$ and $\mathbf{\Sigma}_x$. For simplicity of further notations, we define

$$\tilde{\mathbf{F}} = \sqrt{\mathbf{F}^2 - 1}, \quad (\text{B.3})$$

and

$$\Delta F = F_1 - F_2. \quad (\text{B.4})$$

In order to facilitate the perturbative calculation, we adopt a parametrization of $\mathbf{R} + \delta\mathbf{R}$ as in Eq. (4.38), but with $\mathbf{F} \rightarrow \mathbf{F} + \delta\mathbf{F}$, $\tilde{\mathbf{F}} \rightarrow \tilde{\mathbf{F}} + \delta\tilde{\mathbf{F}}$ and $\mathbf{u} \rightarrow \mathbf{u} + \delta\mathbf{u}$, in which

$$\delta\tilde{\mathbf{F}} = \sqrt{(\mathbf{F} + \delta\mathbf{F})^2 - 1} - \sqrt{\mathbf{F}^2 - 1}. \quad (\text{B.5})$$

Substituting this into Eqs. (4.46) and (4.45) we obtain two coupled equations for $\delta\mathbf{F}$ and the 2×2 matrix \mathbf{S} which captures the incremental change of the polarization basis,

$$\mathbf{S} = 1 + \mathbf{u}^\dagger \delta\mathbf{u}, \quad (\text{B.6})$$

as

$$\mathbf{S}(\mathbf{F} + \delta\mathbf{F})\mathbf{S}^\dagger = \mathbf{F} + \mathbf{F}^{(1)} + \mathbf{F}^{(2)}, \quad (\text{B.7a})$$

$$\mathbf{S}(\tilde{\mathbf{F}} + \delta\tilde{\mathbf{F}})\mathbf{S}^T = \tilde{\mathbf{F}} + \tilde{\mathbf{F}}^{(1)} + \tilde{\mathbf{F}}^{(2)}, \quad (\text{B.7b})$$

We have introduced perturbation terms on the r.h.s. of the two equations as

$$\mathbf{F}^{(1)} = -\mathbf{F}\mathbf{\Lambda}_L + \mathbf{\Lambda}_L\mathbf{F} + \mathbf{\Sigma}_L\tilde{\mathbf{F}} + \tilde{\mathbf{F}}\mathbf{\Sigma}_L^*, \quad (\text{B.8a})$$

$$\mathbf{F}^{(2)} = -\mathbf{\Lambda}_L\mathbf{F}\mathbf{\Lambda}_L + \mathbf{\Sigma}_L\mathbf{F}\mathbf{\Sigma}_L^* + \mathbf{\Lambda}_L\tilde{\mathbf{F}}\mathbf{\Sigma}_L^* - \mathbf{\Sigma}_L\tilde{\mathbf{F}}\mathbf{\Lambda}_L, \quad (\text{B.8b})$$

$$\tilde{\mathbf{F}}^{(1)} = -\tilde{\mathbf{F}}\mathbf{\Lambda}_L^* + \mathbf{\Lambda}_L\tilde{\mathbf{F}} + \mathbf{\Sigma}_L\mathbf{F} + \mathbf{F}\mathbf{\Sigma}_L, \quad (\text{B.8c})$$

$$\tilde{\mathbf{F}}^{(2)} = -\mathbf{\Lambda}_L\tilde{\mathbf{F}}\mathbf{\Lambda}_L^* + \mathbf{\Sigma}_L\tilde{\mathbf{F}}\mathbf{\Sigma}_L + \mathbf{\Lambda}_L\mathbf{F}\mathbf{\Sigma}_L - \mathbf{\Sigma}_L\mathbf{F}\mathbf{\Lambda}_L^*, \quad (\text{B.8d})$$

where $\mathbf{F}^{(1)}$ and $\tilde{\mathbf{F}}^{(1)}$ are linear in disorder, while $\mathbf{F}^{(2)}$ and $\tilde{\mathbf{F}}^{(2)}$ are quadratic. Additionally, $\mathbf{F}^{(1)}$ and $\mathbf{F}^{(2)}$ are *Hermitian*, but $\tilde{\mathbf{F}}^{(1)}$ and $\tilde{\mathbf{F}}^{(2)}$ are *symmetric*.

We expand $\delta\mathbf{F}$ and $\delta\mathbf{u}$ in disorder strength. From the latter we calculate the corresponding variations of angular variables. Without going into the details of the calculation, we present the results up to the second order in disorder.

To first order the corrections

$$\delta\vec{\lambda}^{(1)} = (\delta F_1^{(1)}, \delta F_2^{(1)}, \delta\theta^{(1)}, \delta\psi^{(1)}, \delta\phi^{(1)}, \delta\varphi^{(1)}) \quad (\text{B.9})$$

are given by

$$\delta F_\varrho^{(1)} = \mathbf{F}_{\varrho,\varrho}^{(1)}, \quad \varrho \in \{1, 2\}, \quad (\text{B.10a})$$

$$\delta\theta^{(1)} = \frac{2}{\Delta F} \text{Re}\left(\mathbf{F}_{2,1}^{(1)} e^{i\psi}\right), \quad (\text{B.10b})$$

$$\delta\psi^{(1)} = \frac{1}{2} \left(\frac{\text{Im}\tilde{\mathbf{F}}_{2,2}^{(1)}}{\tilde{F}_2} - \frac{\text{Im}\tilde{\mathbf{F}}_{1,1}^{(1)}}{\tilde{F}_1} \right) - \delta\varphi^{(1)} \cos\theta, \quad (\text{B.10c})$$

$$\delta\phi^{(1)} = -\frac{1}{2} \left(\frac{\text{Im}\tilde{\mathbf{F}}_{2,2}^{(1)}}{\tilde{F}_2} + \frac{\text{Im}\tilde{\mathbf{F}}_{1,1}^{(1)}}{\tilde{F}_1} \right), \quad (\text{B.10d})$$

$$\delta\varphi^{(1)} = \frac{2}{\Delta F} \text{Im}\left(\mathbf{F}_{2,1}^{(1)} e^{i\psi}\right) \csc\theta, \quad (\text{B.10e})$$

where the subscripts denote the matrix elements of the ‘‘perturbations’’ $\mathbf{F}^{(1)}$ in Eq. (B.10).

We recall that the ‘‘perturbations’’ in Eq. (B.10) are L dependent.

The second-order corrections,

$$\delta\vec{\lambda}^{(2)} = (\delta F_1^{(2)}, \delta F_2^{(2)}, \delta\theta^{(2)}, \delta\psi^{(2)}, \delta\phi^{(2)}, \delta\varphi^{(2)}), \quad (\text{B.11})$$

are more complicated. However, we recall that our aim is to calculate the correlators $\overline{\delta\lambda_i^{(1)}\delta\lambda_j^{(1)}}$ and $\overline{\delta\lambda_i^{(2)}}$ in Eq. (4.51). To avoid repeating calculation, we should express the $\delta\vec{\lambda}^{(2)}$'s in terms

of the first-order corrections Eq. (B.10) as far as possible. We obtain

$$\delta F_\varrho^{(2)} = \mathbf{F}_{\varrho,\varrho}^{(2)} - (-1)^\varrho \frac{|\mathbf{F}_{2,1}^{(1)}|^2}{\Delta F}, \quad \varrho \in \{1, 2\}, \quad (\text{B.12a})$$

$$\delta\theta^{(2)} = \frac{2}{\Delta F} \text{Re}\left(\mathbf{F}_{2,1}^{(2)} e^{i\psi}\right) + a^{(1)} \delta\theta^{(1)} + \frac{1}{4} \sin 2\theta (\delta\varphi^{(1)})^2, \quad (\text{B.12b})$$

$$\delta\psi^{(2)} = a_-^{(2)} + b_-^{(1)} \delta\phi^{(1)} + b_+^{(1)} d^{(1)} + c_+ e^{(2)} - a_-^{(1)} c_+^{(1)} - \frac{1}{2} \sin \theta \delta\theta^{(1)} \delta\varphi^{(1)} - \cos \theta \delta\varphi^{(2)}, \quad (\text{B.12c})$$

$$\delta\phi^{(2)} = -a_+^{(2)} - b_+^{(1)} \delta\phi^{(1)} - b_-^{(1)} d^{(1)} + c_- e^{(2)}, \quad (\text{B.12d})$$

$$\delta\varphi^{(2)} = \frac{2}{\Delta F} \text{Im}\left(\mathbf{F}_{2,1}^{(2)} e^{i\psi}\right) \csc \theta + a^{(1)} \delta\varphi^{(1)} - \cot \theta \delta\theta^{(1)} \delta\varphi^{(1)}, \quad (\text{B.12e})$$

in which

$$a^{(1)} = \frac{1}{\Delta F} \left(\delta F_2^{(1)} - \delta F_1^{(1)} \right), \quad (\text{B.13a})$$

$$a_\pm^{(2)} = \frac{1}{2} \left(\frac{\text{Im} \tilde{\mathbf{F}}_{2,2}^{(2)}}{\tilde{F}_2} \pm \frac{\text{Im} \tilde{\mathbf{F}}_{1,1}^{(2)}}{\tilde{F}_1} \right), \quad (\text{B.13b})$$

$$b_\pm^{(1)} = \frac{1}{2} \left(\frac{F_1}{\tilde{F}_1^2} \delta F_1^{(1)} \pm \frac{F_2}{\tilde{F}_2^2} \delta F_2^{(1)} \right), \quad (\text{B.13c})$$

$$c_\pm = \frac{1}{2} \left(\frac{\tilde{F}_1}{\tilde{F}_2} \pm \frac{\tilde{F}_2}{\tilde{F}_1} \right), \quad (\text{B.13d})$$

$$d^{(1)} = \delta\varphi^{(1)} \cos \theta + \delta\psi^{(1)}, \quad (\text{B.13e})$$

$$e^{(2)} = \frac{1}{4} \left[(\delta\varphi^{(1)})^2 \sin^2 \theta - (\delta\theta^{(1)})^2 \right] \sin 2\psi + \frac{1}{2} \delta\varphi^{(1)} \delta\theta^{(1)} \sin \theta \cos 2\psi. \quad (\text{B.13f})$$

In practice, we first calculate all the correlators $\overline{\delta\lambda_i^{(1)} \delta\lambda_j^{(1)}}$ by Eq. (B.10). At the same time we obtain the correlators relevant for the products of first-order terms on the r.h.s. of Eq. (B.12). Finally, after evaluating the disorder average of $a_\pm^{(2)}$ in Eq. (B.13b), $\overline{\delta\lambda_i^{(2)}}$ s can be obtained.

Appendix C

Coefficients of Eq. (4.67)

The coefficients of Eq. (4.67) are

$$c_1 = -2 \frac{\tilde{F}_1^2}{\Delta F} \Gamma_6, \quad (\text{C.1a})$$

$$c_2 = 2 \frac{\tilde{F}_2^2}{\Delta F} \Gamma_6, \quad (\text{C.1b})$$

$$c_3 = \frac{1}{\Delta F^2} \left[(F_1^2 - F_2^2 - 2) (\Gamma_5 + \Gamma_4) + 2F_1F_2 (\Gamma_5 - \Gamma_4) - (\tilde{F}_1^2 + \tilde{F}_2^2) (1 - u^2) \partial_u \Gamma_6 \right] - 4 \frac{1}{\Delta F^2} \tilde{F}_1 \tilde{F}_2 u \Gamma_6 \cos 2\psi, \quad (\text{C.1c})$$

$$c_4 = \frac{1}{\Delta F} \left[\left(\tilde{F}_1 \tilde{F}_2 + \frac{F_2}{\tilde{F}_2} \tilde{F}_1 - \frac{F_1}{\tilde{F}_1} \tilde{F}_2 \right) \Gamma_3 + 2 \frac{\tilde{F}_1 \tilde{F}_2}{\Delta F} \frac{u}{\sqrt{1 - u^2}} (\Gamma_5 - \Gamma_4) + \frac{F_1}{\tilde{F}_1} \tilde{F}_2 \partial_u \Gamma_4 + \frac{F_2}{\tilde{F}_2} \tilde{F}_1 \partial_u \Gamma_5 - 2 \frac{\tilde{F}_1 \tilde{F}_2}{\Delta F} (\Gamma_6 + 2u \partial_u \Gamma_6) \right] \sin 2\psi, \quad (\text{C.1d})$$

$$c_{11} = \tilde{F}_1^2 \Gamma_1, \quad (\text{C.1e})$$

$$c_{12} = 2 \tilde{F}_1 \tilde{F}_2 \Gamma_3 \cos 2\psi, \quad (\text{C.1f})$$

$$c_{13} = \frac{2 \tilde{F}_1}{\Delta F} \left(\tilde{F}_1 + \tilde{F}_2 \cos 2\psi \right) \Gamma_4, \quad (\text{C.1g})$$

$$c_{14} = -\tilde{F}_1 \left(\frac{F_2}{\tilde{F}_2} \Gamma_3 + 2 \frac{\tilde{F}_2}{\Delta F} \frac{u}{\sqrt{1 - u^2}} \Gamma_4 \right) \sin 2\psi, \quad (\text{C.1h})$$

$$c_{22} = \tilde{F}_2^2 \Gamma_2, \quad (\text{C.1i})$$

$$c_{23} = 2 \frac{\tilde{F}_2}{\Delta F} \left(\tilde{F}_2 + \tilde{F}_1 \cos 2\psi \right) \Gamma_5, \quad (\text{C.1j})$$

$$c_{24} = -\tilde{F}_2 \left(\frac{F_1}{\tilde{F}_1} \Gamma_3 + 2 \frac{\tilde{F}_1}{\Delta F} \frac{u}{\sqrt{1-u^2}} \Gamma_5 \right) \sin 2\psi, \quad (\text{C.1k})$$

$$c_{33} = \left[V_3 + \frac{1}{\Delta F^2} \left(\tilde{F}_1^2 + \tilde{F}_2^2 + 2\tilde{F}_1 \tilde{F}_2 \cos 2\psi \right) \Gamma_6 \right] (1-u^2), \quad (\text{C.1l})$$

$$c_{34} = -\frac{1}{\Delta F} \left(\frac{F_1 \tilde{F}_2}{\tilde{F}_1} \Gamma_4 + \frac{\tilde{F}_1 F_2}{\tilde{F}_2} \Gamma_5 - 4 \frac{\tilde{F}_1 \tilde{F}_2}{\Delta F} u \Gamma_6 \right) \sin 2\psi, \quad (\text{C.1m})$$

$$\begin{aligned} c_{44} = & \frac{1}{2} \left[1 + \frac{1}{2} \left(\frac{F_1}{\tilde{F}_1} \right)^2 \right] \Gamma_1 + \frac{1}{2} \left[1 + \frac{1}{2} \left(\frac{F_2}{\tilde{F}_2} \right)^2 \right] \Gamma_2 - \Gamma_6 \\ & + \frac{u}{\sqrt{1-u^2}} \left[\left(2 + \frac{F_1}{\Delta F} \right) \Gamma_4 + \left(2 + \frac{F_2}{\Delta F} \right) \Gamma_5 \right] + \frac{u^2}{1-u^2} \left[\Gamma_3 + \left(1 + \frac{\tilde{F}_1^2 + \tilde{F}_2^2}{\Delta F^2} \right) \Gamma_6 \right] \\ & - \left[\frac{1}{2} \frac{F_1 F_2}{\tilde{F}_1 \tilde{F}_2} \Gamma_3 + \frac{u}{\sqrt{1-u^2}} \frac{1}{\Delta F} \left(\frac{F_1 \tilde{F}_2}{\tilde{F}_1} \Gamma_1 + \frac{\tilde{F}_1 F_2}{\tilde{F}_2} \Gamma_2 \right) + 2 \frac{u^2}{1-u^2} \frac{\tilde{F}_1 \tilde{F}_2}{\Delta F^2} \right] \cos 2\psi, \end{aligned} \quad (\text{C.1n})$$

where the \tilde{F}_ρ 's are the two diagonal elements of the matrix (B.3) and ΔF is defined in Eq. (B.4). The new quantities introduced in Appendix C are defined below. Notice first that the Γ_n are functions of u defined by

$$\Gamma_{1(2)}(u) = V_1 + V_2 + 4V_3 - (+)2(V_2 - V_1)u + (V_1 + V_2 - 4V_3)u^2, \quad (\text{C.2a})$$

$$\Gamma_3(u) = (V_1 + V_2 - 4V_3)(1-u^2), \quad (\text{C.2b})$$

$$\Gamma_{4(5)}(u) = [V_1 - V_2 + (-)(V_1 + V_2 - 4V_3)u](1-u^2), \quad (\text{C.2c})$$

$$\Gamma_6(u) = V_1 + V_2 - (V_1 + V_2 - 4V_3)u^2, \quad (\text{C.2d})$$

where V_1 , V_2 and V_3 are the three Born cross sections defined in Eq. (4.59). In order to solve Eq. (4.77) in the limit $L \gg 1$, we need the values of c_3 and c_{33} in the limit $F_{\max} \gg F_{\min} \gg 1$,

$$\lim_{L \rightarrow \infty} c_3 = (|V_1 - V_2| - \partial_u \Gamma_6)(1-u^2),$$

$$\lim_{L \rightarrow \infty} c_{33} = (V_3 + \Gamma_6) (1 - u^2),$$

which is Eq. (4.78).

Appendix D

Transfer matrix of an “elementary slice” in the basis Eqs. (4.24) and (4.106)

The derivation of Eq. (4.107) goes in parallel with the derivation of Eq. (4.27) in App. A. However, the rotation \mathbf{U}_x is constructed in such a way that

$$\mathbf{U}_x = \begin{pmatrix} \psi_1^+(x) & \psi_1^-(x) & 0 & 0 \\ 0 & 0 & \psi_2^+(1) & \psi_2^-(1) \\ \psi_1^+(x-1) & \psi_1^-(x-1) & 0 & 0 \\ 0 & 0 & \psi_2^+(0) & \psi_2^-(0) \end{pmatrix}, \quad (\text{D.1})$$

where $\psi_{1,2}^\pm(x)$ are defined by Eqs. (4.24) and (4.106). Compared with Eq. (A.5) for the two-channel case, the second and third columns of Eq. (D.1) have been permuted, and the columns corresponding to the evanescent channel are coordinate-independent. The inverse of \mathbf{U}_x is

$$\mathbf{U}_x^{-1} = \begin{pmatrix} -i\psi_1^-(x-1) & 0 & i\psi_1^-(x) & 0 \\ i\psi_1^+(x-1) & 0 & -i\psi_1^+(x) & 0 \\ 0 & -\psi_2^-(0) & 0 & \psi_2^-(1) \\ 0 & \psi_2^+(0) & 0 & -\psi_2^+(1) \end{pmatrix}. \quad (\text{D.2})$$

The transfer matrix of an elementary slice (4.107) is

$$\mathbf{m}_x = \mathbf{U}_{x+1}^{-1} \tilde{\mathbf{m}}_x \mathbf{U}_x = \mathbf{m} + \delta \mathbf{m}_x, \quad (\text{D.3})$$

where \mathbf{m} and $\delta \mathbf{m}_x$ take the form given in Eq. (4.108). Following the same procedure as in App. A, one can also obtain the symmetry constraints on the matrix \mathbf{m}_x , which is imposed by the reality and symplecticity of the matrix $\tilde{\mathbf{m}}_x$. Without going into details we present the following results: The reality relation (A.2) gives

$$\mathbf{m}_x^* = \mathbf{\Lambda}_1 \mathbf{m}_x \mathbf{\Lambda}_1, \quad \mathbf{\Lambda}_1 = \begin{pmatrix} \sigma_1 & 0 \\ 0 & \mathbf{1} \end{pmatrix}; \quad (\text{D.4})$$

The symplecticity relation (A.1) gives

$$\mathbf{m}_x^\dagger \mathbf{\Lambda}_3 \mathbf{m}_x = \mathbf{\Lambda}_3, \quad \mathbf{\Lambda}_1 = \begin{pmatrix} \sigma_3 & 0 \\ 0 & \sigma_2 \end{pmatrix}. \quad (\text{D.5})$$

Finally, it is not hard to show that the Lyapunov exponents of the products (4.30) satisfy the symmetry property stated in Eq. (4.113).

Acknowledgements

I would like to express my gratitude to all those who gave me the possibility to complete this dissertation. I want to thank International School for Advanced Studies and International Centre for Theoretical Physics for supporting me to do the necessary research work and to use the departmental resource.

I am deeply indebted to my supervisor, Professor Michele Fabrizio, Coordinator of Physics Area, International School for Advanced Studies. He patiently provided the encouragement and advise necessary for me to proceed through the doctoral program and complete my dissertation.

I would like to express my deep and sincere gratitude to my supervisor, Professor Vladimir E. Kravtsov, Head of Condensed Matter and Statistical Physics Section, International Centre for Theoretical Physics. His motivation, enthusiasm, and insightful comments have had a remarkable influence on my research career.

I owe my most sincere gratitude to my supervisor, Professor Markus Müller, Research Scientist, International Centre for Theoretical Physics. He provided me sound ideas, detailed and constructive comments, and great efforts to explain things clearly and simply. I would have been lost without him.

I would like to thank my Master supervisors, Professor Yu-Liang Liu and Professor Tao Li, Department of Physics, Renmin University of China. They enlightened me the first glance of scientific research.

My sincere thanks are also given to Professor Erio Tosatti and Professor Giuseppe Mussardo. Their advises for the attitude in theoretical physics research were of great benefits of me.

I give my gratitude to the many people who have taught me numerical techniques, especially, to Dr. Federico Becca, Prof. Sandro Sorella, Prof. Giuseppe Santoro, and to Prof. Stefano Baroni, Prof. Andrea Dal Corso, and Prof. Stefano de Gironcoli.

I am grateful to many experts for stimulating discussions, especially, to Prof. Carlo Beenakker, Prof. Hélène Bouchiat, Prof. Ferdinand Evers, Prof. Yan Fyodorov, Dr. Richard Maxime, Prof. Yuri Rubo, Dr. Peter Schmitteckert, Dr. Alessandro Silva, Prof. Felix von Oppen.

I am indebted to my many colleagues for providing a stimulating environment where to learn and grow. I am especially grateful to Xiao-Quan Yu, and to Dr. Alexei Andreanov, Pier Paolo Baruselli, Francesco Buccheri, Mauro Iazzi, and Iacopo Mastromatteo, and to Bagheri Varnosfaderani Behnaz, Robinson Okanigban, and Amini Abchuyeh Mohsen.

I wish to thank the secretaries for assisting me in many different ways. Ricardo Iancer, Fedrica Tuniz, and Lorena Bencina in International School for Advanced Studies, and Milena Poropat in International Centre for Theoretical Physics, deserve special mention.

I warmly thank Chinese Student and Scholars Union in Trieste for friendly help, where my good friends Xiao-Chuan Ge, Ye Luo, Bai-Lu Si, and Chang Su deserve special gratitudes.

I wish to thank my best friend Roberto Pitton for sharing infinite biking trips in Italy, Slovenia, and Austria. His kind support and guidance have been of great value in my doctoral study.

I owe my loving thanks to my parents, Xi-Ming Xie and Wei-Dong Jiang, for giving birth to me at the first place and supporting me spiritually throughout my life.

Bibliography

- [1] L. D. Landau and E. M. Lifshitz, *Physical Kinetics: Course of Theoretical Physics Vol. 10* (Butterworth-Heinemann, Reprint Edition, 1981).
- [2] A. F. Ioffe and A. R. Regel, *Progr. Semicond.* **4**, 237 (1960).
- [3] N. F. Mott, *Philos. Mag.* **26**, 1015 (1972).
- [4] J. H. Mooij, *Phys. Stat. Sol.* **a17**, 521 (1973).
- [5] L. P. Gorkov, A. I. Larkin, and D. E. Khmel'nitskii, *Sov. Phys. JETP Lett.* **30**, 248 (1979).
- [6] P. A. Lee and T. V. Ramakrishnan, *Rev. Mod. Phys.* *57*, 287 (1985).
- [7] A. I. Larkin and D. E. Khmel'nitskii, *Sov. Phys. Usp.* **25(3)**, 185 (1982).
- [8] H. Wiesmann, M. Gurvitch, H. Lutz, A. Ghosh, B. Schwartz, M. Strongin, P. B. Allen, and J. W. Halley, *Phys. Rev. Lett.* **38**, 782 (1977).
- [9] G. J. Dolan and D. D. Osheroff, *Phys. Rev. Lett.* **43**, 721 (1979).
- [10] N. Giordano, W. Gilson, and D. E. Prober, *Phys. Rev. Lett.* **43**, 725 (1979).
- [11] D. J. Bishop, D. C. Tsui, and R. C. Dynes, *Phys. Rev. Lett.* **44**, 1153 (1980).
- [12] M. Pepper, and M. J. Uren, *J. Phys. C* **15**, L617 (1982).
- [13] P. W. Anderson, *Phys. Rev.* **109**, 1492 (1958).
- [14] Y. Imry, *Introduction to Mesoscopic Physics* (Oxford University Press, 1997).
- [15] B. Kramer and A. MacKinnon, *Rep. Prog. Phys.* **56**, 1469, (1993).
- [16] N. F. Mott, *Philos. Mag.* **17**, 1259 (1968).
- [17] N. F. Mott and G. A. Davis, *Electronic Properties of Noncrystalline Materials (2nd edition)*, (Clarendon Press, Oxford, 1979).
- [18] F. Evers and A. D. Mirlin, *Rev. Mod. Phys.* **80**, 1355 (2008).
- [19] N. W. Ashcroft and N. D. Mermin, *Solid State Physics* (Brooks Cole, New York, 1976)
- [20] J. Hubbard, *Proc. Roy. Soc. London* **A277**, 237 (1964).

- [21] N. F. Mott, *Metal-Insulator Transitions* (Taylor & Francis, London, 1974).
- [22] P. Fazekas, *Lecture Notes on Electron Correlation and Magnetism* (World Scientific, Singapore, 1999).
- [23] D. Jérôme, T. M. Rice, and W. Kohn, Phys. Rev. **158**, 462 (1967).
- [24] E. Abrahams (editor), *50 years of Anderson Localization* (World Scientific, Singapore, 2010).
- [25] D. S. Wiersma, P. Bartolini, A. Lagendijk, and R. Righini, Nature **390**, 671 (1997).
- [26] J. Fröhlich and T. Spencer, Phys. Rep. **103**, 9 (1984); J. Fröhlich, F. Martinelli, E. Scoppola, and T. Spencer, Commun. Math. Phys. **101**, 22 (1985).
- [27] E. Abrahams, P. W. Anderson, D. C. Licciardello, and T. V. Ramakrishnan, Phys. Rev. Lett. **42**, 673 (1979).
- [28] D. J. Thouless, Phys. Rev. Lett. **39**, 1167 (1977).
- [29] F. Weger, Z. Phys. B **35**, 207 (1979).
- [30] L. Schäfer and F. Weger, Z. Phys. B **38**, 113 (1980).
- [31] K. B. Efetov, A. I. Larkin, and D. E. Khmel'nitskii, Sov. Phys. JETP **52**, 568 (1980).
- [32] K. B. Efetov, *Supersymmetry in Disordered and Chaos* (Cambridge University Press, New York, 1997).
- [33] A. Mackinnon and B. Kramer, Phys. Rev. Lett. **47**, 1546 (1981).
- [34] A. MacKinnon and B. Kramer, Z. Phys. B **53**, 1 (1983).
- [35] S. Hikami, A. I. Larkin, and Y. Nagaoka, Prog. Theor. Phys. **63**, 707 (1980).
- [36] D. R. Grempel, J. Phys. C **20**, 3143 (1987).
- [37] T. Ando, Phys. Rev. B **40**, 5325 (1989).
- [38] Y. Asada, K. Slevin, and T. Ohtsuki, Phys. Rev. Lett. **89**, 256601 (2002).
- [39] P. Markös and L. Schweitzer, J. Phys. A **39**, 3221 (2006).
- [40] B. Huckestein, Rev. Mod. Phys. **67**, 357 (1995).
- [41] T. Brandes and S. Kettmann (editors), *Anderson Localization and Its Ramifications: Disorder, Phase Coherence and Electron Correlations*, Lect. Notes Phys. Vol. 630 (Springer, Berlin, 2003).
- [42] T. N. Zavaritskaya and E. I. Zavaritskaya, Sov. Phys. JETP Lett. **45**, 609 (1987).
- [43] S. V. Kravchenko and M. P. Sarachik, in Ref. [24], p.361.

- [44] A. F. Hebard and M. A. Paalanen, Phys. Rev. Lett. **65**, 927 (1990).
- [45] M. A. Paalanen, A. F. Hebard, and R. R. Ruel, Phys. Rev. Lett. **69**, 1604 (1992).
- [46] A. Goldman and N. Markovic, Phys. Today **51**, 39 (1998).
- [47] T. I. Baturina, A. Yu. Mironov, V. M. Vinokur, M. R. Baklanov, and C. Strunk, Phys. Rev. Lett. **99**, 257003 (2007).
- [48] G. Sambandamurthy, L. W. Engel, A. Johansson, E. Peled, and D. Shahar, Phys. Rev. Lett. **94**, 017003 (2005).
- [49] A. M. Finkelstein, Sov. Phys. JETP **57**, 97 (1983).
- [50] C. Catellani, C. Di Castro, P. A. Lee, and M. Ma, Phys. Rev. B **30**, 527 (1984).
- [51] L. Fleishman and P. W. Anderson, Phys. Rev. B **21**, 2366 (1980).
- [52] B. L. Altshuler, A. G. Aronov, and D. E. Khmel'nitskii, J. Phys. C **15**, 7367 (1982).
- [53] D. M. Basko, I. L. Aleiner, and B. L. Altshuler, Ann. Phys. **321**, 1126 (2006); In *Problems of condensed matter physics: quantum coherence phenomena in electron-hole and coupled matter-light systems*, edited by A. L. Ivanov and S. G. Tikhodeev (Oxford University Press, 2008).
- [54] B. L. Altshuler, Y. Gefen, A. Kamenev, and L. S. Levitov, Phys. Rev. Lett. **78**, 2803 (1997).
- [55] I. V. Gornyi, A. D. Mirlin, and D. G. Polyakov, Phys. Rev. Lett. **95**, 206603 (2005).
- [56] P. W. Anderson, J. Phys. Chem. Solids **11**, 26 (1959).
- [57] M. Ma and P. A. Lee, Phys. Rev. B **32**, 5658 (1985).
- [58] M. P. A. Fisher, P. B. Weichman, G. Grinstein, and D. S. Fisher, Phys. Rev. B **40**, 546 (1989).
- [59] M. Müller, Annalen der Physik **18**, 849 (2009).
- [60] I. L. Aleiner, B. L. Altshuler, and G. V. Shlyapnikov, Nat. Phys. **6**, 900 (2010).
- [61] M. V. Feigel'man, L. B. Ioffe, V. E. Kravtsov, and E. Cuevas, Ann. Phys. **325**, 1368 (2010).
- [62] M. V. Feigel'man, L. B. Ioffe, and M. Mézard, Phys. Rev. B **82**, 184534 (2010).
- [63] K. Winkler, G. Thalhammer, F. Lang, R. Grimm, J. H. Denschlag, A. J. Daley, A. Kantian, H. P. Bchler and P. Zoller, Nature **441**, 853 (2006).
- [64] O. N. Dorokhov, Sov. Phys. JETP **71**, 360 (1990).
- [65] D. L. Shepelyansky, Phys. Rev. Lett. **73**, 2607 (1994).

- [66] Y. M. Blanter, Phys. Rev. B **54**, 12807 (1996).
- [67] U. Sivan, F. P. Milliken, K. Milkove, S. Rihston, Y. Lee, J. M. Hong, V. Boegli, D. Kern, and M. de Franza, Europhys. Lett. **25**, 605 (1994).
- [68] U. Sivan, Y. Imry, and A. G. Aronov, Europhys. Lett. **28**, 115 (1994).
- [69] A. D. Mirlin and Y. V. Fyodorov, Phys. Rev. B **56**, 13393 (1997).
- [70] P. G. Silvestrov, Phys. Rev. Lett. **79**, 3994 (1997); Phys. Rev. E **58**, 5629 (1998); Phys. Rev. B **64**, 113309 (2001).
- [71] D. Weinmann, J. L. Pichard, and Y. Imry, J. Phys. I France **7**, 1559 (1997).
- [72] A. Trichet, L. Sun, G. Pavlovic, N.A. Gippius, G. Malpuech, W. Xie, Z. Chen, M. Richard, and L. S. Dang, Phys. Rev. B **83**, 041302(R) (2011).
- [73] F. Manni, K. G. Lagoudakis, B. Pietka, L. Fontanesi, M. Wouters, V. Savona, R. André, and B. Deveaud-Plédran, Phys. Rev. Lett. **106**, 176401 (2011).
- [74] V. Savona, Phys. Rev. Lett. **78**, 4470 (1997).
- [75] V. Savona, J. Phys.: Condens. Matter **19**, 295208 (2007).
- [76] V. E. Kravtsov, cond-mat/09110639.
- [77] A. D. Mirlin, Phys. Rep. **326**, 259 (2000).
- [78] H. Kamimura, in *Electron-Electron interactions in Disordered Systems*, edited by A. L. Efros and M. Pollak (North Holland, 1985).
- [79] E. A. Akkermans and J. L. Pichard, Eur. Phys. J. B **1**, 233 (1998).
- [80] Y. Imry, Europhys. Lett. **30**(7), 405 (1995).
- [81] K. Frahm, A. Müller-Groeling, J.-L. Pichard, Phys. Rev. Lett. **76**, 1509 (1996).
- [82] D. L. Shepelyansky, Phys. Rev. Lett. **78**, 923 (1997).
- [83] K. M. Frahm, Eur. Phys. J. B **10**, 371 (1999).
- [84] F. von Oppen, T. Wettig, and J. Müller, Phys. Rev. Lett. **76**, 491 (1996).
- [85] P. H. Song and F. von Oppen, Phys. Rev. B **59**, 46 (1999).
- [86] R. A. Römer, M. Schreiber, and T. Vojta, Phys. Status Solidi **211**, 681 (1999).
- [87] D. O. Krimer, R. Khomeriki, and S. Flach, JETP Lett. **94**, 406 (2011).
- [88] H. Y. Xie, unpublished.
- [89] H. Fehske, J. Schleede, G. Schubert, G. Wellein, V. S. Filinov, and A. R. Bishop, Phys. Lett. A **373**, 2182 (2009).

- [90] M. Ortuño and E. Cuevas, *Europhys. Lett.* **46**, 224 (1999).
- [91] E. Cuevas, *Phys. Rev. Lett.* **83**, 140 (1999).
- [92] H. Y. Xie (unpublished).
- [93] D. L. Shepelyansky and O. P. Sushkov, *Europhys. Lett.* **37**, 121 (1997).
- [94] O. Halfpap, *Ann. Phys. (Leipzig)* **10**, 623 (2001).
- [95] H. Huang and S. W. Koch, *Quantum Theory of the Optical and Electronic Properties of Semiconductors* (World Scientific, 2004).
- [96] S. I. Pekar, *Sov. Phys. JETP* **7**, 813 (1958).
- [97] J. J. Hopfield, *Phys. Rev.* **112**, 1555 (1958).
- [98] V. M. Agranovich, *Sov. Phys. JETP* **37**, 307 (1960).
- [99] J. J. Hopfield and D. G. Thomas, *Phys. Rev.* **132**, 563 (1963).
- [100] D. Sanvitto and V. Timofeev (editors), *Exciton Polaritons in Microcavities: New Frontiers* [Springer Series in Solide-State Sciences 172] (Springer-Verlag, Berlin, 2012).
- [101] C. Weisbuch, M. Nishioka, A. Ishikawa, and Y. Arakawa, *Phys. Rev. Lett.* **69**, 3314 (1992).
- [102] D. M. Whittaker, P. Kinsler, T. A. Fisher, M. S. Skolnick, A. Armitage, A. M. Afshar, M. D. Sturge, and J. S. Roberts, *Phys. Rev. Lett.* **77**, 4792 (1996).
- [103] V. A. Kosobukin, *Fiz. Tverd. Tela* **45**(6), 1091 (2003) [*Phys. Solid State* **45**(6), 1145 (2003)].
- [104] W. Zhang, R. Yang, Y. Zhao, S. Duan, P. Zhang, and S. E. Ulloa, *Phys. Rev. B* **81**, 214202 (2010).
- [105] A. U. Thomann, V. B. Geshkenbein and G. Blatter, *Phys. Rev. B* **79**, 184515 (2009).
- [106] J. Kasprzak, M. Richard, S. Kundermann, A. Baas, P. Jeambrun, J. M. J. Keeling, F. M. Marchetti, M. H. Szymańska, R. André, J. L. Staehli, V. Savona, P. B. Littlewood, B. Deveaud, and L. S. Dang, *Nature* **443**, 409 (2006).
- [107] F. M. Marchetti, J. Keeling, M. H. Szymańska and P. B. Littlewood, *Phys. Rev. B* **76**, 115326 (2007).
- [108] E. Wertz, L. Ferrier, D. D. Solnyshkov, R. Johne, D. Sanvitto, A. Lemaître, I. Sagnes, R. Grousson, A. V. Kavokin, P. Senellart, G. Malpuech and J. Bloch, *Nature Phys.* **6**, 860 (2010).
- [109] I. L. Aleiner, B. L. Altshuler and Y. G. Rubo, *Phys. Rev. B* **85**, 121301(R) (2012).
- [110] M. H. Anderson, J. R. Ensher, M. R. Matthews, C. E. Wieman, and E. A. Cornell, *Science* **269**, 198 (1995).

- [111] A. V. Kavokin, J. J. Baumberg, G. Malpuech and F. P. Laussy, *Microcavities* (Oxford University Press, 2007).
- [112] H. Deng, H. Huang, and Y. Yamamoto, *Rev. Mod. Phys.* **82**, 1498 (2010).
- [113] H. Y. Xie, V. E. Kravtsov, and M. Müller, *Phys. Rev. B* **86**, 014205 (2012).
- [114] V. L. Berezinskii, *Sov. Phys. JETP* **38**, 620 (1974).
- [115] V. I. Mel'nikov, *Sov. phys. Solid State* **23**, 444 (1981).
- [116] V. E. Kravtsov and V. I. Yudson, *Phys. Rev. B* **82**, 195120 (2010); *Annals of Physics*, **326**, 1672 (2011).
- [117] M. E. Gertsenshtein and V. B. Vasil'ev, *Theor. Probab. Appl.*, **IV**, 391 (1959).
- [118] O. N. Dorokhov, *Solid State Commun.* **44**, 915 (1982).
- [119] P. A. Mello and N. Kumar, *Quantum Transport in Mesoscopic Systems: Complexity and Statistical Fluctuations* (Oxford University Press, 2004).
- [120] P. A. Mello, P. Pereyra and N. Kummar, *Ann. Phys.* **181**, 290 (1988).
- [121] C. W. J. Beenakker and B. Rejaei, *Phys. Rev. Lett.* **71**, 3689 (1993); *Phys. Rev. B* **49**, 7499 (1994).
- [122] A. V. Tartakovski, *Phys. Rev. B* **52**, 2704 (1985).
- [123] M. Kasner and W. Weller, *Phys. Stat. Solidi (b)* **148**, 635 (1988).
- [124] M. Hamermesh, *Group Theory and This Applications to Physical Problem*, (Addison-Wesley, 1962).
- [125] Z. Shi and A. Z. Genack, *Phys. Rev. Lett.* **108**, 043901 (2012).
- [126] G. Benettin, L. Galgani, A. Giorgilli, J. M. Strelcyn, *Meccanica* **15**, 9,21 (1980); A. Crisanti, G. Paladin, A. Vulpiani, *Products of Random Matrices in Statistical Physics* [Springer Series in Solid-State Sciences 104], (Springer-Verlag, 1993).
- [127] B. P. Nguyen and K. Kim, *J. Phys.: Cond. Matter* **24**, 135303 (2012).
- [128] P. F. Bagwell, *Phys. Rev. B* **41**, 10354 (1990).
- [129] J. Heinrichs, *Phys. Rev. B* **68**, 155403 (2003).
- [130] J. H. Davies, *The Physics of Low-Dimensional Semiconductors: An Introduction*, (Cambridge University Press, 1998).
- [131] J. Billy, V. Josse, Z. Zuo, A. Bernard, B. Hambrecht, P. Lugan, D. Clement, L. Sanchez-Palencia, P. Bouyer, and A. Aspect, *Nature (London)*, **453**, 891 (2008).
- [132] G. Roati, C. D'Errico, L. Falani, M. Fattori, C. Fort, M. Zaccanti, G. Modugno, M. Modugno, and M. Inguscio, *Nature (London)*, **453**, 895 (2008).

- [133] H. A. Bethe, Proc. Roy. Soc. London Ser A, **150**, 552 (1935).
- [134] R. J. Baxter, *Exactly solved models in statistical mechanics* (Academic Press, 1982).
- [135] R. Abou-Chacra, P. W. Anderson, and D. J. Thouless, J. phys. C **6**, 1734 (1973).
- [136] R. Abou-Chacra and D. J. Thouless, J. phys. C **7**, 65 (1973).
- [137] A. D. Mirlin and Y. V. Fyodorov, Nucl. Phys. B **366**, 507 (1991).
- [138] J. D. Miller and B. Derrida, J. Stat. Phys. **75**, 357 (1994).
- [139] C. Monthus and T. Garel, J. Phys. A **42**, 075002 (2009).
- [140] G. Biroli, G. Semerjian, M. Tarzia, Prog. Theor. Phys. Suppl. **184**, 187 (2010).
- [141] H. Kunz and B. Souillard, J. Physique Lett. **44**, L411 (1983).
- [142] V. Acosta and A. Klein, J. Stat. Phys. **69**, 277 (1992).
- [143] A. Klein, Commun. Math. Phys. **177**, 755 (1996); Adv. Math. **133**, 163 (1998).
- [144] M. Aizenman R. Sims, and S. Warzel, Prob. Theor. Rel. Fields **136**, 363 (2006); Comm. Math. Phys. **264**, 371 (2006).
- [145] M. Aizenman and S. Warzel, Phys. Rev. Lett. **106**, 136804 (2011).